People's Democratic Republic of Algeria
Ministry of Higher Education and Scientific Research
University Mohamed Khider of Biskra
Faculty of Exact Sciences and Sciences of Nature and Life

Department of Matter Sciences
Domain of Matter Sciences
Section of Physics

Thesis submitted to obtain the Degree of Doctorate

In Physics

Speciality: Physics of thin films

Optimization of indium oxide thin films properties prepared by sol gel spin coating process for optoelectronic applications

Presented by:

Yahia Anouar

To the Jury composed by:

Mr. Attaf Nadhir	*Professor*	*University of Constantine 1*	*President*
Mr. Attaf Abdallah	*Professor*	*University Med Khider of Biskra*	*Reporter*
Mme. Saidi Hanane	*Professor*	*University Med Khider of Biskra*	*Co-Reporter*
Mr. Saad Rahmane	*Professor*	*University Med Khider of Biskra*	*Examiner*
Mr. Gueddim Ahmed	*Professor*	*University Ziane Achour of Djelfa*	*Examiner*

Academic Year
2019-2020

بسم الله الرّحمن الرّحيم

﴿الحَمْدُ لله الذِّيْ هَدَانَا لِهَذَا ومَا كُنَّا

لِنَهْتَدِيَ لَوْلَا أَنْ هَدَانَا الله﴾

﴿وَقُلْ رَبِيْ زِدْنِي عِلْمَا﴾

صدق الله العظيم

DEDICATION

To everyone who contributed in this humble work

From near or far

With a lot or a little

In openly or in secretly

I mentioned him or not

I knew him or not

I dedicate this thesis

May Allah reward you with all goodness

ACKNOWLEDGEMENT

Firstly, I thank ***GOD*** *the whole powerful for having agreed his infinite kindness, courage, the force and patience to complete this modest work.*

I wish to express my deep sense of gratitude to ***Attaf Abdallah****. Professor and Head, Faculty of Exact Sciences and Sciences of Nature and Life in University Mohamed Khider of Biskra for suggesting the problem and his unstinted guidance and supervision throughout the course of this work.*

I should thank from the bottom of my heart to ***Saidi Hanane*** *professor at the department of sciences of matter at faculty of exact sciences and sciences of nature and life in University Mohamed Khider of Biskra, for her constant encouragement and kind help extended to my work.*

I take immense pleasure in thanking to ***Attaf Nadhir*** *professor at the University of Constantine 1, Department of physic, who agreed to be the president of the doctoral committee.*

I am also thankful to ***Saad Rahmane*** *professor at the department of sciences of matter at faculty of exact sciences and sciences of nature and life in University Mohamed Khider of Biskra, who agreed to accept to belong to the jury and to examine my work.*

I owe my heartful thanks to ***Gueddim Ahmed*** *professor at the physics department in Ziane Achour University of Djelfa, who showed great interest in my research work and accepted to belong to the jury and to examine my work.*

I am indebted to ***Prof. Tibermacine Toufik*** *for his help during the progress of my work. I express my sincere thanks to my fellow research scholars* ***Dr. Dahnoun Mohamed, Dr. Labed Mohamed*** *and* ***Dr. Bouhdjer Adel.***

I thank my beloved Parents for their love and care. I wish also to express my gratitude to my brothers and sisters for their constant encouragement and untired support towards the completion of my research work.

Lastly, I offer my regards to many people who have helped me at various stages of my work then and there needed. This work would not be possible without their help.

Anouar Yahia

ABSTRACT

Optimization of indium oxide thin films properties prepared by sol gel spin coating process for optoelectronic applications

Indium oxide thin films have been deposited by sol-gel spin coating technique using indium (III) nitrate hydrate, absolute ethanol and acetylacetone as precursor solution, solvent and stabilizer, respectively. The effect of the molar concentration, annealing temperature, titanium doping and cupric doping on the structural, morphological, optical and electrical properties of In_2O_3 films have been studied.

All films have been characterized by multiple techniques such as X-ray diffraction (XRD), UV-Visible spectroscopy, scanning electron microscope (SEM), photoluminescence (PL) spectroscopy, Fourier transform infrared (FTIR) spectroscopy and four probe method to investigate the physical properties of indium oxide films. X-ray diffraction analysis showed that the films are polycrystalline in nature having cubic crystal structure with preferred growth orientation along (222) plane. SEM images show that the films are homogenous, uniform and dense without any pin holes and cracks**.** The transmittance of In_2O_3 films was high up to 90% and it is probably related to the good crystalline quality of the films. The optical gap was found to vary between 3.5 and 4.0 eV. The photoluminescence measurements revealed mainly three emission peaks (ultraviolet, blue and green) corresponding to the near band edge (NBE) and defect levels (DL) emissions. The broad ultraviolet luminescence peak 310-420 nm is assigned to NBE emission. The blue and green luminescence are attributed to DL emission. The electrical measurements revealed that prepared Cu doped In_2O_3 films have a low resistivity (about 1.77×10^{-3} – 6.34×10^{-3} (Ω.cm)) which made these films suitable for optoelectronic applications.

Keywords: Thin film, indium oxide, sol-gel, spin coating technique, doping, optical properties, electrical properties**.**

ملخص

تحسين خصائص الشرائح الرقيقة لأكسيد الإنديوم المحضرة بواسطة تقنية الطرد المركزي سائل – هلام للتطبيقات الكهروضوئية

تم ترسيب الشرائح الرقيقة لأكسيد الإنديوم بواسطة تقنية الطرد المركزي سائل – هلام باستخدام نترات الإنديوم الثلاثي المميه، الإيثانول وأسيتيل الأسيتون كمصدر، مذيب ومثبت على التوالي. وقد تم دراسة تأثير كل من التركيز المولي، درجة الحرارة، التطعيم باستخدام التيتانيوم والنحاس على الخصائص البنيوية، المورفولوجية، الضوئية والكهربائية لشرائح أكسيد الإنديوم الرقيقة.

تم توصيف كل الشرائح باستعمال عدة طرق مثل انعراج الأشعة السينية، المطيافية فوق البنفسجية والمرئية، المجهر الإلكتروني الماسح، مطيافية التألق الضوئي، مطيافية الأشعة تحت الحمراء (FTIR) وتقنية المسابير الأربعة. أظهرت تحاليل انعراج الأشعة السينية أن الشرائح ذات طبيعة متعددة التبلور ببنية مكعبية الشكل مع اتجاه مفضل للنمو وفق المستوي (222). كما بينت صور المجهر الالكتروني الماسح أن الشرائح ذات سطح متجانس، متماثل وكثيف دون وجود أي مسامات أو شقوق. إضافة إلى ذلك كانت نفاذية شرائح أكسيد الإنديوم عالية بحيث وصلت إلى النسبة 90%، وقد يعود ذلك للتبلور الجيدة لهذه الشرائح.كما تتراوح قيم فجوة النطاق الممنوع ما بين 3.5 و 4.0 إلكترون فولط. وأيضا كشفت قياسات التألق الضوئي بشكل أساسي قمما للانبعاث (فوق البنفسجي والأزرق والأخضر) توافق الانبعاثات من حافة النطاق القريب ومستويات العيوب بحيث قمة التألق الواسعة للأشعة فوق البنفسجية في المجال 310 – 420 نانومتر تعود للانبعاث من حافة النطاق القريب، بينما التألق للأشعة الزرقاء والخضراء يعود إلى الانبعاث من مستويات العيوب. فضلا عن ذلك، أظهرت القياسات الكهربائية أن شرائح أكسيد الإنديوم المطعمة بالنحاس تملك أقل مقاومية من بين الشرائح المحضرة (تتراوح ما بين 1.77×10^{-3} – 6.34×10^{-3} أوم.سم) مما يجعلها صالحة للاستعمال في التطبيقات الكهروضوئية.

الكلمات المفتاحية: الشرائح الرقيقة، أكسيد الإنديوم، سائل – هلام، تقنية الطرد المركزي، تطعيم، خصائص ضوئية، خصائص كهربائية.

RESUME

Optimisation des propriétés des couches minces d'oxyde d'indium préparées par le procédé sol-gel type spin coating pour des applications optoélectroniques

Les couches minces d'oxyde d'indium ont été déposées par la technique de sol-gel spin coating en utilisant du nitrate hydraté d'indium (III), l'éthanol absolu et l'acétylacétone comme précurseur, solvant et stabilisant, respectivement. Les effets de la concentration molaire, la température de recuit, dopage par le titane et dopage par le cuivre sur les propriétés structurelles, morphologiques, optiques et électriques des films d'In_2O_3 ont été étudiés.

Tous les films ont été caractérisés par de nombreuses techniques telles que la diffraction des rayons X (DRX), la spectroscopie UV-Visible, le microscope électronique à balayage (MEB), la spectroscopie à photoluminescence (PL), la spectroscopie infrarouge à transformée de Fourier (IR-TF) et la méthode de quatre points pour étudier les propriétés physiques des films d'oxyde d'indium. L'analyse par diffraction des rayons X a montré que les films sont de nature polycristalline et présentent une structure cristalline cubique avec une orientation de croissance préférée selon le plan (222). Les images de MEB montrent que les films sont des surfaces homogènes, uniformes et denses, sans aucune de porosité et fissures. La transmittance des couches d'In_2O_3 était élevée jusqu'à 90% et est probablement liée à la bonne qualité cristalline des films. Le gap optique variait entre 3,5 et 4.0 eV. Les mesures de photoluminescence ont révélé principalement trois pics d'émission (ultraviolets, bleus et verts) correspondant aux émissions de bord proche de la bande et des niveaux des défauts. Le large pic de luminescence ultraviolet 310-420 nm est attribué à l'émission de bord proche de la bande. Les luminescences bleue et verte sont attribuées à l'émission des niveaux des défauts. Les mesures électriques ont révélé que les couches préparées d'In_2O_3 dopées par Cu ont une faible résistivité (autour de 1.77×10^{-3}–6.34×10^{-3} (Ω.cm)), ce qui rend ces films adaptés aux applications optoélectroniques**.**

Mots-clés: couche mince, oxyde d'indium, sol-gel, technique de spin coating, dopage, propriétés optique, propriétés électrique.

TABLE OF CONTENTS

LIST OF FIGURES

LIST OF TABLES

GENERAL INTRODUCTION

Studies of transparent and highly conducting films (such as indium oxide (In_2O_3) [1], zinc oxide (ZnO) [2] and tin oxide (SnO_2) [3]…,etc) have attracted the attention of many researchers because of their many and varied uses, both in industry and in research fields. Among them, indium oxide (In_2O_3) has received much attention due to his wide band gap, high transparency, considerable chemical stability, high mobility and electrical conductivity. It is commonly used for extent applications, like, solar cells [4], heat reflecting mirrors [5], antireflection coatings [6], gas sensors [7] and flat panel displays [8].

Until now, In_2O_3 thin films have been prepared by a variety of thin film deposition techniques such as pulsed laser deposition (PLD) [9], dc magnetron sputtering [10], spray pyrolysis [11], spray ultrasonic [12], sol gel method [13]…,etc. Among these techniques, we chose the sol gel method due to many merits and benefits such as the easy control of chemical components, low cost of the equipment and low temperature deposition. Besides, the films can easily be coated in a variety of shapes and sizes using an inkjet printer.

In the last decades, several published researches studied indium oxide thin films properties prepared by sol gel spin coating process by varying multiple deposition parameters such as: spin coating speed [14], thermal annealing [15], tin doping [16]...,etc. In this work, an attempt has been made to optimize optical and electrical properties of indium oxide thin films using sol gel spin coating method, and that's by changing the following parameters: precursor concentration, annealing temperature, titanium and copper doping. These parameters has been varied to make In_2O_3 thin films suitable for optoelectronic and photovoltaic applications such as: solar cells, buffer layers and gas sensors..., etc.

This thesis contains the following chapters:

The first chapter is a brief survey on structural, optical and electrical properties of indium oxide thin films. It also summarizes the multiple applications of these films in optoelectronic and photovoltaic fields.

The second chapter discusses the various preparation methods and diagnostic techniques used in the analysis of undoped and doped In_2O_3 thin films. In the present study, films were prepared using sol gel via spin coating process and characterized using X-ray diffractometer (XRD), scanning electron microscopy (SEM) and energy dispersive X-ray spectroscopy (EDX) techniques. A few films were analyzed by photoluminescence (PL) spectroscopy and fourier

transform infrared spectroscopy (FTIR). The electrical and optical properties of the films were studied using a four probe set up and UV-Visible spectrophotometer, respectively.

The third chapter deals with the preparation and characterization of indium oxide (In_2O_3) films deposited by sol gel spin coating technique on glass substrates with different precursor concentration ranging from 0.05 to 0.25 M.

In chapter IV, the influence of annealing temperature on the properties of prepared indium oxide thin films by sol gel technique was investigated.

Chapter V gives an account of titanium doped indium oxide (InTiO) films prepared by spin coating on microscopic glass substrates. The films were prepared at optimum conditions.

Preparation and characterization of copper doped indium oxide films are discussed in chapter VI. The films were prepared at the optimum conditions on glass substrates with different mol.% of Cu doping.

Finally, we present general conclusion with future outlooks about the results obtained in this work.

Chapter I: Indium oxide thin films: an overview

I.1. Introduction

Rapid and significant advances have been taking place in the field of semiconductor physics during the past few decades. In the field of research and industry, semiconductors are the subject of great interest because of their numerous practical applications. Scientists are interested in developing those materials, which maintain their required properties under extreme environmental conditions. One of the most important fields of current interest in material science is the fundamental aspects and applications of semiconducting transparent thin films. Such materials are highly conducting and exhibit high transparency in the visible region of the electromagnetic spectrum. Because of this unique property, transparent conducting oxides (TCOs) are finding wide range of applications in research and industry. They are essential part of technologies that require large area electrical contact and optical access in the visible portion of the light spectrum.

A TCO is a wide band gap semiconductor that has relatively high concentration of free electrons in the conduction band. These arise either from defects in the material or from extrinsic dopants, the impurity levels of which lie near the conduction band edge. The high carrier concentration causes absorption of electromagnetic radiations in both visible and IR portions of the spectrum [17]. A TCO must necessarily represent a compromise between electrical conductivity and optical transmittance; a careful balance between these properties is required. Reduction of the resistivity involves either an increase in carrier concentration or in the mobility. But increase in the former will lead to an increase in the visible absorption while the increase in mobility has no adverse effect on the optical properties. So the search for new TCO materials must focus on achieving materials with higher electron motilities. The above target can be achieved by making material with longer electron relaxation times or by identifying materials with lower electron effective masses.

Most of the useful oxide-based materials are n-type conductors that ideally have a wide band gap (>3 eV), the ability to be doped to degeneracy, and a conduction band shape that ensures that the plasma absorption edge lies in the infrared range. The transparency of the TCO films in the visible region is a result of the wide band gap of the material and the n type conductivity is mainly due to the oxygen ion vacancies that contribute to the excess electrons in the metal atoms [18].

I.2. Transparent conductive oxides

I.2.1. Historical Development of TCOs

The first report on TCO was published in 1907 by Badeker [19]. He reported that thin films of

Cadmium metal deposited in a glow discharge chamber could be oxidized to become transparent while remaining electrically conducting. Since then, the commercial value of these thin films has been recognized, and the list of potential TCO materials has expanded to include Aluminum doped ZnO [20], SnO_2 [21], Fluorine doped In_2O_3 [22], etc. Most of the research to develop highly transparent and conducting thin films has focused on n-type semiconductors consisting of metal oxides. Historically, TCO films composed of binary compounds which were developed by means of physical and chemical deposition methods [23,24]. One of the advantage of using binary compound as TCO material is that their chemical composition in film deposition is relatively easier to control than that of ternary and multicomponent oxides. Until now, undoped and impurity doped films such as SnO_2, In_2O_3, ZnO, CdO were developed. These materials have a free electron concentration of the order of 10^{20} cm^{-3} provided by native donors such as oxygen vacancies and interstitial metal atoms. Since impurity doped materials can use both native and impurity donors, undoped binary materials have got limited range of applications. In addition to these binary compounds, ternary compounds such as Cd_2SnO_4, $CdSnO_3$ and $CdIn_2O_4$ were also developed prior to 1980 [25,26]. In order to get TCO films suited for specialized applications, new TCO materials have been studied actively. TCO materials consisting of multicomponent oxides have been developed in 1990s. In these material systems, TCO materials consisting of ternary compounds such as Zn_2SnO_4 [27], $MgIn_2O_4$ [28], $ZnSnO_3$ [29], $GaInO_3$ [30] as well as multicomponent oxides composed of combinations of these ternary compounds were developed. The advantage of the multicomponent oxide materials is the fact that their electrical, optical, chemical and physical properties can be controlled by altering their chemical compositions.

I.2.2. Opto-electrical properties of TCOs

The induction of electrical properties of TCOs can be understood by the semiconductor band theory. For electrical conduction to occur within the semiconductor material, ground state electrons must be excited from the valence band to the conduction band minimum (CBM), across the band gap by absorbing photon energy. A wider band gap requires a higher energy photon in order for an electron to become excited into conduction. Therefore, widening the band gap (i.e. $E_g > 3.0$ eV) in a material permits transparency to the visible portion of the spectrum by placing a greater separation between the valance band maximum (VBM) and CBM of the material, thus decreasing the probability of exciting an electron into conduction [31].

TCOs have been developed by doping materials in order to facilitate the charge carrier generation within the structure. In the description of the band model, there is an important difference between the fundamental band gap (i.e. the energy separation of the E_{vb} and E_{cb}; an intrinsic property of the material) and the optical band gap (an extrinsic property), which

corresponds to the lowest-energy allowed for an optical transition. The optical band gap determines the transparency of a material which is important in TCO applications.

In order to achieve n-type conducting properties, electrons are injected from a nearby defect donor level directly into the conduction band. The point defects in a metal oxide crystal, such as oxygen vacancies, proton or metal interstitials and certain substitutional defects, effectively create an excess of electrons close to the defect site in n-type TCOs. If there is sufficient orbital overlap, it permits delocalization of electrons from the defect sites such that electronic states at the CBM become filled or in other words Fermi level shifts above the CBM. This leads to an effect known as the Moss–Burstein shift, which effectively widens the optical band gap.

$$E_g = E_{CBM} - E_{VBM} \tag{I.1}$$

$$E_g^{opt} = E_g^{MB} + E_g = E_F - E_{VBM} \tag{I.2}$$

Since the Moss–Burstein shift is:

$$E_g^{MB} = E_F - E_{CBM} \tag{I.3}$$

where E_g is the fundamental energy gap separating the VBM and CBM, E_g^{opt} is the optical band gap corresponding to the smallest allowed optical transition from the VB to the CB, E_g^{MB} is the Moss–Burstein shift and E_F is the Fermi level (Figure I.1). Thus, lattice defects in TCOs can simultaneously promote both electrical conductivity and optical transparency.

Apart from the Moss–Burstein shift the fundamental band gap is tapered due to the band gap narrowing effect which led by exchange interactions in the free-electron gas and electrostatic interactions between free electrons and ionized impurities [32].

The optical band gap is a key aspect in designing a TCO. However, the CBM depth or electron affinity (EA) in other words, the difference between vacuum energy and CBM which affects the ‘dopability’ of the TCO is also equally important in determining the conducting properties. A higher value of EA indicates greater ease of introducing charge carriers, i.e. a greater dopability [33,34]. A large separation (E_g > 3.1 eV) between the Fermi level in the conduction band and the next electronic energy level (CBM + 1) helps to prevent excitation of electrons to higher states within the conduction band, which prevents undesirable optical absorption [20].

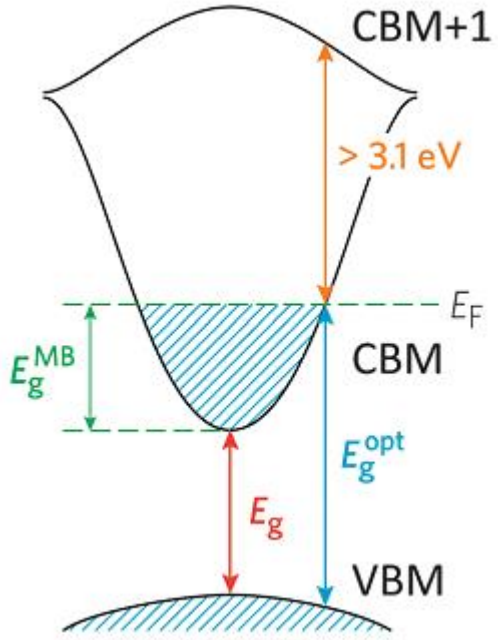

Figure I. 1. Diagram of the optical widening effect of the Moss–Burstein shift.[31].

The conductivity of a TCO is determined by the number of charge carriers and their mobility within the crystal lattice, which is inversely proportional to their effective mass. The effective mass is a quantity used to express the mass that the electrons appear to have when moving within a crystalline solid, in which their mobility is affected by their response to local forces within the crystal, expressed relative to their true mass (m_e). The local forces in TCO crystal lattice is controlled by the orbital overlap between the metal cation in a host lattice and the oxygen. The electron mobility, electron density and conductivity of inorganic materials are linearly related as described in the Boltzmann equation:

$$\sigma = n.e.\mu \tag{I.4}$$

where σ is the electrical conductivity defined in $S.cm^{-1}$, n is the density of free charge carriers (*i.e.* electrons in an n-type TCO), e is the electronic charge and μ is the electron mobility. The electrical resistivity (ρ), expressed in Ω.cm, as below:

$$\rho = \frac{1}{\sigma} \tag{I.5}$$

There are three distinct domains amongst inorganic materials regarding electrical properties: namely the semimetals (high carrier density, low electron mobility), highly conductive metals (both high carrier density and mobility) and semiconductors (low carrier density, high mobility). While the introduction of a donor level close to the conduction band permits a wide optical band gap from the VBM to the CBM, the optical absorption associated with the promotion of electrons from the CBM to higher states places an upper limit on the carrier concentration in the CBM, such that the absorption coefficient α of the TCO is proportional to the density of free

electrons n as found in equation I.6:

$$\alpha = \sigma . n \tag{I.6}$$

where σ is the absorption cross-section and n is the carrier density.

Therefore, a compromise must be made when designing doped TCOs because of this relationship between the free electron density and the optical absorption. With this limitation, ideal TCO materials need to have a high charge carrier mobility (typically $\mu = 50 - 70\ \mathrm{cm^2.V^{-1}.s^{-1}}$) and a low electrical resistivity (ideally $\rho = 10^{-3} - 10^{-4}\ \Omega.\mathrm{cm}$) whilst keeping the carrier concentration below $2 \times 10^{21}\ \mathrm{cm^{-3}}$, to prevent undesired optical absorption [31].

I.2.3. Mechanism behind simultaneous transparency and conductivity

As far as the properties of a solid are concerned, one can see that optical transparency and electrical conductivity are antonyms to each other. This can be easily proved using the basic equations in electromagnetic theory [35,36] as described below.

For electromagnetic waves passing through an uncharged semiconducting medium, the solution to Maxwell's equation gives the real and complex parts of the refractive index as:

$$n^2 = \frac{\varepsilon}{2}\left[\left\{1 + \left(\frac{2\sigma}{\nu}\right)^2\right\}^{1/2} + 1\right] \tag{I.7}$$

and

$$k^2 = \frac{\varepsilon}{2}\left[\left\{1 + \left(\frac{2\sigma}{\nu}\right)^2\right\}^{1/2} - 1\right] \tag{I.8}$$

where n is the refractive index of the medium, k is the extinction coefficient, ε is the dielectric constant, σ is the conductivity of the medium and ν is the frequency of the electromagnetic radiation. In the case of an insulator $\sigma \to 0$, $n \to \varepsilon^{1/2}$ and $k \to 0$. This implies that an insulator is transparent to electromagnetic waves.

For a perfect conductor, the solution to the Maxwell's equation yields, the reflected and transmitted component of the electric field vector as $\mathrm{E_R} = -\mathrm{E_I}$ and $\mathrm{E_T} = 0$. This means that the wave is totally reflected with a 180° phase difference. Or in other words, a good conductor reflects the radiations incident on it, while a good insulator is transparent to the electromagnetic radiations.

I.3. Indium oxide (In_2O_3): an overview

Indium metal was discovered by Reich and Richter in 1863. Indium is silver white, soft, malleable and ductile material. On heating, it burns in air with blue flame. It dissolves in all acids, but not in alkalies. Indium is used in a wide variety and range of industrial products.

Indium in its usual form has a tetragonal crystal structure with lattice parameters a = 0.3252 nm and c = 0.4946 nm. Table I.1 lists the properties of indium metal [37].

Table I. 1. Properties of indium (In) metal.

Parameter	Value
Atomic number	49
Atomic radius (nm)	0.166
Atomic weight (g/mol)	114.82
Boiling point (K)	2273
Chemical valence	1, 2, 3
Density (kg/m^3)	7280
Electrical resistivity (Ω. m)	8.37×10^{-8}
Ionic radius (nm)	(In^{3+}) 0.08
Melting point (K)	429

I.3.1. Basics of In_2O_3

Indium Oxide (In_2O_3) is a wide band gap n-type semiconductor possessing variable electrical conductivity and high optical transparency [38] and gaining interest in power electronics and switching devices [39]. It is yellowish in color and has a good physical and chemical stability [40]. It has a direct band gap of 3.2 – 3.7 eV and indirect band gap of around 2.7 eV [41]. But, there is always a debate about the nature of band gap of indium oxide. It has been reported that the indirect band gap is 0.9 – 1.1 eV smaller than the direct band gap [42]. Due to high transparency of In_2O_3, it has been used for different applications like photovoltaic devices [43], transparent conductive electrode in electronic devices, liquid crystal displays [44], transparent conducting electrodes in flat panel displays and solar cells [45], photo-detectors [46], gas sensors [47] and different other optoelectronics applications. In_2O_3 is an n-type degenerate non-stoichiometric transparent conducting oxide. It has been found in different structures like thin film, nanowires, nanoparticles and single crystals.

The research started 60 years ago on In_2O_3 when Rupprecht oxidized an evaporation-deposited indium layer at high temperature in air forming polycrystalline, transparent and conductive material [48]. Not only do polycrystalline In_2O_3 films have its applications in microelectronics but amorphous In_2O_3 films are also used for optoelelectronics applications [49].

There are different methods to grow different forms of In_2O_3. The common methods used to grow the thin films of In_2O_3 are metal oxide chemical vapor deposition (MOCVD), sol gel method, electron-beam evaporation, dc magnetron sputtering, chemical vapor deposition, spray

pyrolysis, atomic layer deposition (ALD), pulsed laser deposition, etc. Different other techniques have been used for the growth of other forms of In_2O_3 structure. Single crystals of In_2O_3 can be grown by solution dispersed method and flux method.

In_2O_3 has many properties similar to other transparent conducting oxide (TCO) such as ZnO, SnO_2, CdO, Ga_2O_3 which can be used for TCO's contact applications by doping with higher donor impurity. Indium oxide has some important properties which might favor it with respect to Ga_2O_3 because of single phase and higher symmetry cubic structure. It has been often doped with some other materials to increase its conductivity near to the value of metals and to higher transparency in the visible range. Most of the application of In_2O_3 comes in the form of widely used TCO material Sn doped In_2O_3 which is commonly referred as ITO and has been widely used in window layers in solar cells, transparent electrodes in liquid crystal display (LCD) and organic light emitting diode (OLED) [50]. But In_2O_3 has been doped with some other materials like Molybdenum [51] to increase the charge mobility, Titanium [52] to increase the electro-conductivity, tungsten [53] used for organic solar cells.

The optical band gap energy of In_2O_3 has been found to depend on various parameters like annealing temperature, oxidations conditions and the types of substrate used to grow the film and there are reports which suggests that the optical band gap of In_2O_3 thin films can be controlled by growth temperatures optimizing the way for growth temperatures to develop the high quality films and devices. It has also been figured that the growth temperature actually influence the structural, morphological, optical and electrical properties of In_2O_3 thin films and temperature is the most important parameter to grow high quality thin films [54]. Pure indium oxide which is conducting and transparent can be grown on Si substrates below temperature 400°C using trimethylindium (TMIn) and H_2O vapor [44]. Most of the growth methods include TMIn and H_2O with H_2O vapors used for oxygen precursors. But in some cases, N_2O is also used as the oxygen precursor to grow high quality In_2O_3 films on sapphire substrates at high temperature.

I.3.2. Crystal structures of In_2O_3

Indium oxide crystallizes in two phases: the cubic type and metastable rhombohedral type. The cubic structure is also referred as bixbyite Mn_2O_3 or C-type rare earth oxide structures (rare earth is a crystal prototype structure, not the elements). According to the Wyckoff [55] the bcc-In_2O_3 unit cell with space group Ia3 consists of 16 molecules with 80 atoms with the lattice constant a = 10.118 Å. In this lattice, 8 of the 32 cations sit on site b and the other 24 are in d-site. The bixbyite structure is made of edge-sharing InO_6 octahedra arranged in a 2×2×2 array. The b-site, like d-site, is six-fold coordinated by oxygen in a distorted octahedral geometry with In-O bond distance of 2.18 Å. In the b-site, two interstitial sites are located at body-diagonal

positions of the cubic structure. In d-site structure, vacancies occupy the facial-diagonal sites with each two oxygen atoms in distances of 2.13, 2.19 and 2.23 Å [56]. Figure I.2 (b) reveals the difference in the symmetry between 24d sites and 8b sites. B-site is centrosymmetric (S_6 or C_{3i} symmetry), while d-site shows a noncentrosymmetric (C_2) state [57]. Differences in the symmetry of b-site and d-site, cations show distinct spectroscopic properties in these two sites.

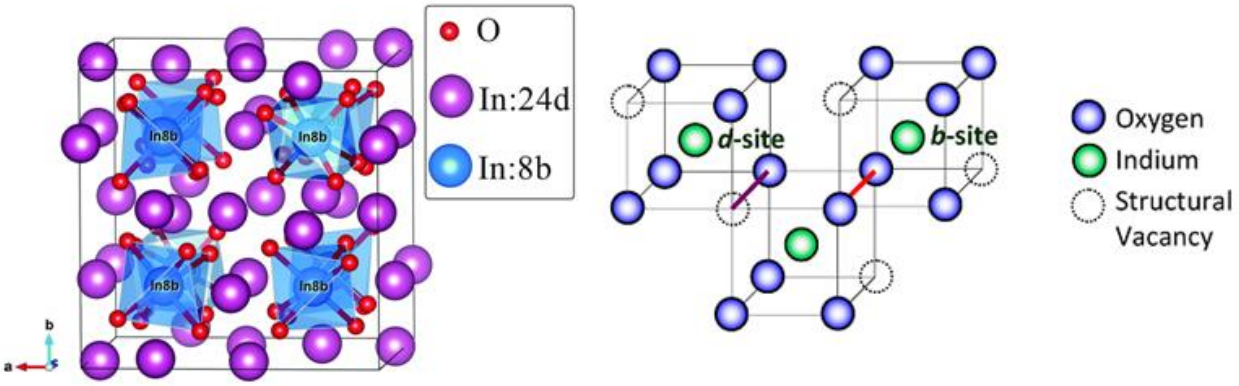

Figure I. 2. (a) In_2O_3 cubic bixbyte structure. (b) The coordination arrangement of In atoms in In_2O_3 cubic bixbyte structure [58,59].

Shannon [60] has described one of the first reports on the formation of metastable rhombohedral (corundum) indium oxide (rh-In_2O_3). Phase transformation from bixbyite to rhombohedral can happen at elevated temperature and pressure (6.5 GPa and 1250 °C); elimination of the pressure will not change the crystal structure. Stability of rh-In_2O_3 has been observed up to 12 GPa and 900 °C. Although initial study claims that rh-In_2O_3 is a high-pressure product, but recent reports present the formation of rh-In_2O_3 under ambient conditions (1 bar, 250 °C) [61]. Rhombohedral structure with space group $R\bar{3}c$ can be considered as an arrangement of hexagonal close pack oxygens, which is slightly distorted, and In^{3+} cations lying in two-thirds of the octahedral holes in the oxygen sublattice. The lattice parameters are a = 5.49 Å and c = 14.52 Å. In this arrangement, the six coordinated In^{3+} cations are surrounded with three oxygens in distance of 2.07 Å and three in 2.27 Å [61]. The unit cell with six formula units contains 12 In and 18 O (Figure I.3).

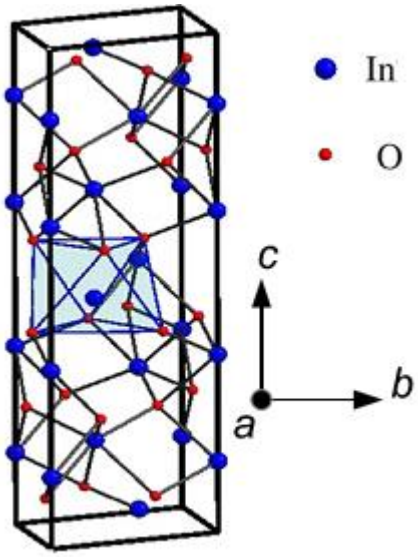

Figure I. 3. One unit cell of In_2O_3: the large and small spheres represent the In and O atoms, respectively [48].

I.3.3. Electrical and optical properties of In_2O_3

Most of the research work on In_2O_3 have been condensed on tin doped indium oxide and very few works have been done on undoped and as-grown indium oxide. In_2O_3 can be grown by different methods applying various growth conditions and changing different parameters and using different precursor sources.

In_2O_3 generally lacks stoichiometry due to oxygen-array vacancies. If the O_2 vacancies are high, a vacancy band will be formed and it overlaps with the bottom of the conduction band producing a degenerate semiconductor. The O_2 vacancies act as doubly ionized donors and contribute two electrons to the electrical conductivity [62]. Most of the transparent metal oxide films are anion (oxygen) deficient and hence are n-type semi-conductors. In doped films donor impurities (Sn, Sb, Zn, Mo, As, etc.) are added in a controlled manner. Indium tin oxide (ITO) is formed by substitutional doping of In_2O_3 with Sn. Sn replaces the In^{3+} atoms from the cubic bixbyte structure of indium oxide. Sn thus forms an interstitial bond with oxygen and exists either as SnO or SnO_2 accordingly it has a valency of +2 or +4 respectively [63]. This valency state has a direct bearing on the ultimate conductivity of ITO. The lower valence state results in a net reduction in carrier concentration since a hole is created which acts as a trap and reduces conductivity. On the other hand, predominance of the SnO_2 state means Sn^{4+} acts as an n-type donor releasing electrons to the conduction band. However, in ITO, both substitutional tin and oxygen vacancies contribute to the high conductivity and the material can be represented as $In_{2-x}Sn_xO_{3-2x}$. The direct optical band gap of ITO films ranges from 3.5 to 4.06 eV [64]. The high optical transmittance of these films is a direct consequence of the wide band gap nature. The band structure of ITO is assumed to be parabolic as shown in Figure I.4:

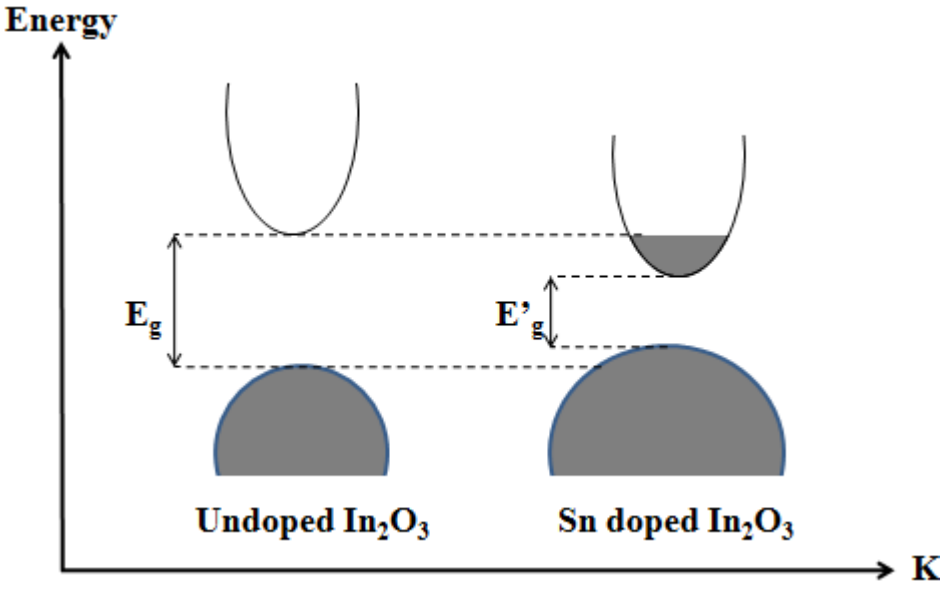

Figure I. 4. The parabolic band structure of undoped In_2O_3 and Sn doped In_2O_3 films [65].

The conduction band is curved upwards, the valence band is curved downwards and the Fermi level is located at mid band gap for the undoped material; addition of Sn dopants results in the formation of donor states just below the conduction band. As the doping density is increased, these merge with the conduction band at a critical density, N_C, which was calculated to be 2.3×10^{19} cm^{-3} by Gupta et al. [65]. Free electron properties are exhibited by the material when the density of electrons from the donor atoms exceeds this value. As all the reported values of carrier concentration are greater than N_C, all ITO films are expected to be degenerate in nature. Once the material becomes degenerate, the mutual exchange and columbic interactions shift the conduction band downwards and the valence band upwards effectively narrowing the band gap from E_g to E_g'. The band gap increase by the Burstein-Moss shift is partially compensated by this effect. The reported value for the refractive index of ITO is 1.96 [66]. The transmittance of ITO films is also influenced by a number of minor effects which include surface roughness and optical homogeneity in the direction normal to the film surface. Dark brown (effectively translucent) metallic films of ITO have also been reported. This opaqueness has been attributed to unoxidized Sn metal grains on the ITO surface as a result of instability due to absence of sufficient oxygen during deposition [67].

I.3.4. Photoconductivity

Photoconductivity is an important phenomenon in some semiconductors by which the conductivity of the sample increases due to the incident radiation. It includes the generation and recombination of charge carriers and provides useful and valuable information about the physical properties of materials which can be utilized in photo-detection and radiation measurements [68]. The term dark conductivity is used for room conductivity.

Intrinsic photoconductivity refers to the photoconductivity whenever the energy provided by the irradiated light is sufficient to excite the electrons from the valence band to the conduction band thus creating holes in the valence band and free electrons in the conduction band. But, if the energy of incident light is much smaller compared to the band gap of the sample, the energy matches the ionization energy of the impurity atoms creating an extra electron in the conduction band thereby increasing photoconductivity. This is known as extrinsic photoconductivity. Figure I.5 (a) shows intrinsic photoconductivity due to absorption of photon of energy greater than band gap which excites electrons from the valence band to the conduction band and Figure I.5 (b) shows that a photon of energy less than the band gap energy excites electrons from the defects and traps to the conduction band increasing charge carriers.

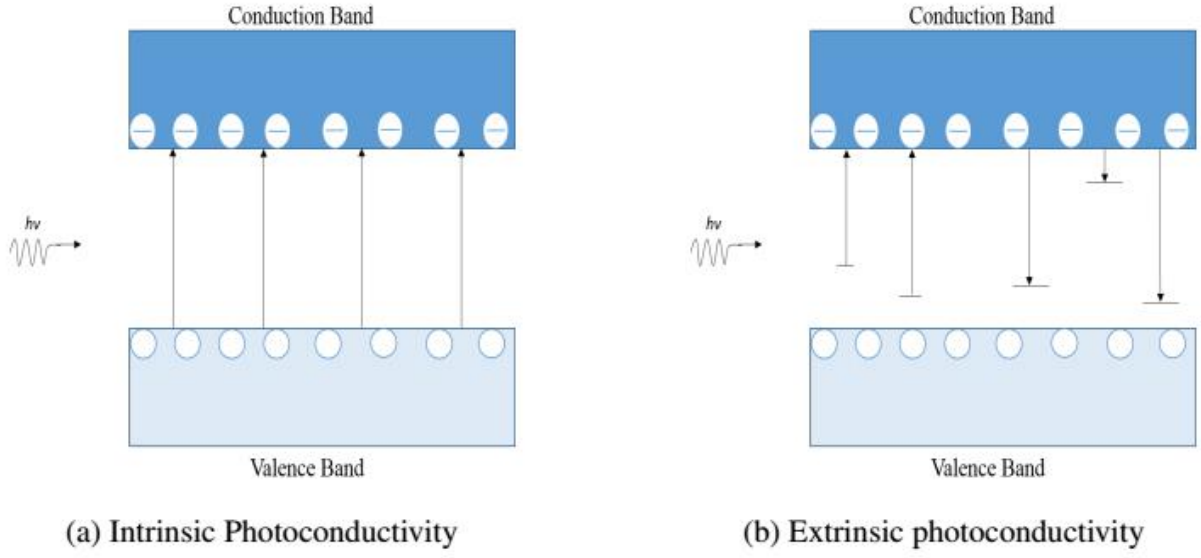

Figure I. 5. Sketch of photoconductivity phenomena showing intrinsic and extrinsic photoconductivity in a semiconductor [69].

The photoconductivity experiment consists of a monochromatic light source which is shined on the sample creating excess densities of charge carriers, that leads to the change in the conductivity creating excess holes (Δp) and electrons (Δn) given by:

Before illumination:

$$\Delta n = \Delta p = 0 \tag{I.9}$$

After illumination:

$$\Delta\sigma = \sigma_{ph} = q\left(\mu_n \Delta n + \mu_p \Delta p\right) \tag{I.10}$$

where q is the electronic charge and μ_n and μ_p are mobilities of electrons and holes and σ_{ph} is the steady state photoconductivity.

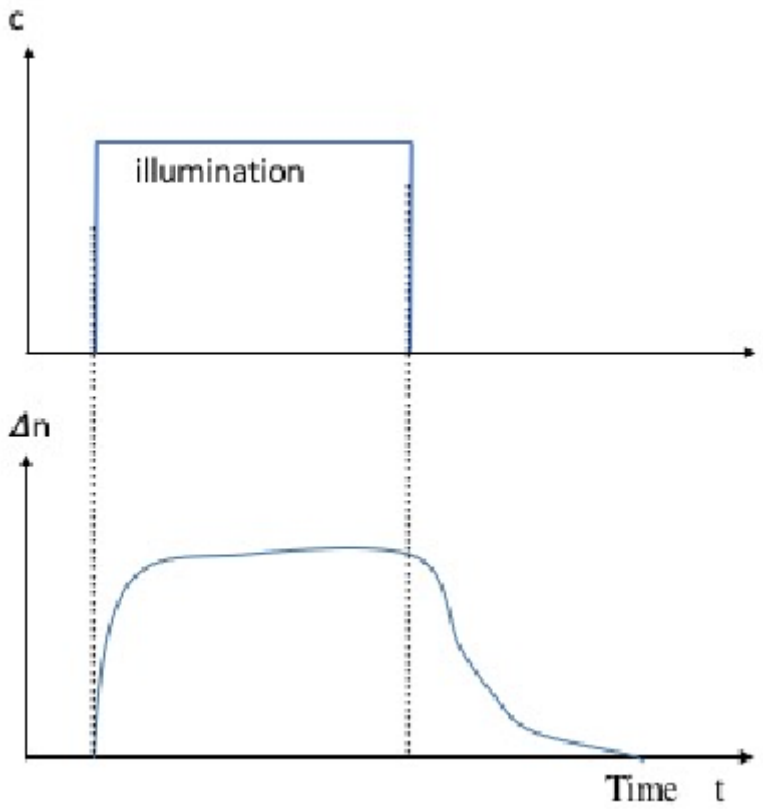

Figure I. 6. Schematic of change in charge carriers due to illumination of light [69].

In Figure I.6, it shows the change in charge carriers in response to the incident photon. Initially, when there is no illumination of light, the material shows no change in charge carriers. As the material is illuminated, charge carriers can quickly increase to the maximum value or gradual increase of charge carriers can be observed depending on the energy and intensity of the incident light as well as defect levels present in the material. The charge carrier increases and reaches saturation, which points the maximum conductivity. After the light is turned off, charge carriers of the materials decay and reach to the same value before illumination.

I.4. Importance of In_2O_3 thin films

The transparent conducting oxides exhibit high reflectivity (over 80%) in the IR region. This high IR reflectivity is useful for eliminators of heat flow through windows in buildings so that the heat input from outside in summer, and heat output from within during winter through windows are minimized. The thermal energy conservation property of indium oxide coatings is utilized in air condition residential buildings green houses, flat panel and tubular solar collectors. Undoped and doped indium oxide films have high electrical conductivity and very low absorption in the visible and near infrared regions of the solar spectrum. Because of these properties, they are used in a vast majority of applications. The major application of In_2O_3 and

ITO films include their use as wide band gap semiconductors in SIS solar cells [70], transparent electrodes for hetero-junction solar cells, liquid crystal displays [71] and antireflection coatings for silicon solar cells [72,73]. ITO film is an excellent heat mirror to transmit light radiation and reflect heat radiation [74]. Low dimensional and nanostructured semi conducting oxides, e.g. ZnO [75], CdO [76] and In_2O_3 [77,78] have recently attracted much attention due to their novel properties differing from those of thin films, and due to their applications in nanoelectronics, photonics and sensor technology. Indium oxide nanoparticles are used for transparent conductive coatings and as electrically conductive thin films in modern electronics and optoelectronics. One-dimensional In_2O_3 nanostructures have been demonstrated to be sensitive to NO_2 and NH_3 gases [79,80] as well as to biomolecules [81]. In_2O_3 thin films have been used as active layers in ozone (O_3) gas sensors [82–84].

Photoluminescence study of In_2O_3 nanoparticles dispersed within pores of mesoporous silica annealed at different temperatures are reported by Zhou et al. [85]. Zheng et al [86] reported PL band in the wavelength range of 300-360 nm for nanowire arrays formed on anodic alumina membranes by electro deposition technique. A strong PL emission peak at 398 nm was detected upon excitation of In_2O_3 nanowires embedded in alumina template at 274 and 305 nm under room temperature [87].

I.5. Applications of In_2O_3 thin films

Indium oxide has a variety of applications in microelectronics and optoelectronic devices because of high optical transmittance and high conductivity. They are therefore used for flat panel display devices, heat reflecting mirrors, transparent electrodes in displays, thin film transistors [88] and gas sensors of different oxidizing gases. It is often found doped with other material like tin used mostly for liquid crystal display (LCD), molybdenum to enhance the conductivity and use for novel optoelectronic devices. Some of the applications are discussed below:

I.5.1. Electronic Displays

Electronic displays are used for interfacing electronic equipment with human operators. Different components and device structures are required, such as liquid crystal displays [89], organic light emitting diodes (OLEDs) [90], electroluminescent displays, plasma and fluorescent displays and electrochromic displays, etc. The fabrication of these displays requires transparent and conductive films, luminescent or fluorescent films as well as dielectric and insulating layers.

I.5.2. Optical coatings

Optical coatings are applied for antireflection purposes, as interference filters on solar panels,

as plate glass infrared solar reflectors, and for laser optics. In the fabrication of filter optics, thin films with refractive index gradients are deposited on preforms from which the optical fibers are drawn. These coatings require dielectric materials with precisely defined indices of refraction and absorption coefficients. Laser optics requires metal reflective coatings which can withstand high radiation intensities without degradation. Infrared reflecting coatings are applied to filament lamps to increase the luminous flux intensity.

I.5.3. Magnetic films for data storage

Thin films of magnetic materials have found wide commercial applications for data storage in computers and control systems. The substrates can be metal, glass or plastic polymeric materials. Thin film deposition processes for magnetic materials and for materials with a high degree of hardness are required. Thin films are finding increasing commercial use for optical data storage devices in compact disks and computer memory applications. Processes for the deposition of organic polymer materials as storage media and as protective overcoats are required for this technology.

I.5.4. Antistatic coatings

Thin films of conductive or semi-conductive materials are deposited to provide protection from electrostatic discharges. Thin film coatings of carbides, silicates, nitrides, and borides are finding increased uses to improve the wear characteristics of metal surfaces for tools, bearings, and machine parts. Of particularly great current interest are films of diamond-like carbon because of this material's heat dissipation properties, electrical insulation, hardness, and resistance to high-temperature and high-energy radiation.

I.5.5. Solar cells

There has been interest in recent years directed towards the development of conducting transparent oxide-based solar cell. These oxides offer the possibility of fabrication of solar cell with performance characteristics suitable for large-scale terrestrial applications. Transparent conducting oxides are particularly effective in solar cell applications because of the following advantages.

a) The conducting transparent film permits transmission of solar radiation directly to the active region with little or no attenuation, so that solar cells based on these materials result in improved sensitivity in the high photon-energy portion of the solar spectrum.
b) Ease of fabrication of the junction because of lower junction formation temperature.
c) These films can serve simultaneously as low resistance contact to the junction and antireflective coating for the active region.

I.5.6. Gas sensors

Semiconductor material whose conductance is modulated directly by interaction with an active gas has been studied for many years. There is reversible chemisorptions of reactive gases at the surface of the certain metal oxides. The electron concentration in semiconductor sensors varies less linearly with pressure up to eight decades, while the variation in the mobility was less than a factor of two over the same pressure range. This suggests that gas chemisorptions into the surface of the semiconductor materials are useful for the fabrication of gas sensing electronic devices.

In_2O_3 has been widely used for sensing application because of high sensitivity to the chemical environment. The sensing process is governed by oxygen vacancies on the surface that influence the electronic properties of In_2O_3. Upon oxidation, via adsorption of molecules such as NO_2 at vacancy sites that accept electrons, electrons are withdrawn and effectively depleted from the conduction band, leading to a reduction of conductivity. On the other hand, reducing molecules such as H_2 can react with surface-adsorbed oxygen, leaving behind an electron and hence higher conductivity. In_2O_3 films deposited by spray pyrolysis: gas response to reducing (CO, H_2) gases have been prepared by Korotcenkov et al. [91].

Chapter II: Thin films: Preparation and characterization techniques

II.1. Introduction

The growth technique plays a significant role in controlling the properties of In_2O_3 films, because the same material deposited by two different techniques, usually has different physical properties. This is due to the fact that the electrical and optical properties of the films strongly depend on the structure, morphology and nature of impurities present. Moreover the films grown using any particular technique might have different properties due to the variation of the deposition parameters and hence the properties can be tailored by controlling the deposition parameters. It is, therefore, important and necessary to make a detailed investigation on the different techniques used for the deposition of In_2O_3 thin films. The major category of thin film deposition is given as physical deposition method and chemical deposition method. Among them, there are many techniques are employed so as to tailor the deposition results.

II.2. Thin film preparation techniques

Deposition techniques fall into two broad categories:

II.2.1. Physical deposition techniques

Physical processes proceed along the following sequence of steps:

a) The solid material to be deposited is physically converted to vapor phase;
b) The vapor phase is transported across a region of reduced pressure from the source to the substrate;
c) The vapor condenses on the substrate to form the thin film.

The conversion from solid to vapor phase is done through physical dislodgement of surface atoms by addition of heat in evaporation deposition or by momentum transfer in sputter deposition. The third category of PVD technique is the group of so called augmented energy techniques including ion, plasma or laser assisted depositions [92,93].

II.2.1.1. Evaporation

Evaporation or sublimation techniques are widely used for the preparation of thin layers. A very large number of materials can be evaporated and, if the evaporation is undertaken in vacuum system, the evaporation temperature will be considerably reduced and the amount of impurities in the growing layer will be minimized. In order to evaporate materials in a vacuum, a vapor source is required that will support the evaporant and supply the heat of vaporization while allowing the charge of evaporant to reach a temperature sufficiently high to produce the desired vapor pressure, and hence rate of evaporation, without reacting chemically with the evaporant. To avoid contamination of the evaporant and hence of growing film, the support material itself must have a negligible vapor pressure and dissociation temperature of the operating temperature

[94,95]. Laser beam evaporation has also come in to use recently. The laser source is situated outside the evaporation system and the beam penetrates through a window and is focused onto the evaporate material, which is usually fine powder form [96].

II.2.1.2. Sputtering

If a surface of target material is bombarded with energetic particles, it is possible to cause ejection of the surface atom: this is the process known as sputtering. The ejected atoms can be condensed on to a substrate to form a thin film. This method has various advantages over normal evaporation techniques in which no container contamination will occur. It is also possible to deposit alloy films which retain the composition of the parent target material. DC sputtering, radio frequency sputtering and magnetron sputtering methods are the oldest types of sputtering used by Behrisch [97]. High pressure oxygen sputtering and facing target sputtering are the two new methods introduced for deposition of thin films for applications in superconducting and magnetic films [98].

II.2.1.3. Ion plating

In this atomistic, essentially sputter-deposition process the substrate is subjected to a flux of high energy ions, sufficient to cause appreciable sputtering before and during film deposition. The advantages of physical methods are laid in dry processing, high purity and cleanliness, compatibility with semiconductor integrated circuit processing and epitaxial film growth. However, there are certain disadvantages such as slow deposition rates, difficult stoichiometry control, high temperature post deposition annealing often required for crystallization and high capital expenditure [99].

II.2.2. Chemical deposition techniques

Among chemical methods the most important are chemical bath deposition, cathode electrolytic deposition (also called electro-deposition), anodic oxidation, chemical vapor deposition and sol gel.

II.2.2.1. Chemical bath deposition (CBD)

There is considerable interest in the deposition of compound semiconductors by methods, which involve relatively low capital expenses and are technically undemanding on the experimentalist. One process to meet these criteria is chemical bath deposition. The chemical bath deposition technique involves the controlled precipitation from solution of a compound on a suitable substrate. The technique offers many advantages over the more established vapor phase synthetic routes to semiconductor materials, such as chemical vapor deposition (CVD), molecular beam epitaxy (MBE) and spray pyrolysis.

Factors such as control of film thickness and deposition rate by varying the solution pH,

temperature and reagent concentration are allied with the ability of chemical bath deposition to coat large areas, in a reproducible and low cost process. The first report of CBD was in 1884 by J. E. Reynolds [100] for the deposition of PbS. A wide range of chalcogenide (*e.g.* CdS, ZnS and MnS) and chalcopyrite materials (*e.g.* $CuInS_2$ and $CuInSe_2$) have been prepared by CBD methods.

The chemical bath deposition process uses a controlled chemical reaction to effect the deposition of a thin film by precipitation. In the most typical experimental approach, substrates are immersed in an alkaline solution containing the chalcogenides source, the metal ion, added base and complexing agent. The latter is used to control the speciation of the metal ion. The chemical bath technique appears to be a relatively simple inexpensive method to prepare a homogeneous film with controlled composition. Chemical bath deposition has been widely applied to the fabrication of semiconductor layers for photovoltaic application.

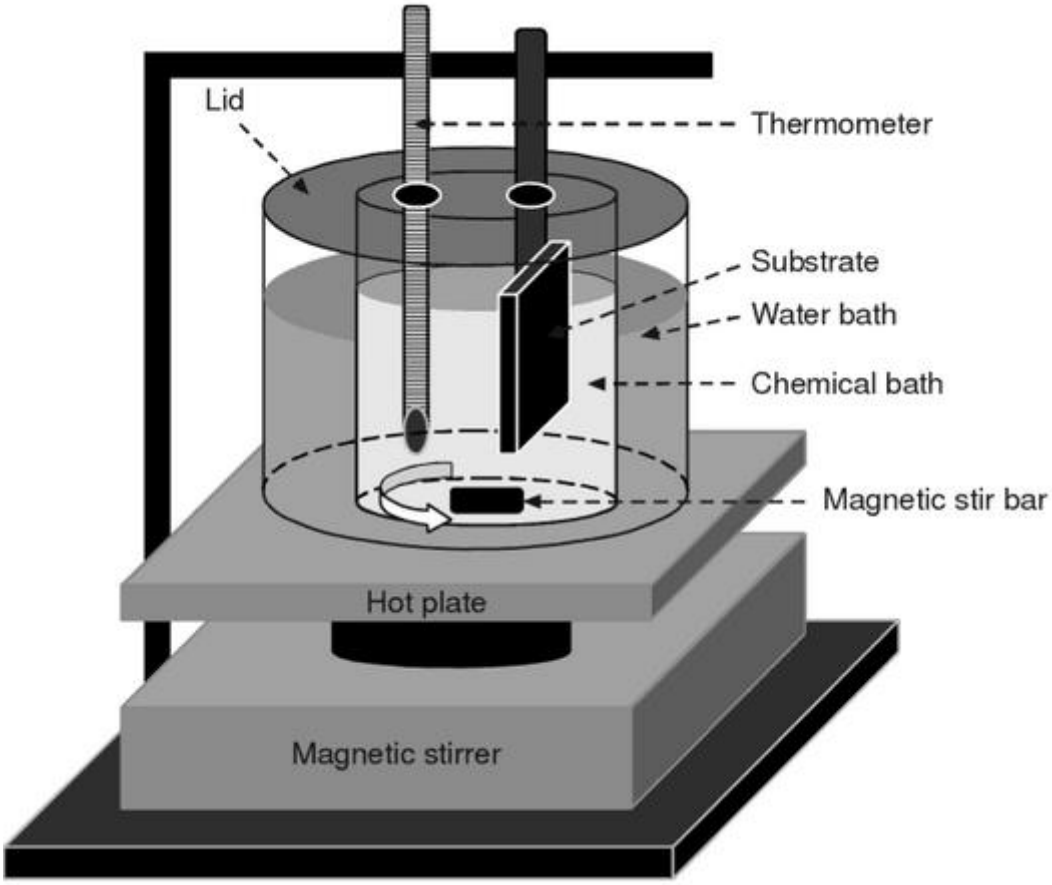

Figure II. 1. Schematic diagram of a CBD system **[101]**.

II.2.2.2. Cathodic deposition

In cathode electrolytic deposition, the substance (metal) to be deposited is present in a solution or melt in the form of ions. If we insert two electrodes into the solution (or melt) the positive ions of the metal will be attracted to the cathode where the metal will be deposited. The mass of the substance deposited is proportional to the amount of electricity used. The

proportionality constant is the electrochemical equivalent of the given substance, which, for example, is 2.04×10^{-3} g/C for Au and 0.09×10^{-3} g/C for Al. The properties of the deposited films, as, for example, its adhesion to the substrate, its crystal structure (the size of microcrystals), etc., may be influenced by the composition of the electrolyte. By this method it is, of course, possible to deposit films only on metallic substrates and the films may be contaminated by substances in the electrolyte [96].

II.2.2.3. Anodic oxidation

Anode oxidation (anode electrolytic deposition) is used mainly in the formation of films of the oxides of certain metals, e.g. Al, Ta, Nb, Ti and Zr. The oxidized metal is an anode dipped in the electrolyte from which it attracts the oxygen ions. The ions pass through the already formed oxide film by diffusion forced by a strong electric field and combine with metallic atoms to form molecules of the oxide. Because the growth rate of the film depends exponentially on the intensity of the electric field, the film thus formed is homogeneous owing to the fact that random fluctuations are immediately smoothed out. For anode oxidation it is possible to use either the constant-current or constant-voltage method. Solutions or melts of various salts, or in some cases acids, are used as electrolytes [96]. This is an electrolytic method for producing oxide films on the surface of metal.

II.2.2.4. Chemical vapor deposition (CVD)

Chemical vapor deposition (CVD) can be defined as a material synthesis method in which the constituents of vapor phase react together to form a solid film at a surface [102]. The chemical reaction is an essential characteristic of this method; therefore, besides the control of the usual deposition process variables, the reaction of the reactants must be well understood. Various types of chemical reactions are utilized in CVD for the formations of solids are pyrolysis, reduction, oxidation, hydrolysis, synthetic chemical transport reaction etc. It has emerged one of the powerful techniques of thin film growth. Among the reasons for the growing adoption of CVD methods is the ability to produce a large variety of films and coatings of metals, semiconductors, and compounds in a crystalline or amorphous form, possessing high purity and desirable properties. Furthermore, the capability of controllably creating films of widely varying stoichiometry makes CVD unique among deposition techniques. Other advantages include relatively low cost of the equipment and operating expenses, suitability for both batch and semi continuous operation, and compatibility with other processing steps. The detailed steps of CVD process are demonstrated in Figure II.2. CVD has numerous other names and adjectives associated with it such as Vapor Phase Epitaxy (VPE) when CVD is used to deposit single crystal films, Metal-organic CVD (MOCVD) when the precursor gas is a metal-

organic species, Plasma Enhanced CVD (PECVD) when a plasma is used to induce or enhance decomposition and reaction, and Low Pressure CVD (LPCVD) when the pressure is less than ambient.

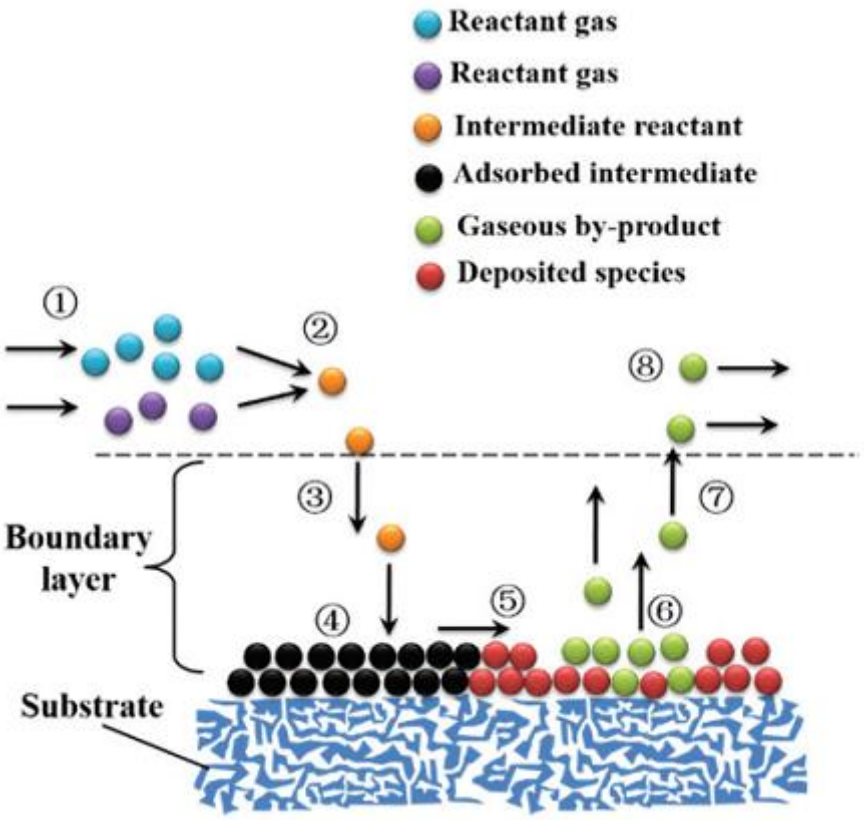

Figure II. 2. Schematic model of a CVD process [103].

II.2.2.5. Sol gel

A colloid is a suspension in which the dispersed phase is so small (~ 1–1000 nm) that gravitational forces are negligible and interactions are dominated by short range forces, such as Van Der Waals attraction and surface charges. A sol may be defined as a colloidal suspension of solid particles in a liquid. The sol may be produced from inorganic or organic precursors and may consist of dense oxide particles or polymeric clusters. In the sol-gel process, the precursors (starting compounds) for preparation of a colloid consist of a metal or metalloid elements surrounded by various ligands. The precursor most widely used in sol-gel research [104] is termed as an alkoxide. Metal alkoxides are members of the family of metalorganic compounds, which have an organic ligand attached to a metal or metalloid atom. The most thoroughly studied example is silicon tetraethoxide (or tetraethoxy-silane, or tetraethyl orthosilicate, TEOS), $Si(OC_2H_5)_4$. Metal alkoxides are popular precursors because they react readily with water. The reaction is called hydrolysis, because a hydroxyl ion becomes attached to the metal atom. Key steps in sol-gel processing are the hydrolysis of the alkoxides and the condensation of the hydrolysis products, both of which are stimulated by catalysts such as acids. The hydrolysis step

is described by:

$$M(OR)_4 + H_2O \rightarrow HO - M(OR)_3 + ROH \quad \text{(II.1)}$$

R represents a proton (hydrogen atom) or other ligand and ROH is an alcohol. In reaction (II.1) the metal alkoxide $M(OR)_4$ is partially hydrolyzed forming a suitable species for polymerization as shown in the reaction:

$$(OR)_3M - OR + HO - M(OR)_3 \rightarrow (OR)_3M - O - M(OR)_3 + ROH \quad \text{(II.2)}$$

By definition, condensation liberates small molecules, such as water or alcohol. This type of reaction can continue to build up larger and larger molecules by the process of polymerization. Dilute solutions containing these polymerized species can then be used to coat substrates by spinning or dip coating.

a) Dip coating

In dip coating process, film formation takes place by evaporation of the solvent from a polymer solution. The substrate is dipped into the polymer solution, taken out at a constant speed and dried by allowing the solvent to evaporate, leaving behind a solid polymer film on the substrate. Scriven et al. [105] divided the dip coating process into five stages: (a) immersion, (b) start-up, (c) deposition, (d) drainage and (e) evaporation, shown in Figure II.3. The thickness of the deposited film is related to the position of the streamline dividing the upward and downward moving layers. There are five forces in the film deposition region governing the thickness of the film and the position of the streamline: (1) viscous drag upward on the liquid by the moving substrate, (2) force of gravity, (3) resultant force of surface tension in the concavely curved meniscus, (4) inertial force of the boundary layer liquid arriving at the deposition region, and (5) surface tension gradient [106].

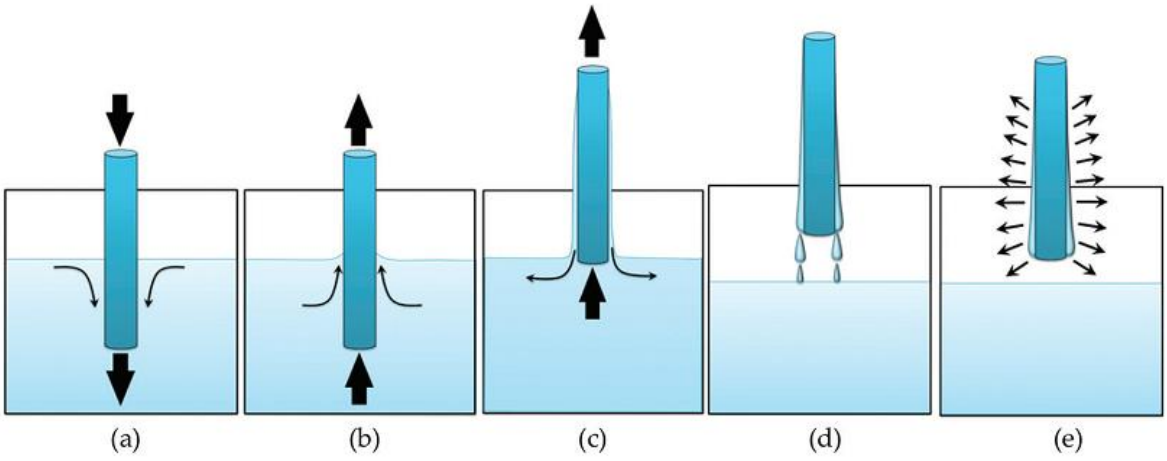

Figure II. 3. Dip-coating stages: (a) immersion; (b) start-up; (c) deposition; (d) drainage and (e) evaporation **[103]**.

The thickness of the coating layer depends on the following factors:

1) The speed at which the substrate is taken out,
2) The concentration of the solution,
3) The viscosity of the solution,
4) The rate of solvent evaporation,
5) The angle at which the substrate is taken out,
6) The surface tension of the solution,
7) The vapor pressure,
8) Temperature and relative humidity above the coating bath,
9) The precise control of air velocity, and the temperature of substrate and solution.

b) Spin coating:

Films may also be formed by spinning the solution on a rotating substrate. Bornside et al. [107] divided spin coating into four stages: (1) deposition, (2) spin-up, (3) spin-off, and (4) evaporation, shown in Figure II.4. An excess of liquid is dispensed on the surface during the deposition stage. In the spin-up stage, the liquid flows radially outward, driven by centrifugal force. In the spin-off stage, excess liquid flows to the perimeter and leaves as droplets. As the film thins, the rate of removal of excess liquid by spin-off slows down, because the thinner the film, the greater the resistance to flow, and also because the concentration of the nonvolatile components increases raising the viscosity. In the fourth stage, evaporation takes over as the primary mechanism of thinning [108].

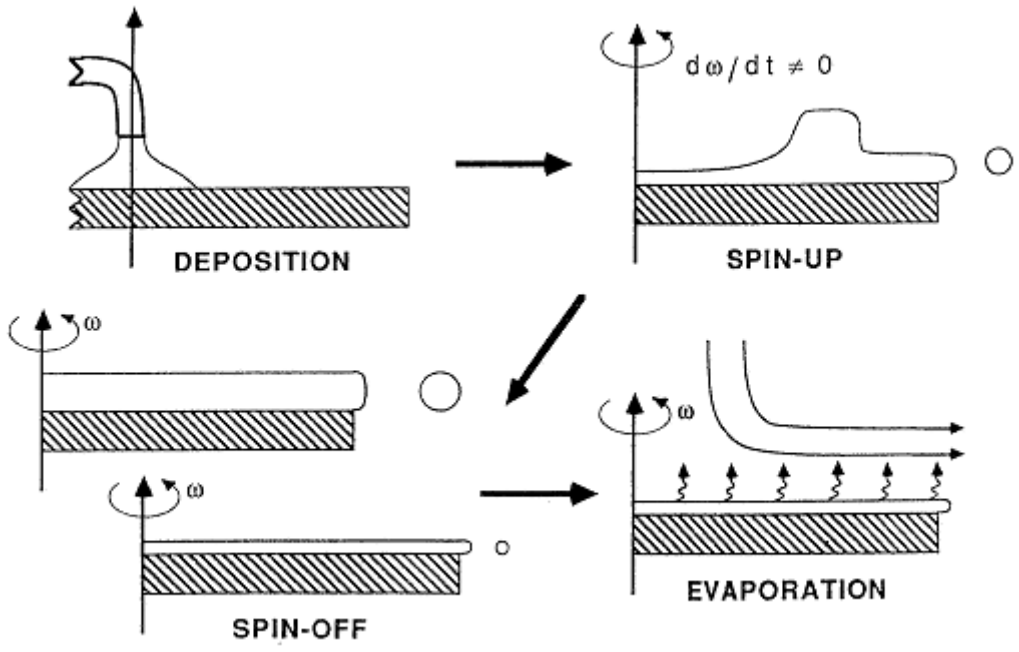

Figure II. 4. The four stages of the batch spin-coating process [106].

According to Scriven [105], an advantage of spin coating is that a film of liquid tends to become uniform in thickness during spin-off and once uniform, tends to remain so provided that the viscosity is not shear dependent and does not vary over the substrate. This tendency arises due to the balance between the two main forces: centrifugal force, which drives flow radially outward, and viscous force (friction), which acts radially inward. During spin-up, the centrifugal force overwhelms the force of gravity, and the rapid thinning quickly squelches all inertial forces other than centrifugal force [104].

The final thickness of film depends on the following factors:

1) Initial thickness,
2) Time between spin-up and spin-off,
3) Angular velocity,
4) The evaporation rate in spin coating,
5) The viscosity of the liquid.

In comparison with other thin film deposition technologies the sol-gel process has the following advantages:

(i) It gives wide possibility to vary the film properties by changing the composition of the solution (change in film microstructure, introduction of dopants, etc.);

(ii) Low process cost, specially for large scale substrates;

(iii) It is possible to coat on the desired shape and area without using expensive and complicated equipment;

(iv) Better purity and homogeneity from raw materials;

(v) Low temperature of preparation which can:

a) save energy;
b) minimize evaporation losses;
c) minimize air pollution;
d) minimize reactions with containers, thus producing purity;
e) bypass phase separation;
f) bypass crystallization.

(vi) While for thin films applied by vacuum techniques it is difficult to provide a stoichiometric ratio of the elements [109] and appropriate quality of the dielectric semiconductor interface (as a result of bombardment of the substrate by high energy particles), the sol-gel method allows one to overcome these problems.

Some disadvantages [110] of the sol-gel process are:

(i) High cost of raw materials;

(ii) Large shrinkage during processing that accompanies drying and sintering;

(iii) Residual fine pores;

(iv) Residual hydroxyl;

(v) Residual carbon;

(vi) Health hazards of organic solutions;

(vii) Long processing times.

II.3. Characterization techniques

The deposited indium oxide (IO) thin films are characterized for their structural, surface morphological, optical and electrical properties. X-ray diffraction (XRD) is used for studying the nature of crystal structure, scanning electron microscopy (SEM) is used to identify the surface morphology and energy dispersive X-ray (EDX) (attached to SEM) to study films elemental composition. The optical parameters have been analyzed from the transmittance and absorbance spectra obtained using UV-Visible spectrophotometer, fourier transform infrared (FTIR) spectrometer was used to obtain information about the chemical bonding in In_2O_3 films and photoluminescence (PL) spectrometer to detect luminescence regions and defect types. The Four point probe technique is employed to measure electrical conductivity of the films.

II.3.1. X-ray diffraction (XRD)

The discovery of X-rays in 1895 enabled scientists to probe crystalline structure at the atomic level. XRD has been used in two main areas, for the fingerprint characterization of crystalline materials and the determination of their structure [111]. Each crystalline solid has its unique characteristic X-ray powder pattern which may be used as a "fingerprint" for its identification. Once the material has been identified, X-ray crystallography may be used to determine its structure, i.e. how the atoms pack together in the crystalline state and what the inter-atomic distance and angle, etc.

The size and the shape of the unit cell for any compound can be determined most easily using XRD. X-rays are the electromagnetic waves of wavelength about 1 Å. When X-rays are incident on a crystal surface, they are reflected from it (Figure II.5).

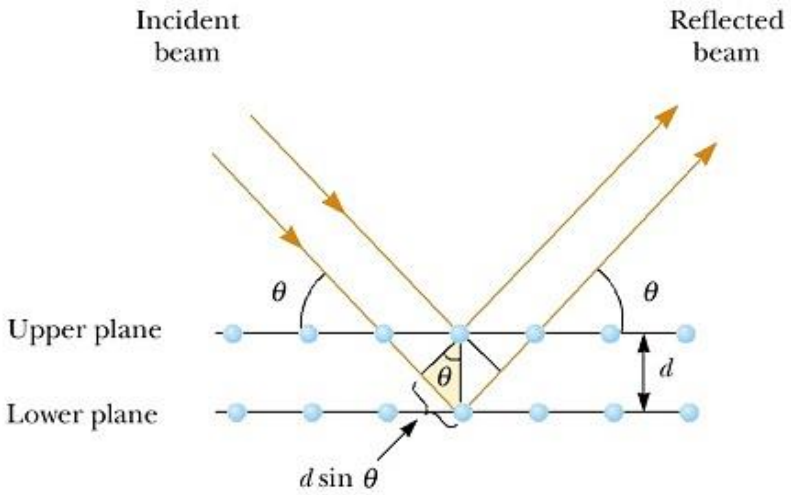

Figure II. 5. Reflection of X-rays from two planes of atoms in a solid.

The reflection obeys the following Bragg's law:

$$2dsin\theta = n\lambda \quad \text{(II.3)}$$

where d is the distance between crystal planes, θ is the incident angle of X-ray, λ is the wavelength of the X-ray and n is a positive integer. Bragg's law also suggests that the diffraction is only possible when $\lambda < 2d$.

From the width of the diffraction line, it is possible to estimate the average grain size of the thin film [112]. Surface thickness in thin films are about 1000 Å, can be investigated using XRD [113]. Thicker films can be characterized by reflection high-energy electron diffraction (RHEED). Analysis of the diffraction patterns obtained by these techniques and comparison with standard JCPDS cards can reveal the existence of different crystallographic phases in the film, their relative abundance, the lattice parameters and any preferred orientations.

Using 'd' values, the set of lattice planes (hkl) are identified from the standard data and the lattice parameters are calculated using the relations. For a cubic crystal structure, the lattice parameters can be determined using the relation:

$$\frac{1}{d^2} = \frac{h^2+k^2+l^2}{a^2} \quad \text{(II.4)}$$

where, h, k and l are the indices of the crystal planes, d is the inter-planar spacing and a is the lattice constant.

Crystallite size (D) generally corresponds to the coherent volume in the material for the respective diffraction peak. It contributes to the peak broadening and as crystallite size decreases, the full width increases. The Crystallite size (D) of the film is determined by using Debye Scherrer's formula [114]:

$$D = \frac{K\lambda}{\beta cos\theta} \quad \text{(II.5)}$$

Where K is a constant known as shape factor and taken as 0.94, λ is the wavelength of X-rays, β

is the full-width at half maximum and θ is Bragg angle.

The origin of micro strain (ε) is calculated using the relation [115]:

$$\varepsilon = \frac{\beta cos\theta}{4} \quad \text{(II.6)}$$

The dislocation density (δ) is the dislocation lines per unit area of the crystal, can also be evaluated from the crystallite size 'D' using the formula [116]:

$$\delta = \frac{1}{D^2} \quad \text{(II.7)}$$

II.3.2. Scanning electron microscope (SEM)

Scanning electron microscope is an instrument that is used to observe the morphology of the solid sample at higher magnification, higher resolution and depth of focus as compared to an optical microscope [117]. When an electron strikes the atom, variety of interaction products are evolved. Figure II.6 illustrates these various products and their use to obtain the various kinds of information about the sample. Scattering of electron from the electrons of the atom results into production of backscattered electrons and secondary electrons. Electron may get transmitted through the sample if it is thin. Primary electrons with sufficient energy may knock out the electron from the inner shells of atom and the excited atom may relax with the liberation of Auger electrons or X-ray photons. All these interactions carry information about the sample. Auger electron, ejected electrons and X-rays are energies specific to the element from which they are coming. These characteristic signals give information about the chemical identification and composition of the sample.

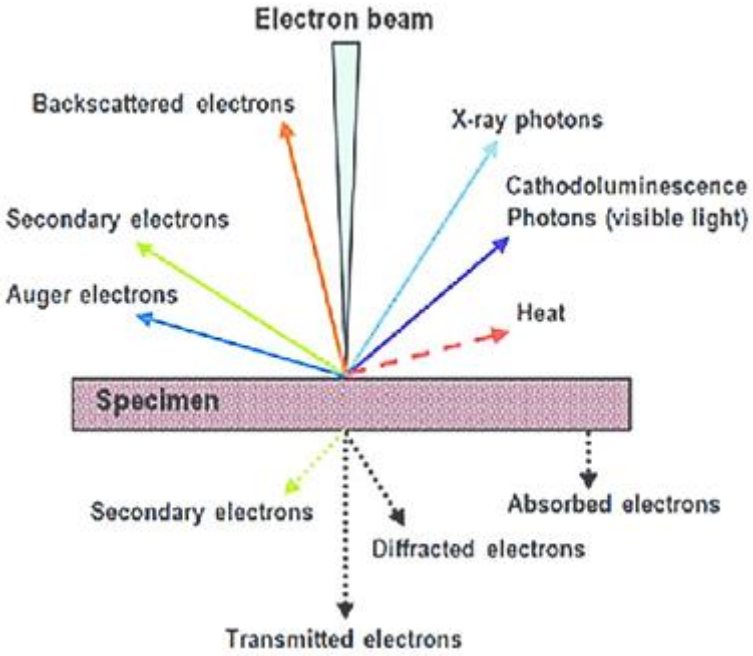

Figure II. 6. Variety of interaction products evolved due to interaction of a primary electron beam and specimen (sample) [118].

Principle of Scanning Electron Microscope

A well-focused mono-energetic (~25 keV) beam is incident on a solid surface giving various signals as mentioned above. Backscattered electrons and secondary electrons are particularly pertinent for SEM application, their intensity being dependent on the atomic number of the host atoms. Each may be collected, amplified and utilized to control the brightness of the spot on a cathode ray tube. To obtain signals from an area, the electron beam is scanned over the specimen surface by two pairs of electro-magnetic deflection coils and so is the cathode ray tubes (C.R.T) beam in synchronization with this.

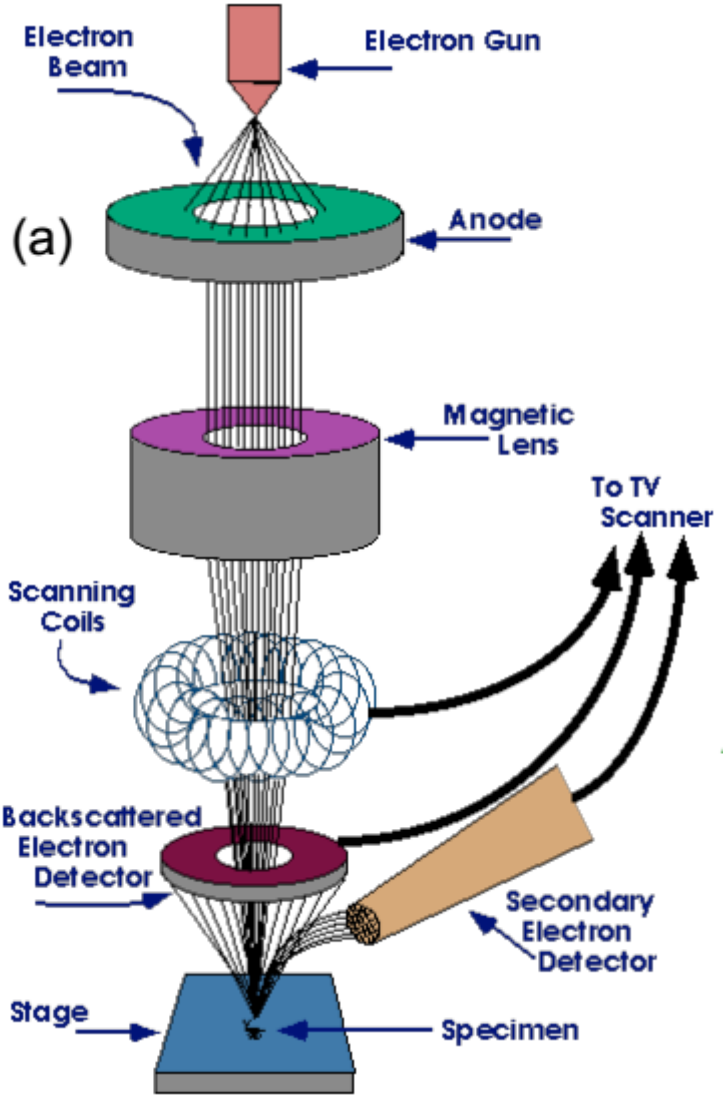

Figure II. 7. Schematic diagram of the scanning electron microscope (SEM) [121].

The signals are transferred from point to point and signal map of the scanned area is displayed on a long persistent phosphor C.R.T. screen. Change in brightness represents change of a particular property within the scanned area of the specimen [119]. The ray diagram of

scanning electron microscope is shown in Figure II.7. The scattering cross section for backscattered electrons is given as [120]:

$$Q = 16.2 \times 10^{-30} \left[\frac{Z}{E}\right]^2 \cot\left(\emptyset/_2\right) \quad \text{(II.8)}$$

where Z is atomic number and E is electric field.

Here the cross-section is proportional to Z^2. Hence, the backscattered electrons are used for the Z contrast or for compositional mapping.

II.3.3. Energy dispersive X-ray spectroscopy (EDS or EDX)

EDX is a chemical microanalysis technique used in conjunction with SEM. EDX can provide elemental analysis on areas as small as nanometer in diameter and it is used to determine the elemental composition of individual points or to map out the lateral distribution of elements from the imaged area. When an incident electron beam hits atoms of the sample, secondary and backscattered electrons are emitted from the sample surface. However, these are not the only signals emitted from the sample. When the incident beam bounces through the sample creating secondary electrons, it leaves thousands of the sample atoms with holes in the electron shells where the secondary electrons used to be. If these "holes" are in inner shells, the atoms are not in a stable state. To stabilize the atoms, electrons from outer shells will drop into the inner shells, however, because the outer shells are at a higher energy state, to do this the atom must lose some energy. It does this in the form of X-rays. The X-rays emitted from the sample atoms are characteristic in energy and wavelength to, not only the element of the parent atom, but which shells lost electrons and which shells replaced them, this permits the elemental composition of the sample to be measured.

An EDX spectrum not only identifies the element corresponding to each of its peaks, but also the type of X-ray to which it corresponds as well. For example, a peak corresponding to the amount of energy possessed by X-rays emitted by an electron in the L-shell going to the K-shell is identified as a K-alpha peak. The peak corresponding to X-rays emitted by M-shell electrons going to the K-shell is identified as K-beta peak [122] (Figure II.8).

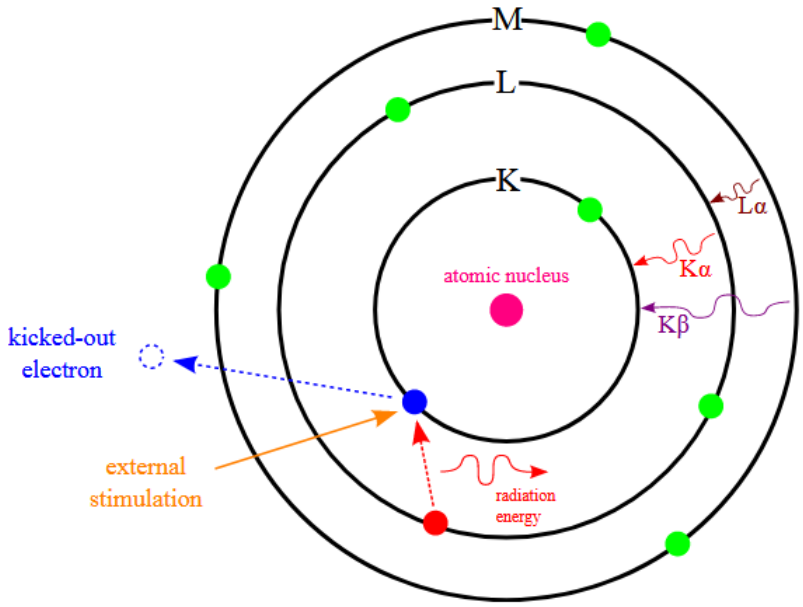

Figure II. 8. Scheme of X-ray excitations in EDX analysis.

II.3.4. Photoluminescence spectroscopy

The spontaneous emission of light from a material under optical excitation is known as photoluminescence (PL). Photoluminescence spectroscopy is a nondestructive method to probe the electric structure of materials. PL spectroscopy can be used to characterize a variety of material parameters. It provides electrical characterization and information on the quality of surfaces and interfaces. It is a direct method to measure various important material properties such as band gap, impurity levels, and defect detection and recombination mechanism. The schematic diagram of the PL measurement set-up is shown in Figure II.9.

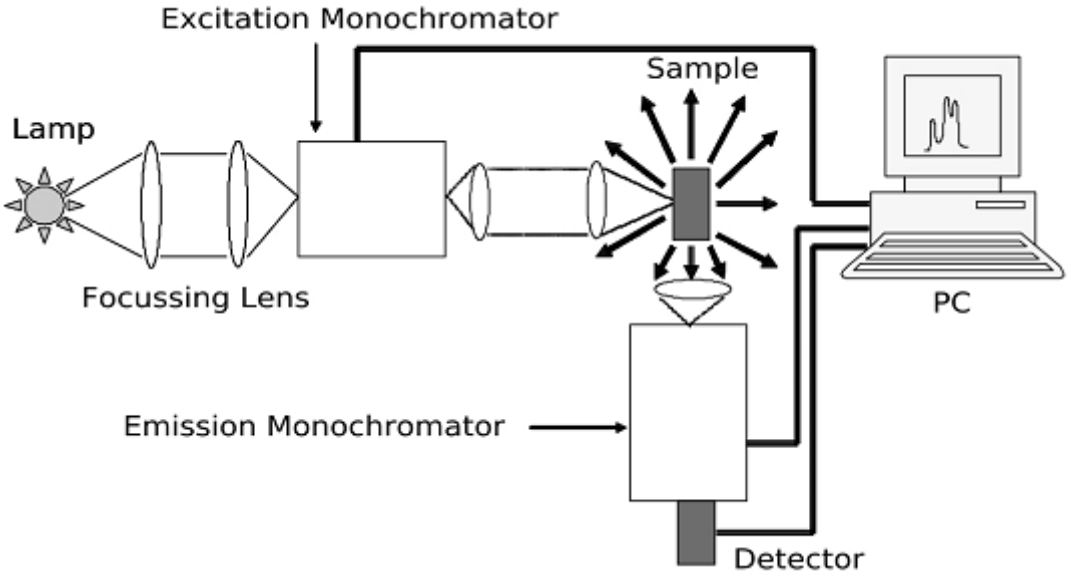

Figure II. 9. Schematic diagram showing elements used to measure photoluminescence spectra [123].

When light of sufficient energy is incident on a material, photons are absorbed. Electrons are excited due to the energy of absorbed photons and goes to the excited state. Eventually, such excited electrons reach to the ground state with emitting radiations in the form of light. This emitted light can be collected and analyzed to get information about the material. After analyzing the signals, transition energies and electronic energy levels can be determined.

II.3.5. Fourier Transform Infrared Spectroscopy (FTIR)

The FTIR is mostly used to identify chemicals that are either organic or inorganic. We can also use it to get information of some compounds of an unknown mixture. The FTIR can be applied to the analysis of solids, liquids and gases. Today, the FTIR is computerized and it has become more sensitive than the other dispersive instruments. The FTIR not only identify chemicals but also identify the types of chemical bonds (functional group). To get absorption spectrum of material it absorbs the wavelength of light. By interpreting the IR absorption spectrum, we can able to determine the chemical bonds in the molecule. We can obtain unique FTIR spectra of pure compounds like a molecular fingerprint. The spectrum of unknown materials can be identified by comparison to a library of known compounds. West coast analytical service (WCAS) has several IR spectral libraries including online computer libraries. Schematic diagram of FTIR is as shown in Figure II.10.

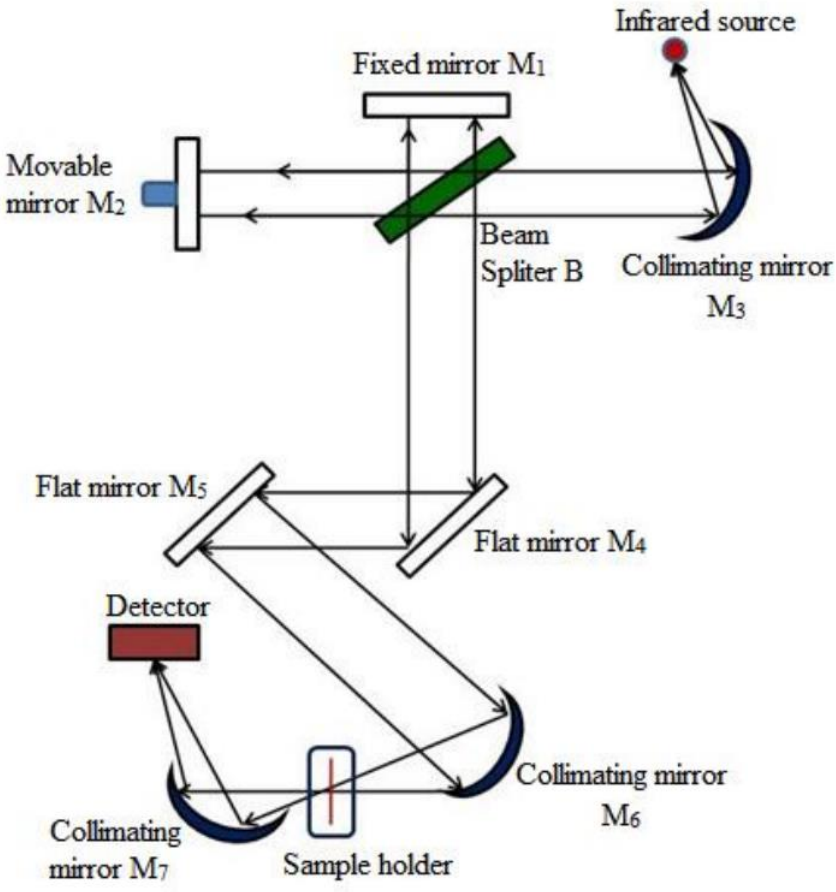

Figure II. 10. Schematic diagram of a Fourier transform infrared spectrometer [124].

A parallel beam of infrared radiation is directed from the source to the interferometer that split by beam splitter (B) and directed towards mirror M_1 and M_2. The beam splitter plate is coated by transparent material, which reflects 50 % of radiation falling on it. Hence, half of the radiation reflects and goes to the mirror M_1 while remaining half to M_2. Both splitted beams return from both these mirrors (M_1 and M_2) along same path and recombine to form a single beam at the beam splitter. The recombined beam interferes and produce fringes relative phase of the recombined beams determines whether the interference will be constructive or destructive. Such signals are recorded and plot a transmittance spectrum [124].

II.3.6. UV-Visible spectroscopy

Ultraviolet-visible spectrophotometer involves the spectroscopy of photons in the ultraviolet region (200–400 nm) and visible region (400–800 nm). It is a type of absorption spectroscopy in which the excitation of the electrons takes place from ground state to excited state while fluorescence measures transitions from excited state to ground state. The method is most often used in a quantitative way to determine concentrations of an absorbing species in sample using the Beer-Lambert law. The principle involved in UV-VIS Spectroscopy states that, when a beam of monochromatic light is passed through a homogeneous medium of an absorbing substance, the rate of decrease in intensity of radiation with respect to thickness of the absorbing medium is directly proportional to the intensity of incident radiation as well as the concentration of the medium.

$$I = I_0 . \exp(-\alpha d) \tag{II.9}$$

where α is the absorption coefficient, d is the thickness of the film, I_0 and I are the intensity of the incident and the transmitted beams, respectively.

The absorption coefficient (α) can be calculated using the following expression:

$$\alpha = \frac{1}{d} \ln\left(\frac{100}{T(\%)}\right) \tag{II.10}$$

where $T(\%)$ is the transmittance (quantity of the transmitted light), and can be directly measured by:

$$T(\%) = \frac{I}{I_0} \times 100 \tag{II.11}$$

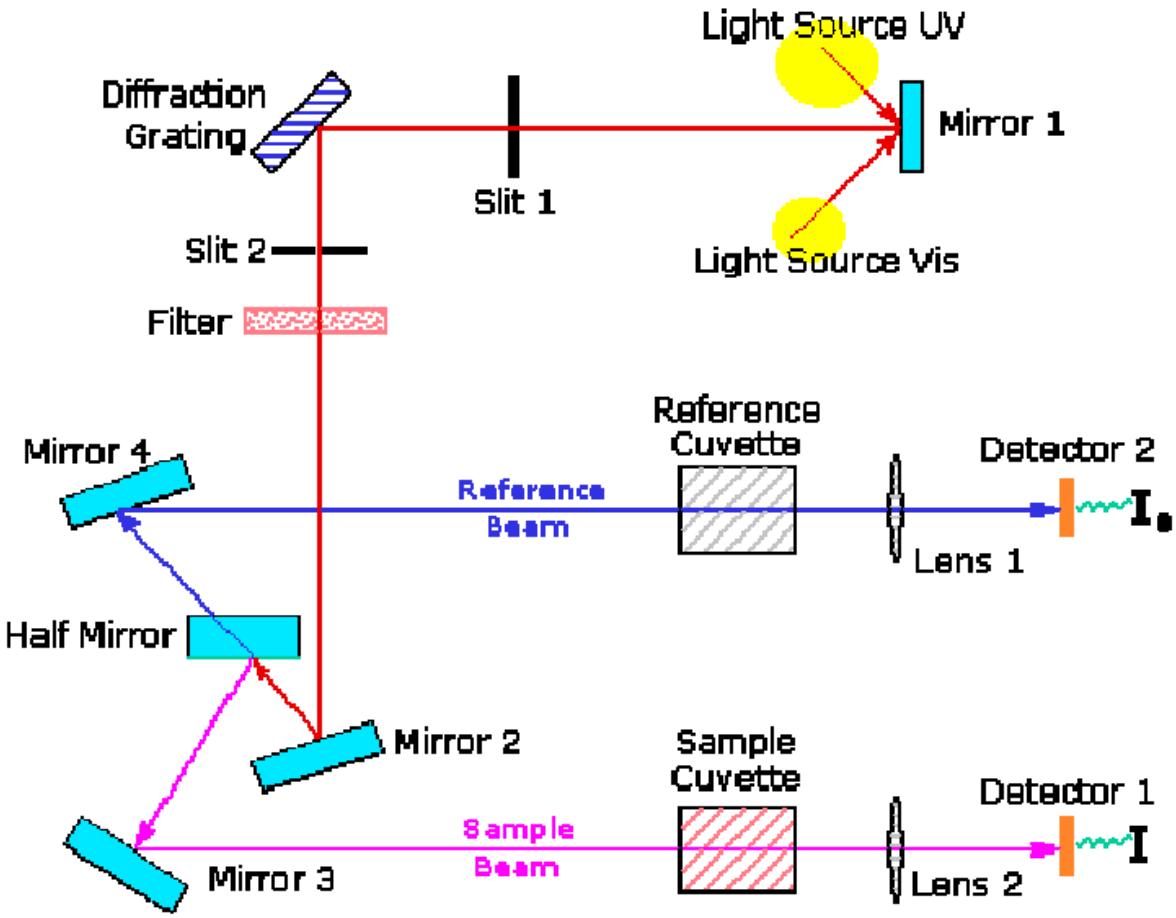

Figure II. 11. Schematic representation of UV-Visible Spectrophotometer [125].

a) Optical band gap (E_g)

The fundamental absorption is related to the band-to-band transitions in a polycrystalline semiconductor, i.e., to the excitation of an electron from the valence band to the conduction band. Therefore, the fundamental absorption can be used to determine the energy gap of the semiconductor. The optical band gap of films can be estimated using Tauc's formula [126]:

$$(\alpha h\nu)^2 = A(h\nu - E_g) \qquad \text{(II.12)}$$

where α is the absorption coefficient, A is a constant (independent of photon energy ($h\nu$)), h is the Planck constant and E_g is the optical band gap. The values of the optical band gap are obtained by extrapolating the tangential line of the data to the abscissa axis in the plot of $(\alpha h\nu)^2$ as a function of $h\nu$ as shown in Figure II.12.

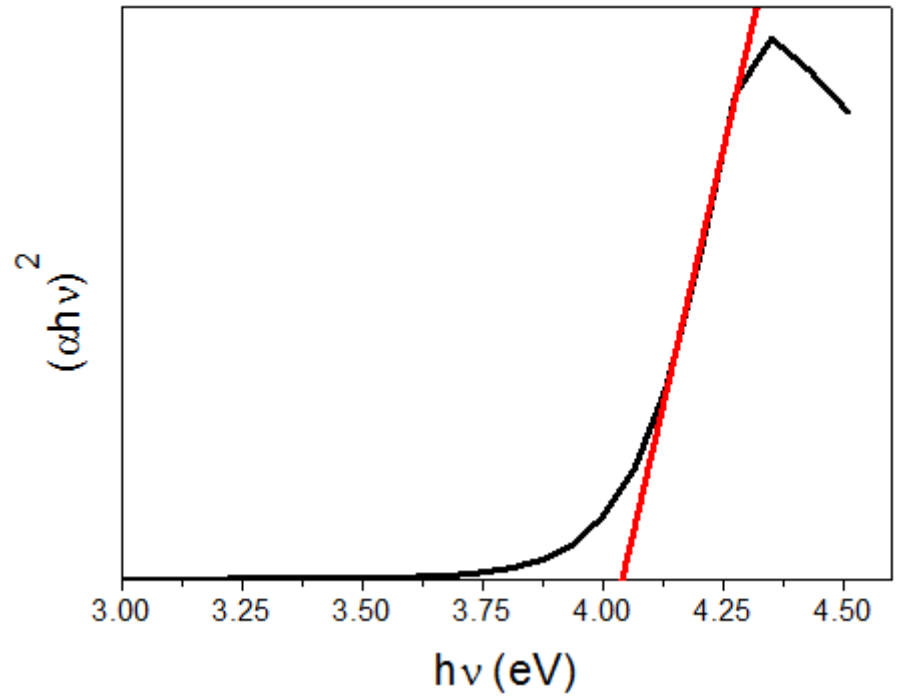

Figure II. 12. Determination of the band gap (E_g).

b) Urbach energy (E_u)

Urbach energy is usually used to describe the width of the localized states in the band gap (but not their positions). Pankove [127] has shown that the value of E_u is related to the impurity concentration. However, Redfield [128] has shown that all defects (point, line and planar defects) lead to local electric fields that cause band tailing. Thus, the Urbach energy can be considered a parameter that includes all possible defects. The relation between the Urbach energy and absorption coefficient is described by [129]:

$$\alpha = \alpha_0 exp\left(\frac{h\nu}{E_u}\right) \quad \text{(II.13)}$$

where α_0 is a constant and E_u is Urbach energy.

By drawing $ln(\alpha)$ versus $h\nu$ we can determine E_u value as the reciprocal of the linear part slope (Figure II.13):

$$ln(\alpha) = ln(\alpha_0) + \frac{h\nu}{E_u} \quad \text{(II.14)}$$

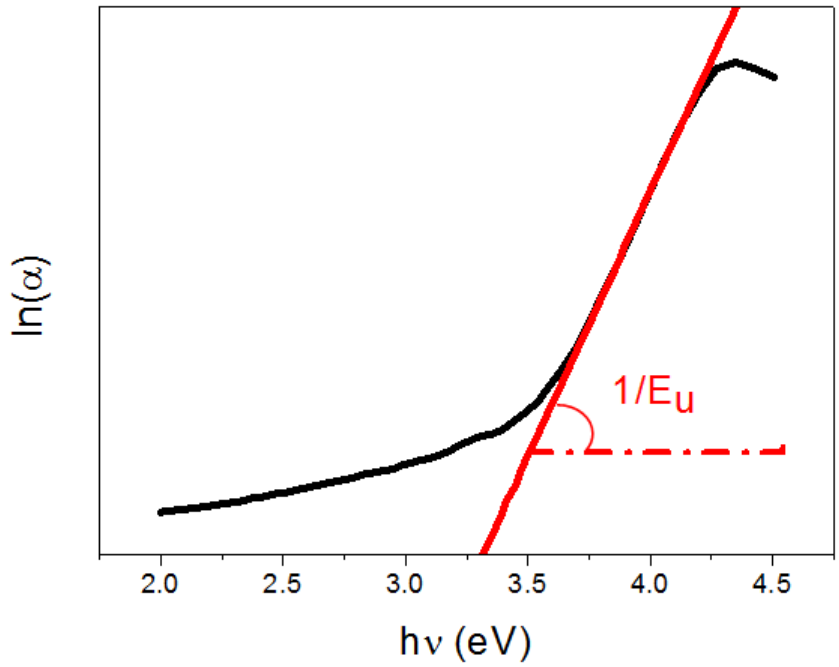

Figure II. 13. Determination of Urbach energy (E_u).

c) Refractive index (n)

The refractive index (n) was determined from the reflectance (R) data using [130]:

$$n = \frac{(1+R)^{1/2}}{(1-R)^{1/2}} \quad \text{(II.15)}$$

d) Extinction coefficient (k)

The extinction coefficient (k) of films is related to the absorption coefficient α through the following relation [131]:

$$k = \frac{\alpha\lambda}{4\pi} \quad \text{(II.16)}$$

e) Dielectric constant

The real (ε_1) and the imaginary (ε_2) parts of dielectric constant are determined by the relations bellow [132]:

$$\varepsilon_1 = n^2 - k^2 \quad \text{(II.17)}$$

$$\varepsilon_2 = 2nk \quad \text{(II.18)}$$

where λ is the wavelength, ε_1 and ε_2 are the real and imaginary parts of the dielectric constant, respectively.

II.3.7. Four point probe method

The four point probe method has proven to be a convenient tool for the resistivity measurement of small size (of the order of mm) specimen. This method is applicable when the distance between the probes is small compared to the smaller dimension of the sample, and provided none of the probe is too close to an edge of the sample. The arrangement of four point

probes is shown in Figure II.14:

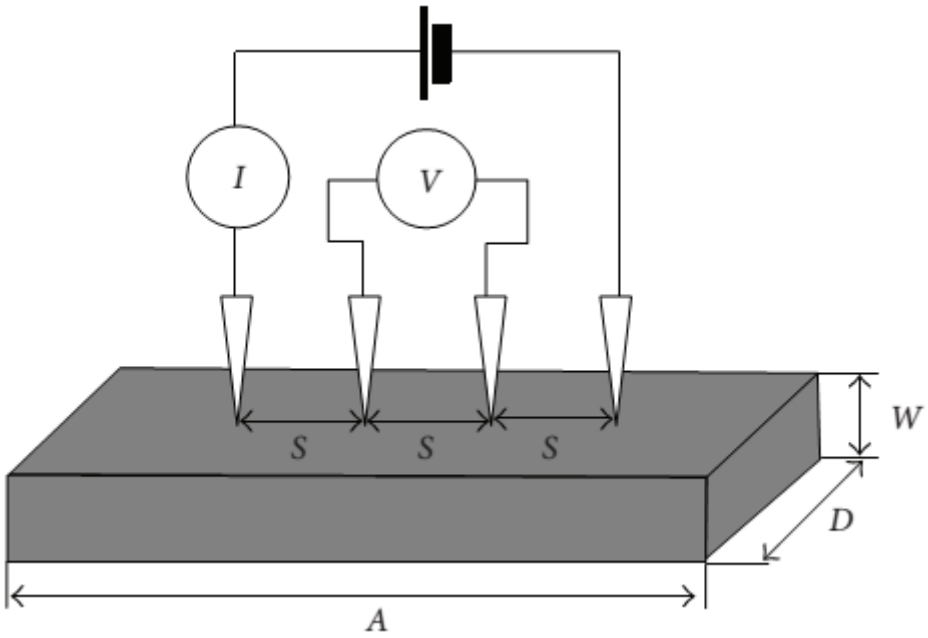

Figure II. 14. Schematic diagram of test circuit for measuring bar specimen resistivity with the four-point probe method [133].

In the case of a four point probe on a sheet, the two outside current points represent the dipole. Therefore, the resistivity in this case can be given by [134]:

$$\rho = \frac{V_D}{I} 2\pi S \qquad \text{(II.19)}$$

Here, the distance between all the four points is equal. I is the current flowing through the sample, V_D is produced voltage across two inner points and S is the distance between the adjacent points. If the distance between contact points is not equal and it is given as S_1, S_2 and S_3 respectively, then the resistivity is given as:

$$\rho = \frac{V}{I}\left[\frac{2\pi}{\left(\frac{1}{S_1}+\frac{1}{S_3}-\frac{1}{S_1+S_2}-\frac{1}{S_2+S_3}\right)}\right] \qquad \text{(II.20)}$$

Where V is the floating potential difference between the inner probes, and I is the current through outer pair of probes.

Conductivity, denoted by σ, can be determined from sheet resistance data according to the definition of resistivity (ρ) [135]:

$$\sigma = \frac{1}{\rho} \qquad \text{(II.21)}$$

Chapter III: Effect of molar concentration on indium oxide thin films properties

The precursor solute concentration is one of the important process parameters that determines the indium ion concentration and hence the film growth, structure and characteristics. So, the influence of the precursor solute concentration on the In_2O_3 film characteristics has been studied with a view to optimize the solute concentration to obtain films with the best possible characteristics.

III.1. Experimental details

III.1.1. Preparation of In_2O_3 films

Indium oxide thin films were prepared by sol gel spin coating method on glass substrates using indium (III) nitrate hydrate [$In(NO_3)_3.xH_2O$], absolute ethanol (C_2H_6O) and acetylacetone ($C_5H_8O_2$) as precursor, solvent and stabilizer, respectively. The substrates were cleaned by rinsing them with soap solution, acetone and alcohol for 5 min, then rinsed with distilled water and dried to remove contaminants. The volume ratio of acetylacetone to ethanol was maintained at 1:10. Five different precursor concentrations from 0.05 to 0.25 M were prepared by taking different amounts of indium (III) nitrate hydrate into a fixed volume of ethanol. The solutions were then stirred for 2 h using a magnetic stirrer at 50 °C and they were aged for 48 h at room temperature. The prepared solutions were deposited on glass substrates and rotated for 30 s at 4000 rpm using a spin coater (bought from Holmarc) to get well coated films. To dry the films, the samples were placed in furnace for 10 min at 250 °C. The spin coating process was repeated six times to achieve the desired thickness. After that, the annealing process was carried out at 500 °C for 2 h to obtain good crystalline films.

III.1.2. Films characterization

The prepared films were characterized by an X-ray diffractometer (X'PERT PRO) to define the crystallite state and structural properties, scanning electron microscope (SEM) to analyze the surface morphology and energy dispersive X-ray (EDX) (attached to SEM) to evaluate films elemental composition. UV-Visible spectrophotometer (Perkin Elmer LAMBDA 950 UV/VIS) to investigate the optical properties (gap energy, Urbach energy, refractive index, real and imaginary parts of dielectric constant), fourier transform infrared (FTIR) spectrometer (BRUKER VERTEX-80V) was used to obtain information about the chemical bonding in In_2O_3 films, photoluminescence (PL) spectrometer (Perkin Elmer LS 55) to detect luminescence regions and defect types. Four probe method to estimate the electrical conductivity (σ).

The overall process used for the preparation and characterization of In_2O_3 thin films based on the sol gel spin coating method is shown in Figure III. 1:

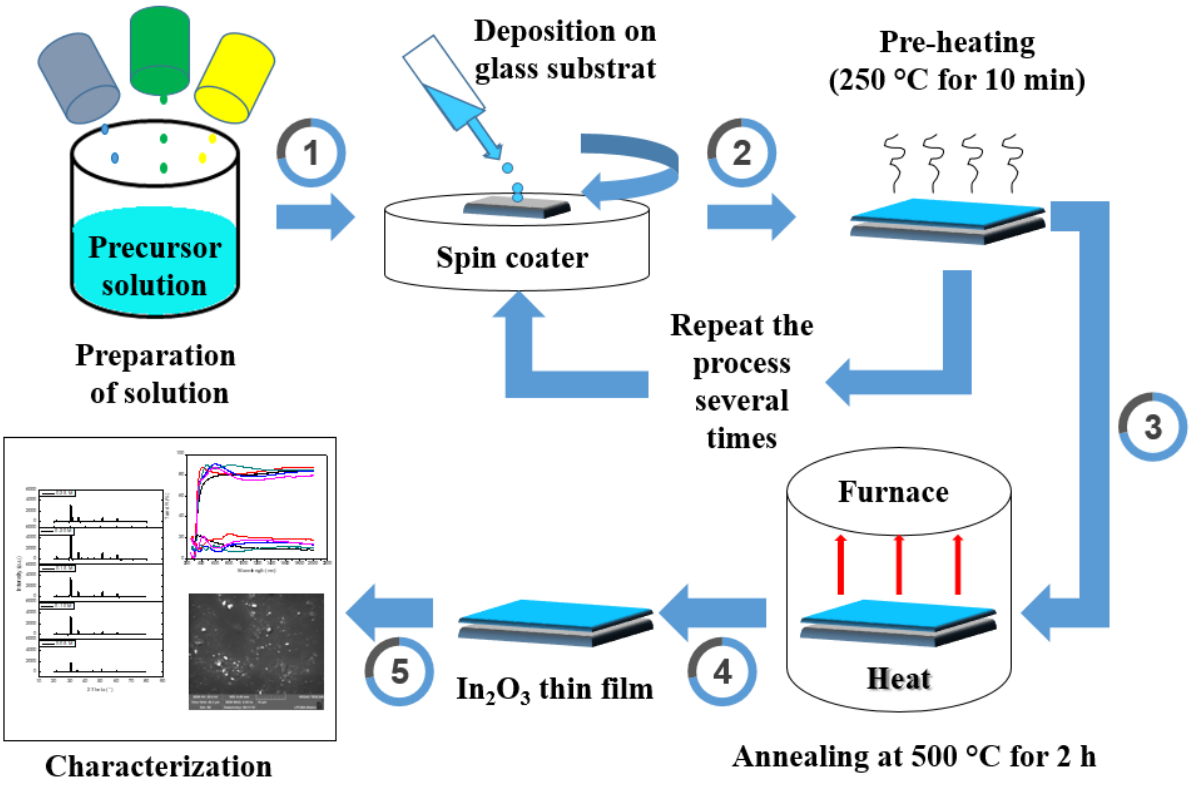

Figure III. 1. Steps of thin film preparation and characterization in sol gel spin coating process.

III.2. Results and discussion

To investigate the adhesion strength, a simple scotch tape test was performed on In_2O_3 coated films on the glass substrates. At room temperature, the scotch tape was set on the coated surfaces. The tape was then peeled by a pulling action. After the peeling of the tape, the coated films have not been removed at all confirming the good adhesion of In_2O_3 films to the substrates.

III.2.1. Film thickness study

The thickness (t) of In_2O_3 thin films is calculated using the weight difference method used by Yahmadi et al. [136]:

$$t = \frac{m}{\rho.A} \qquad \text{(III.1)}$$

where m is the mass of the film (expressed in gram), ρ is the density of the In_2O_3 in the bulk form ($\rho = 7.18\ g/cm^3$) and A (cm^2) is the area of the glass substrate.

The Variation of the film thickness (t) of the In_2O_3 thin films with molar concentration is given in Figure III.2. The figure shows that the film thickness increases almost linearly with the molar concentration. This increase with the molar concentration can be attributed to that the augment of In^{3+} ions in the substrate surface leading to an increase in the electrostatic interaction between indium (In^{3+}) and oxygen (O^{2-}) ions, which in turn enhanced the probability to form In_2O_3 phase

and caused an improvement in the film thickness. Similar thickness variation was reported by Rao et al. [137]. However, according to Langlet [138] and Lau et al. [139] there will be a threshold value of film thickness when the precursor concentration is further increased (above 0.55 M) as the film will crack when it is too thick and this condition is due to the capillary forces induced by post-deposition solvent evaporation.

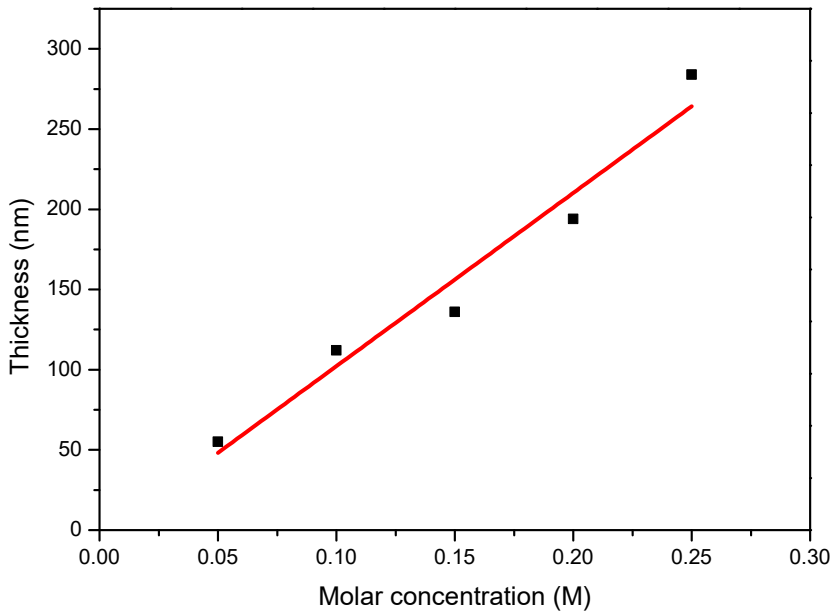

Figure III. 2. Variation of the film thickness (t) of In_2O_3 films with molar concentration.

III.2.2. Structural study

The structural analysis of the prepared In_2O_3 thin films has been carried out using their XRD spectra. The XRD spectra have been obtained using CuKα radiation of wavelength 1.5406 Å in the 2θ range of 20°-80°. The XRD spectra of In_2O_3 thin films deposited using different precursor concentrations of 0.05 M, 0.10 M, 0.15 M, 0.20 M and 0.25 M are displayed in Figure III.3. The presence of several peaks in the XRD spectra (Figure III.3) shows that all the films are polycrystalline in nature. The figure shows that all the films give rise to well defined peaks corresponding to (211), (222), (400), (440) and (622) planes of crystalline In_2O_3 with body centered cubic (BCC) structure [Joint Committee on Powder Diffraction standards (JCPDS) data card No. 06-0416] with preferential orientation along (222) peak. The growth along the (222) plane is due to the low free surface energy found in this direction for In_2O_3 cubic structure [140]. The inter-planar distance (d_{hkl}) for the In_2O_3 phase in all these films works out to be 2.910-2.920 Å which is less than the standard value of 2.921 Å given for In_2O_3 in the JCPDS data card. The figure further shows that the XRD spectrum of the film grown with the highest molar

concentration of 0.25 M contains new growth direction corresponds to (321) plane with slightly small decrease in intensity of previously mentioned planes. Khan et al. [141] have reported the formation of (321) plane in their spin coating deposited In_2O_3 films on glass substrate. Logacheva et al. [142] have suggested that the formation of (321) plane can be attributed to the modification and deviation from In_2O_3 cubic symmetry; which means that the composition (stoichiometry) of the In_2O_3 films is changing as a function of molar concentration.

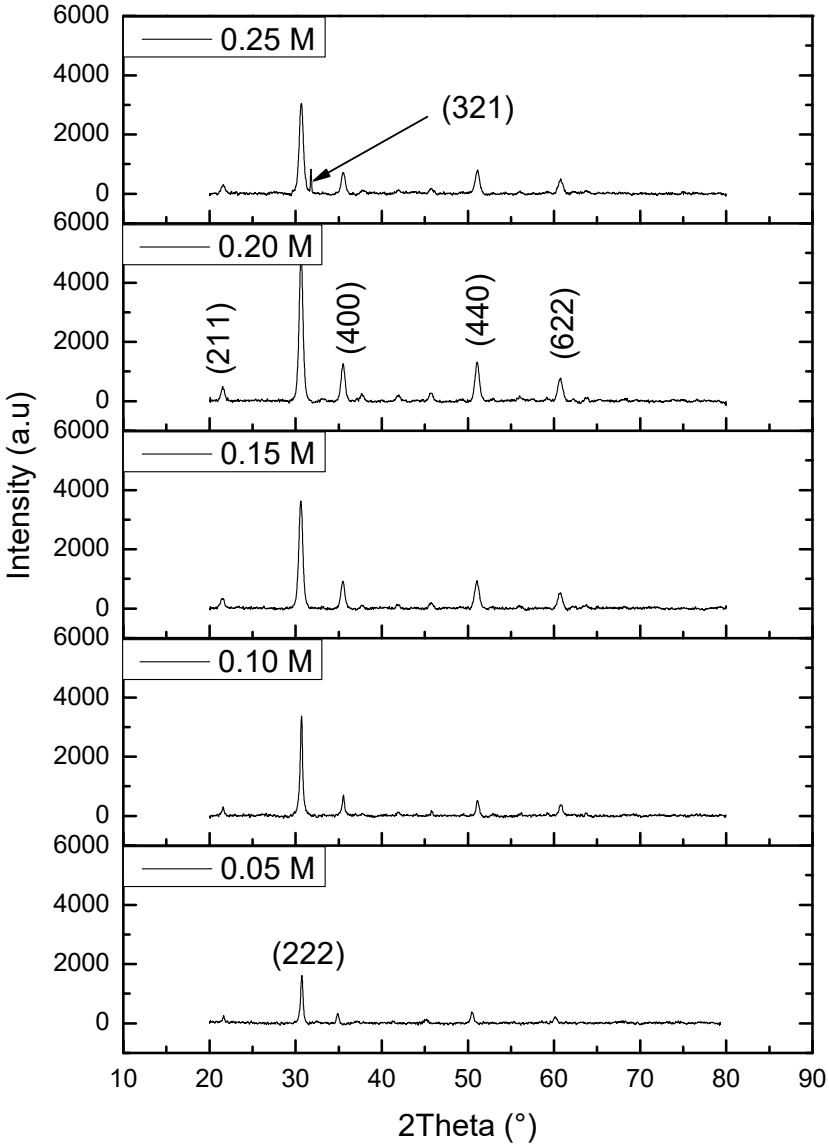

Figure III. 3. XRD patterns of In_2O_3 thin films at different molar concentration.

From the figure, it can be noted that the diffraction intensity of the In_2O_3 phase increases with the molar concentration up to a molar concentration of 0.20 M due to the increase in the film thickness. This result implies that the crystallinity of the In_2O_3 phase improves with the increase

in molar concentration. Similar conclusions have been found by Jothibas et al. [143] from their studies on sprayed In_2O_3 thin films. However, it can also be seen from the figure that the diffraction intensity of In_2O_3 gets reduced when the molar concentration is further increased to 0.25 M even though the film thickness has increased enormously. This means that the crystallinity of the In_2O_3 phase drops when the molar concentration is increased to 0.25 M, inspite of the film thickness increasing sharply. This result is rather surprising. The film contains a new growth direction along (321) plane. So, it is reasonable to take that the appearance of (321) plane in the 0.25 M film may be the cause for the reduced crystallinity of In_2O_3 film observed at this stage. Similar reduction in the crystallinity of In_2O_3 has been reported by Metaferia et al. [144] in their studies on indium oxide films. The reduction indicated the occurrence of restructuring of the In_2O_3.

Table III. 1 summarizes the structural parameters: Bragg's angle (2θ) and the interplanar distance (d_{hkl}) for the predominant (222) peak. The interplanar distance for (222) plane of the In_2O_3 films is found to be smaller than the standard value of $d = 2.921$ Å. This indicates contraction of unit cell volume which in turn reveals the presence of compressive stress in all the films [145].

Table III. 1. The structural parameters of In_2O_3 films corresponding to (222) plane.

Preferred plane (hkl)	**Molar concentration (M)**	**Standard 2θ (°)**	**The observed 2θ (°)**	**Standard d (Å)**	**The observed d_{hkl} (Å)**	**JCPDS Card No. 06-0416**
(222)	0.05	30.58	30.71	2.921	2.910	06-0416
	0.10		30.67		2.909	
	0.15		30.60		2.920	
	0.20		30.63		2.917	
	0.25		30.65		2.910	

The crystallite size and the strain of In_2O_3 films grown at different molar concentrations are shown in Figure III. 4. It is easy to note that the crystallite size and the strain have an opposite variation. The observed decrease in the crystallite size is commonly due to the augment in the internal strain [146]. Prathap et al. [147] reported that the decrease in crystallite size with increased molar concentration is attributed to the short time taken for the formation of crystallite. In addition, the decrease in the crystallite size indicates an increase in the lattice defects, which in turn enhanced internal strain and dislocation density [148] (as it was shown in Figure III.4 and Figure III.5). In the other hand, Jothibas et al. [143] from their studies on In_2O_3 thin films have obtained that the crystallite size increases with the molar concentration.

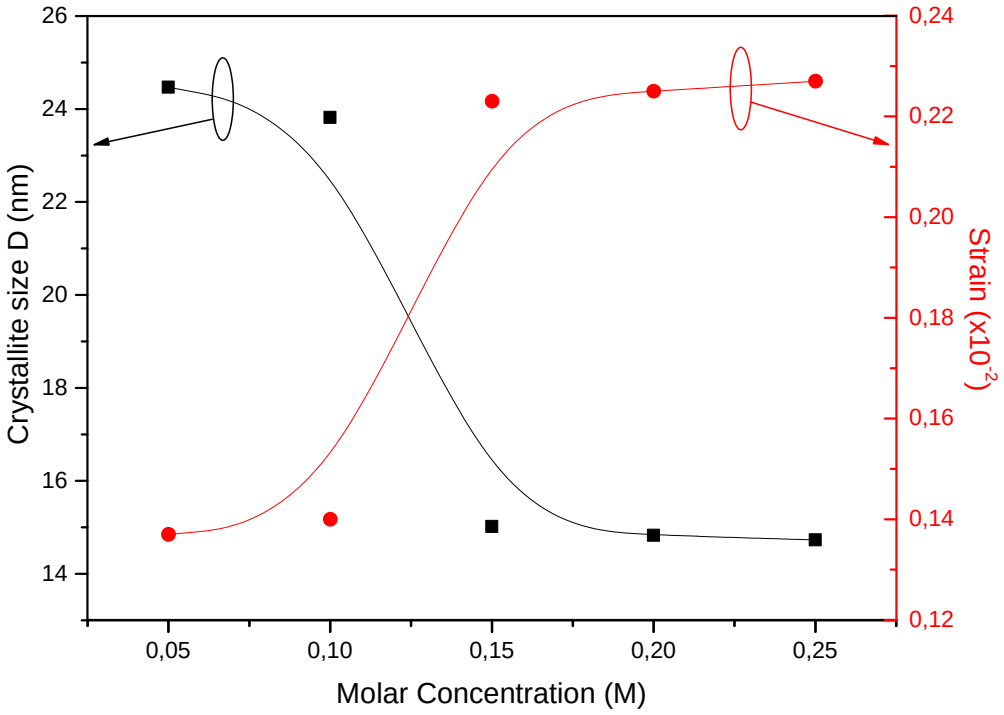

Figure III. 4. Crystallite size and the strain as function of molar concentration.

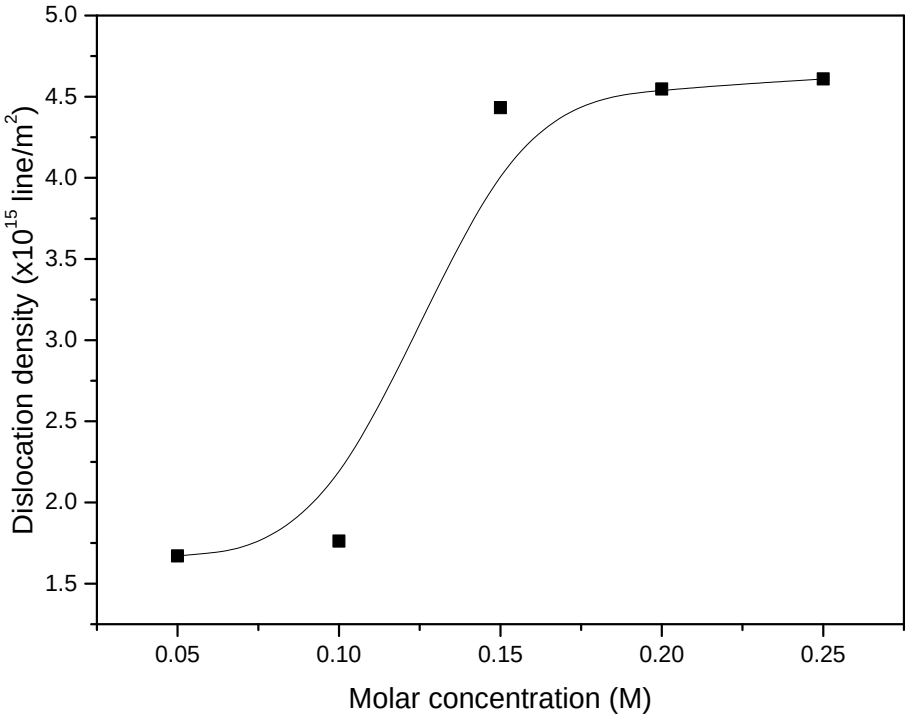

Figure III. 5. The dislocation density of In_2O_3 films.

The dislocation density of In_2O_3 films is illustrated in Figure III. 5. As may be seen below, the dislocation density was about the range of 1.6×10^{15} – 1.7×10^{15} line/m^2 at low molar concentrations, then it increased and stabilized about 4.6×10^{15} line/m^2 beyond 0.10 M. The increase in the dislocation density can be attributed to the decrease in crystallite size. Moreover, dislocations naturally become longer as dislocation lines extend to avoid micro-structural barriers that enhanced by the decrease of crystallite size. May be that is the reason of the abrupt increase of dislocation density beyond 0.10 M. This result can be confirmed by the crystallite size variation.

III.2.3. Surface morphological study

The surface morphology of films depends on the deposition technique, its parameters and it may influence mechanical, electrical and optical properties of the films. Figure III. 6 shows the scanning electron micrographs of In_2O_3 films at different molar concentrations prepared by sol gel spin coating process. It is obvious that all the films have homogenous, uniform and dense surface without any pin holes and cracks indicating that the films are well adherent to the substrates. Moreover, the film deposited at 0.25 M shows more roughness than the other films. The more roughness is probably due to a change in the surface structure of the film by the appearance of new growth in the [321] direction over the film surface, which was confirmed by XRD results.

Energy dispersive X-ray spectroscopy (EDX) is an analytical technique used for the elemental analysis of a sample. The EDX spectra of the prepared In_2O_3 films are shown in Figure III. 7. As may be seen below, all EDX spectra reveal the presence of In and O elements in the deposited films. The peaks of other elements such as Si, Na, Mg and P are attributed to constituents of glass substrate. In addition, the EDX spectra also analyzed both of the weight percentage (wt.%) and atomic percentage (at.%) of the indium and oxygen compounds (see Table III.2). As can be seen, the weight percentage and atomic percentage of In and O elements vary with the precursor molar concentrations.

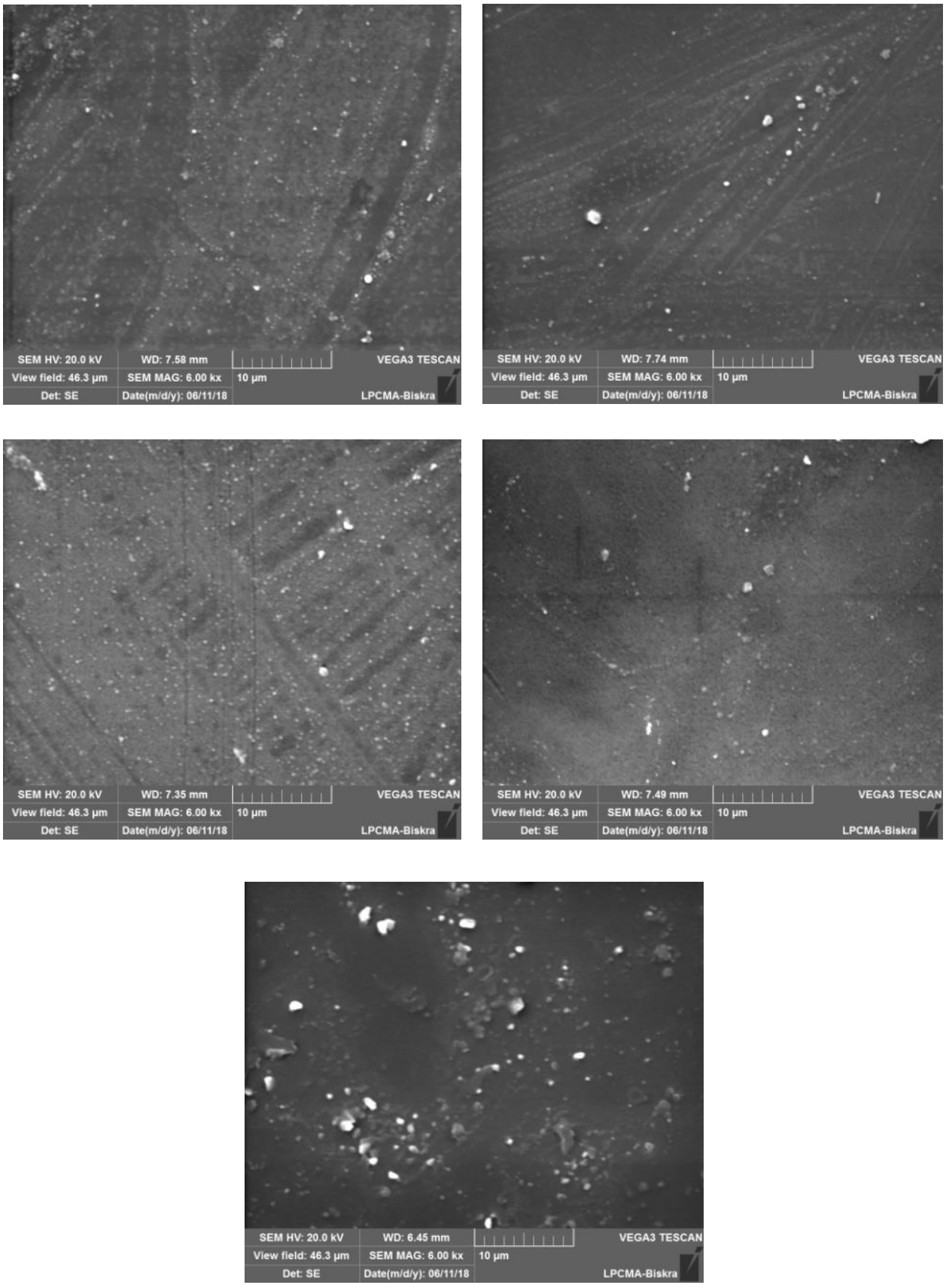

Figure III. 6. Scanning electron microscopy images of prepared In_2O_3 thin films.

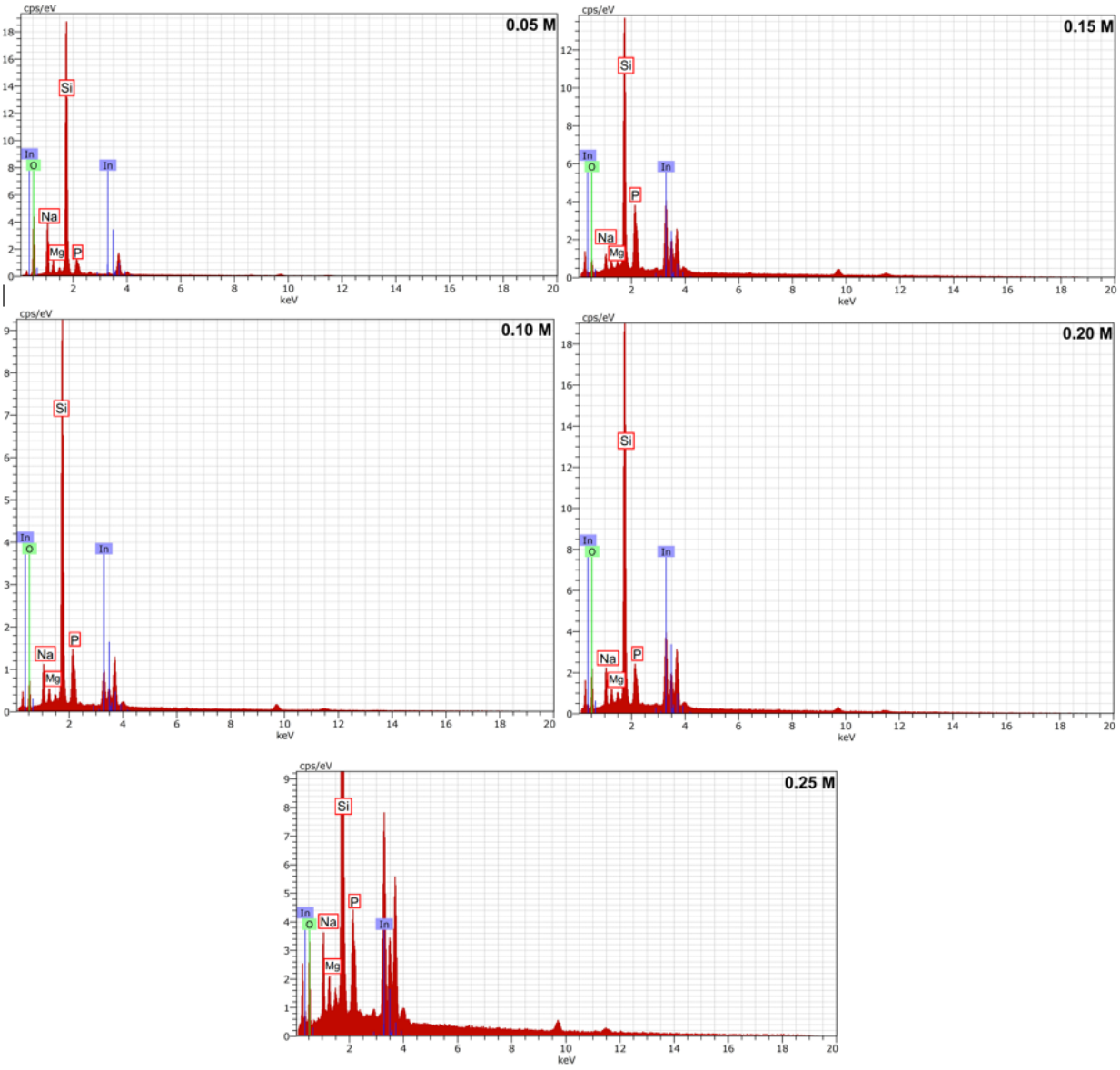

Figure III. 7. Energy dispersive X-ray (EDX) spectra of In_2O_3 films.

Table III. 2. The weight percentage (wt.%) and atomic percentage (at.%) of In_2O_3 thin films.

Molar concentration (M)	Elements			
	wt.%		at.%	
	In	O	In	O
0.05	8.78	91.22	1.32	98.68
0.10	51.02	48.98	12.67	87.33
0.15	71.52	28.48	25.93	74.07
0.20	56.52	43.48	15.34	84.66
0.25	61.49	38.51	18.20	81.80

III.2.4. Optical study

Transmittance is very important to the applications of In_2O_3 thin films and the transmission spectra provide information about their band gap and structure. The transmittance spectra depend on the chemical composition, crystal structure, energy of incident photon, film thickness and film surface morphology. For a given film, the chemical composition and crystal structure are fixed and hence in such a case the film thickness, crystallinity and surface and structural homogeneity are factors that greatly influence the transmittance of the film.

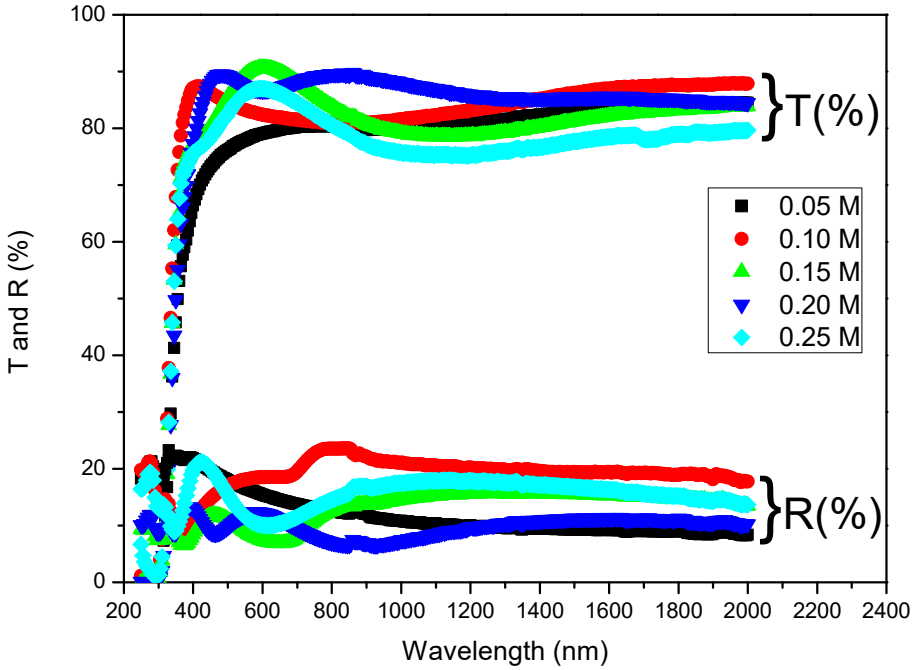

Figure III. 8. The transmittance and reflectance spectra of In_2O_3 thin films.

Figure III. 8 represents the transmittance (T) and reflectance (R) spectra of In_2O_3 thin films measured by Perkin Elmer LAMBDA 950 UV/VIS spectrophotometer in the wavelength range from 250 to 2000 nm. It is found that the In_2O_3 films deposited at different molar concentrations exhibit a high optical transparency about 80-90 % in the visible range while the reflectance is found inside a confined interval 10-25 %. Most of the samples show the presence of interference fringes in both reflectance and transmission spectra in the visible region; this can be attributed to the homogenous and smooth surface of the films [149]. Shinde et al. [150] suggested that interference patterns in reflectance and transmittance show that the films are specular to a great extent. In general, transmittance of the In_2O_3 films increases in the visible region (400 – 800 nm) with increase of precursor molar concentration from 0.05 M to 0.20 M. Furthermore, the transmittance spectra reveal a strong absorbance for all films in the range between 290 and 380 nm due to the excitation and the transition of electrons from the valence band (VB) to the

conduction band (CB). This last phenomenon is very important characteristic for a semiconductor corresponding to the optical band gap energy (E_g).

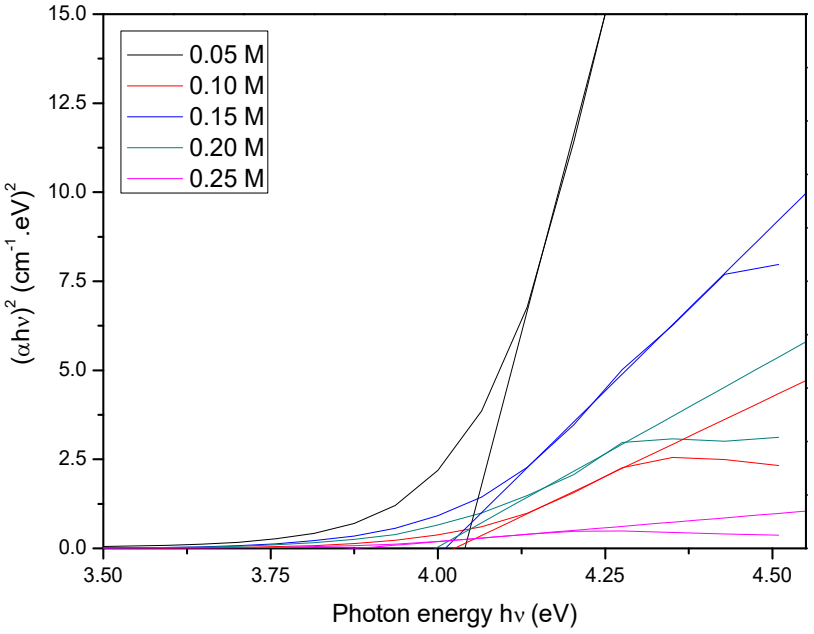

Figure III. 9. Plots of $(\alpha h\nu)^2$ against hν of In_2O_3 films.

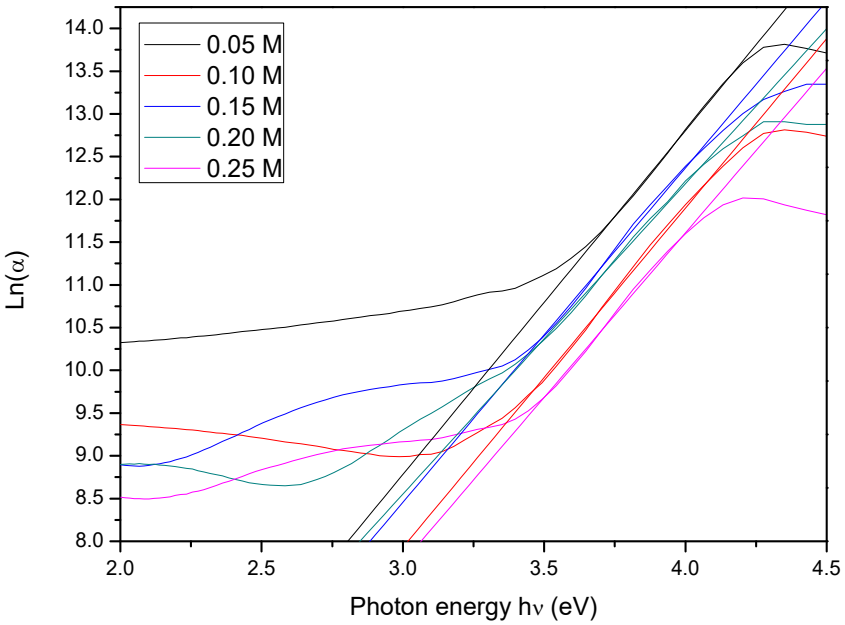

Figure III. 10. Ln(α) vs hν plots of the films.

Consider Figure III. 9, which plots $(\alpha h\nu)^2$ against hν for In_2O_3 films prepared at several precursor concentrations. The optical band gap (E_g) is determined by the extrapolation of the

linear region of the curves to intersect at hν axis. The Urbach energy (E_u) is the band tail width and characterizes the disorder in film network, it is estimated from the plots of Ln(α) vs hν (Figure III. 10) by taken the inverse of the slope of the linear part.

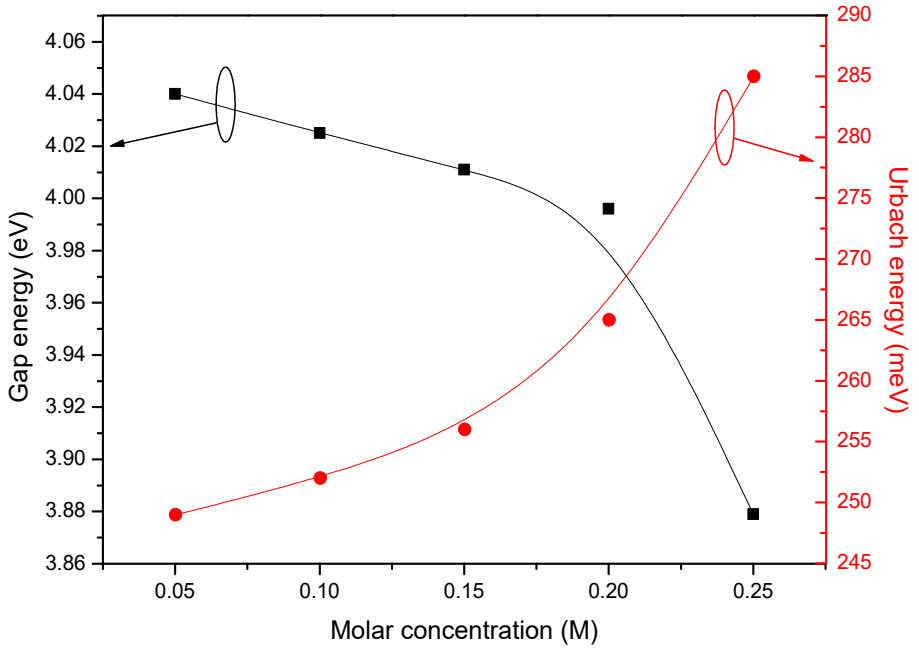

Figure III. 11. Optical band gap and Urbach energy of In_2O_3 films.

The variations of the optical band gap energy and Urbach energy of In_2O_3 films at different molar concentration are given in Figure III. 11. Typically, in polycrystalline semiconductors, the energy band gap can be impacted by the quantum size effect [151], modification in the preferred orientation of the film [152], disorder and dislocation density at the grain boundaries [153]. From this figure it can be seen that the energy band gap was narrowing (from 4.04 to 3.88 eV) with increasing molar concentration. Whereas, the width of the band tails, generally known as Urbach tails, was determined to measure the structural disorder. The estimated Urbach tail energies increased from 249 to 285 meV with the increase of precursor concentration. The reduction of energy band gap with the increase of precursor concentration could be owing to the constitution of localized states in the band gap region. These states might be elicited in the band gap on account of the structural disorder owing to the oxygen vacancy. The high concentration of impurity states stimulates the band structure to dislodge, resulting in a prolonged tail extending into the energy band gap [154]. According to Ali [155], increasing molar concentration causes increase in the density of charges and then every electron is effectively surrounded by an exchange and correlating hole that lowers the energy level of the electrons, and the conduction band is shifted downwards. Moreover, the calculated band gap of prepared In_2O_3 films is higher

than that of In_2O_3 bulk. This is because of the quantum confinement effect due to small crystallite size of the polycrystalline In_2O_3 films [156].

The variation of extinction coefficient (k) with the wavelength (λ) for the grown films at various molar concentrations is shown in Figure III. 12. In these spectra, all the films have maximum k in the ultraviolet region, almost constant and minimum in the visible and near infrared regions. Moreover, extinction coefficient shows high values that reach to 2.25 for 0.05 M in the low wavelengths (<350 nm). Whilst, in the high wavelengths (>350 nm), the extinction coefficient is very low (less than 0.25). The minimum of extinction coefficient in in the visible and near infrared regions established that the films are highly transparent. The rise and the fall in the extinction coefficient (k) are directly related to the absorption of the light [143].

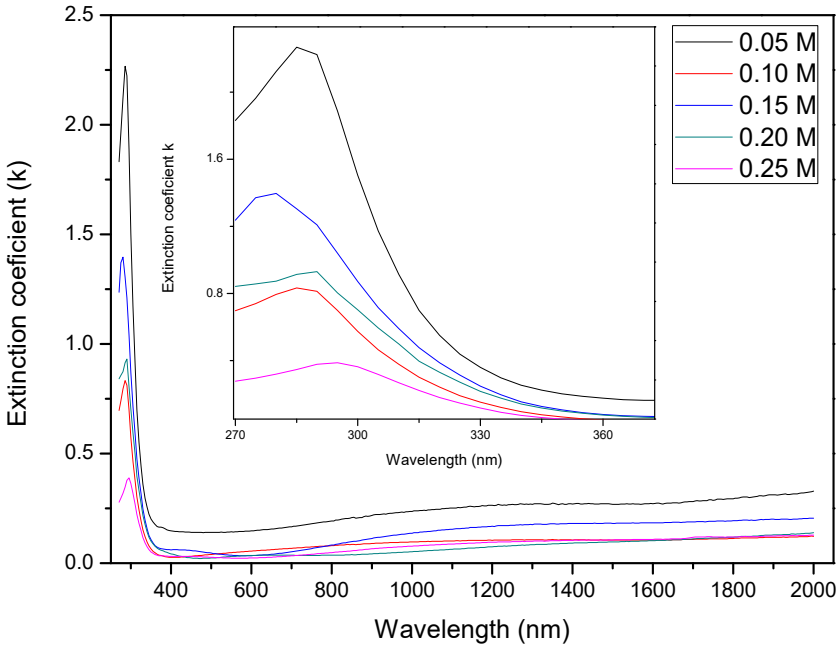

Figure III. 12. Extinction coefficient as a function of wavelength for In_2O_3 films.

The plots of refractive index (n) as function of the wavelength (λ) for In_2O_3 films deposited at different molar concentrations are given in Figure III. 13. From these spectra, it can be seen that n values of In_2O_3 films vary in the range of 1.7-2.9. All films show that the maximum of refractive index (n) is in the UV-Visible region except the films deposited at 0.10 and 0.15 M, which had the maximum refractive index in the near IR region. Panneerdoss et al. [157] said that the maximum refractive index in the near IR region is possibly due to the stoichiometric form of the films. Generally, it is found that the refractive index of all films decreases with increase in molar concentration. Li et al. [158] explained that by the increase in the carrier concentration.

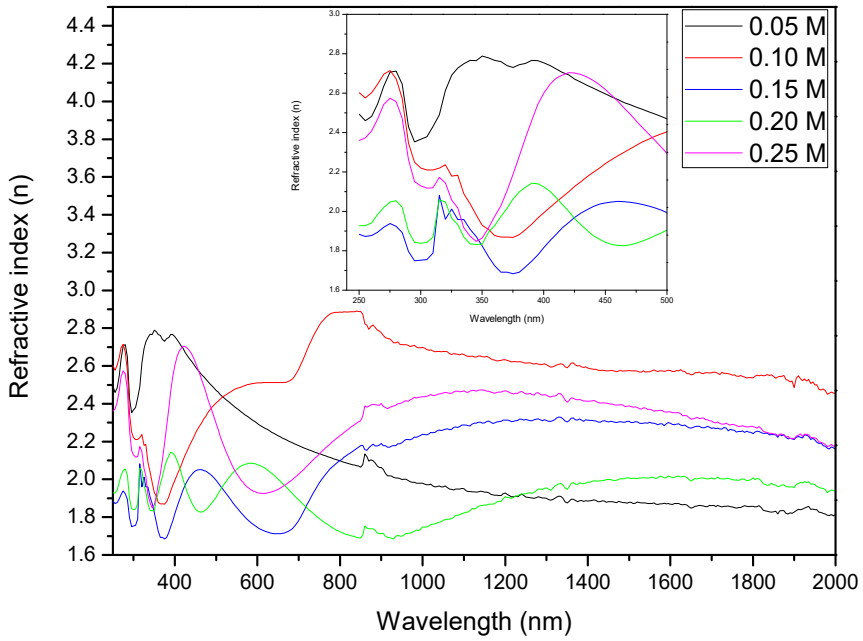

Figure III. 13. The refractive index (n) of In_2O_3 films.

Figure III. 14 presents the variation of the real (ε_1) and imaginary (ε_2) parts of the dielectric constant with various molar concentrations. The values of ε_1 and ε_2 as function of wavelength are around of 1-8.5 and 0.8-12, respectively. Most studies reported that using low solution molar concentrations enhance the dielectric response of thin films due to the crystallite size modification, porosity and preferred orientation [159,160].

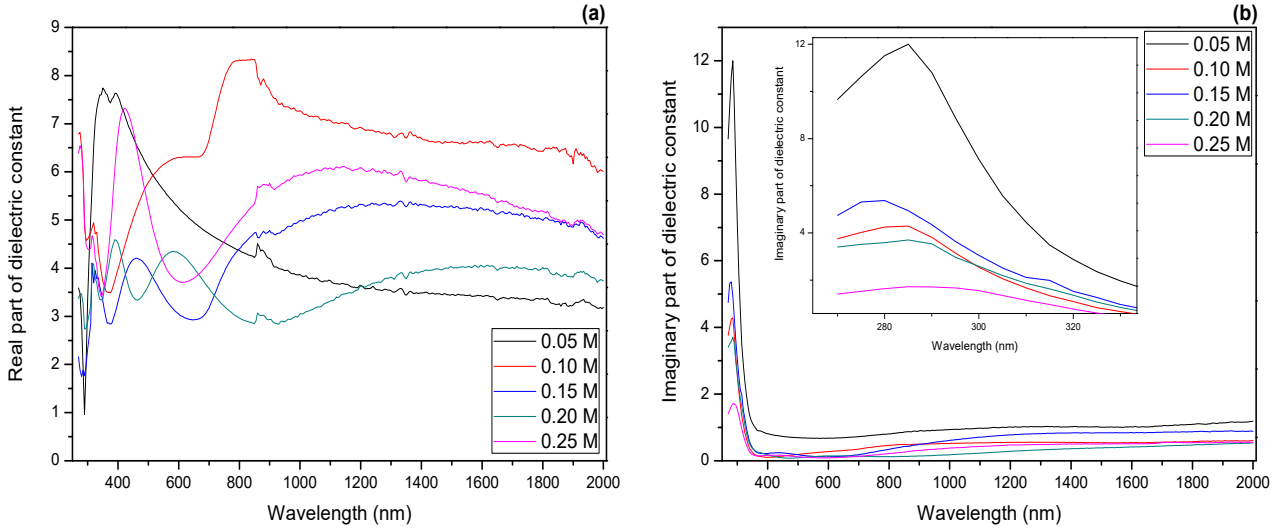

Figure III. 14. The variation of: (a) the real and (b) the imaginary parts of dielectric constant.

Figure III. 15 shows the room temperature photoluminescence (PL) spectra of In_2O_3 films grown at various molar concentrations. Photoluminescence spectra show mainly three emission peaks (ultraviolet, blue and green). The broad ultraviolet luminescence peak 310-420 nm is assigned to the near band edge (NBE) emission, which is attributed to the free exciton recombination between the conduction band (CB) and the valence band (VB) [161]. As can be seen, a decrease observed in the broad ultraviolet emission peak, this could be due to the increased number of trap states in the mid-band gap region for non-radiative transition [162]. The blue emission band at 485 nm is referred to the new defect level that introduced into the band gap by the indium (In) atoms. The origin of green emission at 532 nm is generally ascribed to the deep level defects such as surface defects and singly ionized oxygen vacancies [163].

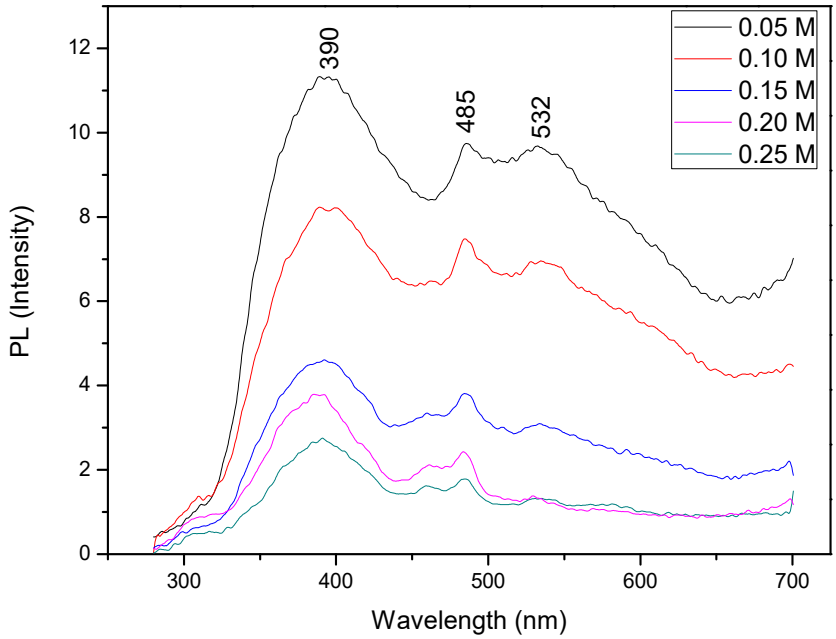

Figure III. 15. PL spectra of indium oxide thin films at various molarities.

FTIR technique is used to obtain information about the chemical bonding and the presence of certain functional groups in the films. The FTIR spectra of indium oxide films with various molar concentrations are shown in Figure III. 16. The absorption bands shown by the films at 410, 565 and 600 cm^{-1} are referred to the In–O bond [164]. Return to the heavy mass of In atoms, the In–O stretching vibration modes are usually observed in the region of 800-300 cm^{-1}. We can also recognize absorption band at 1186 cm^{-1} related to In–O–H bending vibration [165]. It is obvious that the In–O and In–O–H absorption bands intensity increases with the increase of the molar concentration. This can be attributed to the enhancement of In atoms on the substrate surface which in turn leads to an increase in the probability of forming In–O and In–O–H bonds.

However, the intensity of FTIR spectra reduced considerably for 0.25 M due to the degradation of the crystal state. These results are supported by the variation of XRD data.

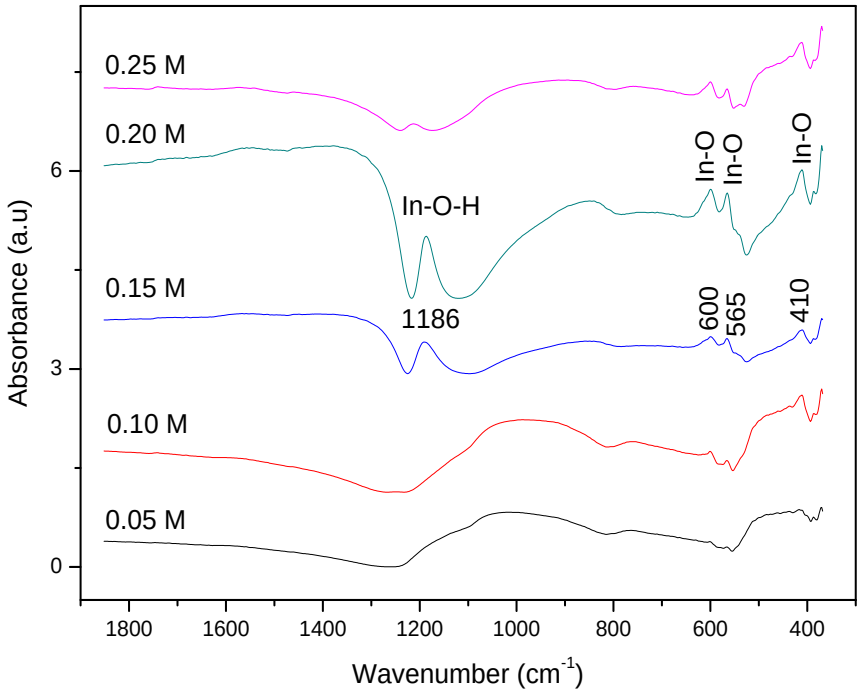

Figure III. 16. FTIR spectra of In_2O_3 films at different molar concentrations.

III.2.5. Electrical study

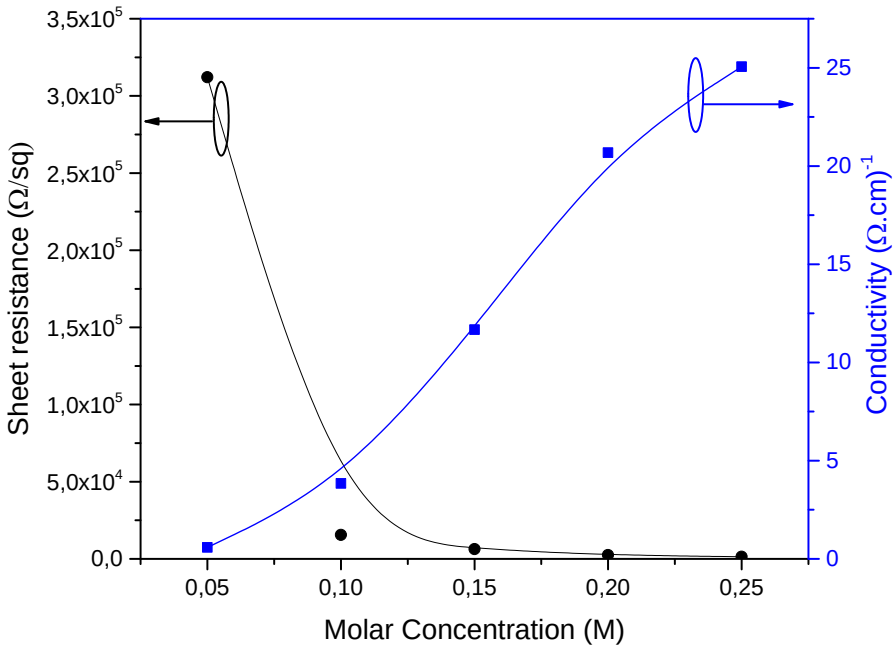

Figure III. 17. Electrical conductivity as a function of molar concentration.

The variation of electrical conductivity and sheet resistance of In_2O_3 films measured by four probe method at various molar concentrations can be found in Figure III. 17. As can be seen, the electrical conductivity of In_2O_3 films increases from 0.58 to 2.5×10^1 $(\Omega.cm)^{-1}$. Whereas, The sheet resistance decreased with increasing precursor molar concentration becomes a minimum of 1405 Ω/sq for 0.25 M. The maximum conductivity value obtained in this work is 2.5×10^1 $(\Omega.cm)^{-1}$ for the film deposited at 0.25 M. Many researchers claimed that the increase of the electrical conductivity is due to the enhancement of free carrier concentration [166]. In this work and in related references it was observed that the raise of electrical conductivity may be resulted from the interstitial indium atoms, which act as charge carrier donors to the conduction band. Moreover, the increase of the electrical conductivity of the film layers after increasing the precursor concentration could, therefore, be ascribed to the modification of properties of the grains or their boundaries. It is ascertained that for the films deposited at five different precursor concentrations, the conductivity improves as indium concentration increases. It is well known that the n-type conductivity in In_2O_3 is owing to oxygen vacancy and interstitial indium atoms, both acting as donors. Hence, it gives rise to higher carrier concentration as In and O concentration increases [154]. The investigation results of the In_2O_3 thin films grown by sol gel spin coating technique assure the stability of the film and their employability in solar cell application.

III.3. Conclusion

Indium oxide thin films with different molar concentrations have been successfully deposited by sol gel spin coating method on glass substrates. Effect of molar concentration on structural, morphological, optical and electrical properties was investigated. XRD patterns revealed that prepared films have a polycrystalline nature with strong orientation along (222) plane corresponding to In_2O_3 cubic structure. We observed an increase in the preferential growth in the (222) plane for films. Furthermore, we noticed emergence of new growth orientation for 0.25 M sample corresponding to (321) plane, which confirms the change in the composition (stoechiometry) at the film surface and the reduction of the preferential orientation. SEM images showed the homogenous and uniform distribution without any voids or cracks. The EDX spectra revealed the presence of In and O elements in the prepared films with their weight (w.%) and atomic (at.%) percentage. Films exhibited a high optical transparency that reaches up to 90 % in the visible range. In addition, we observed that the optical band gap energy (E_g) decreases from 4.04 to 3.88 eV. The decrease in PL peak intensity was indicating the increased number of trap states in the mid-band gap region for non-radiative transition. The presence of In–O and In–O–H

absorption bands was confirmed by FTIR. Electrical measurements showed that molar concentration effectively increases the electrical conductivity from 0.58 to 2.5×10^{1} $(\Omega.cm)^{-1}$. From these findings, we conclude that the prepared In_2O_3 films can be used in optoelectronic applications such as buffer layer and transparent electrodes in solar cells. Also, the sol gel spin coating technique is suitable for producing homogenous and uniform thin films with good quality.

Chapter IV: Influence of annealing temperature on indium oxide thin films properties

The annealing temperature is a parameter that influences the stoichiometry, structure and characteristics of films. Hence, the influence of the annealing temperature on the properties of In_2O_3 thin films has been investigated and the annealing temperature optimized for obtaining films with the best possible characteristics.

IV.1. Experimental details

IV.1.1. Preparation of In_2O_3 films

The indium oxide films were prepared over glass substrate using sol-gel spin coating method. We used indium nitrate hydrate as precursor, ethanol as solvent and acetylacetone as a stabilizer. The substrates were cleaned by rinsing them with soap solution, acetone and alcohol for 5 min, then rinsed with distilled water and dried to remove contaminants. To prepare (0.15 M) of In_2O_3 solution, indium (III) nitrate hydrate [$In(NO_3)_3.xH_2O$] was dissolved in a mixture of ethanol (C_2H_5OH) and acetylacetone ($CH_3COCH_2COCH_3$) with volume ratio maintained at 1:10. The mixture was stirred constantly at 50°C for 2h to yield a clear, transparent, and homogeneous solution. Then the solution was aged at room temperature for 24 h.

The aged indium oxide solutions were deposited on microscopic glass substrates by using a spin coating technique with a controlled rotation speed of 4000 rpm for 30 s at room temperature. The films dried at 250°C for 10 min to evaporate the solvent and remove organic residuals. This process was repeated six times to get well coated films with the desired thickness. Then the films subjected to annealing treatment at different temperatures: 250, 350, 450 and 550°C in a furnace under ambient air for 2 h to get well crystallized In_2O_3 films.

IV.1.2. Films characterization

The films adherence to the substrate was checked by means of the tape method. The X-ray diffraction (XRD) studies were carried out in a BRUKER–AXS type D8 diffractometer (CuKα1 radiation, 1.5406 Å). The transmittance and absorbance spectra of the films were measured by a Perkin Elmer Lambda 25 spectrometer, in the 290–1100 nm wavelength range. The resistivity was achieved by the four aligned probe method.

A schematic representation of the sol gel synthesis and spin coating procedure is shown in Figure IV.1.

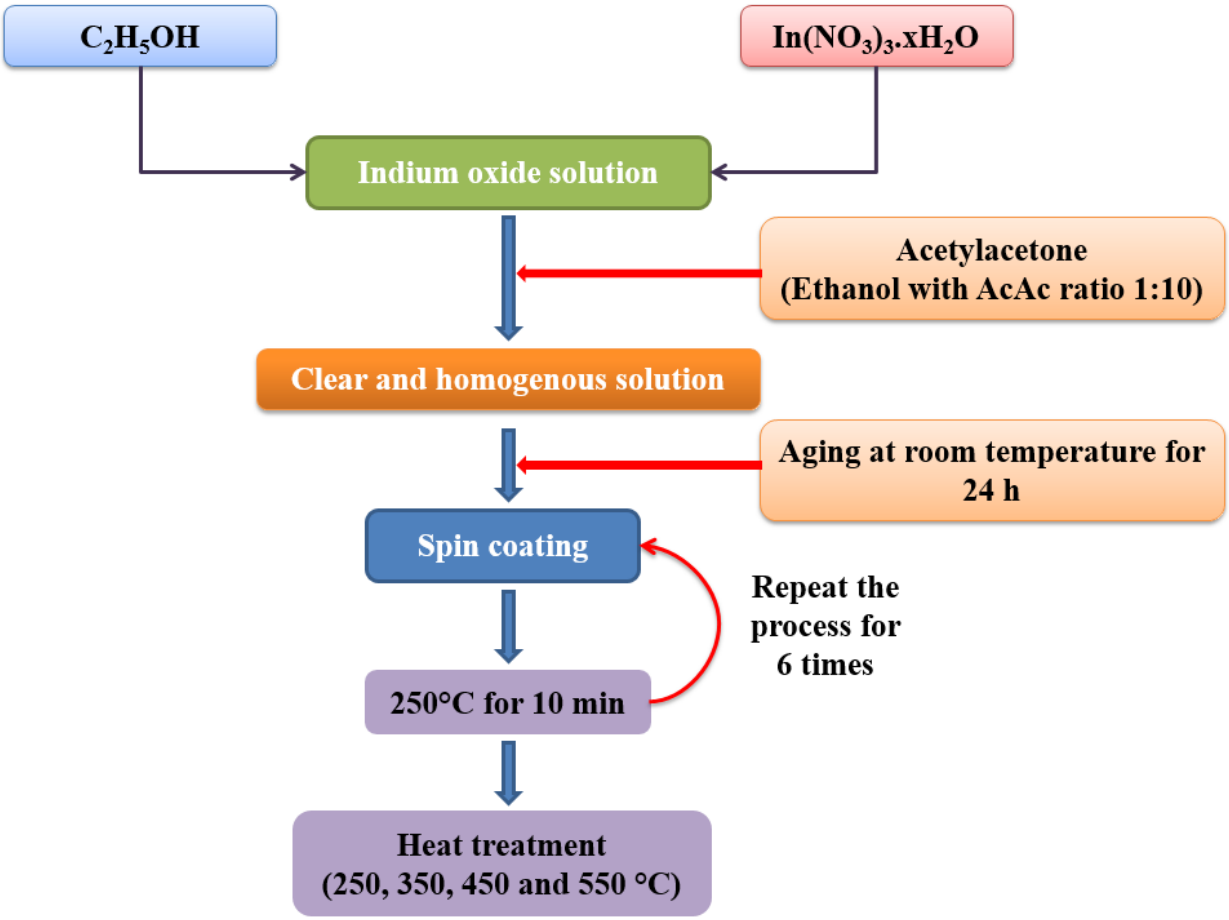

Figure IV. 1. The sol gel synthesis procedure of prepared In_2O_3 thin films.

IV.2. Results and discussion

IV.2.1. Thickness study

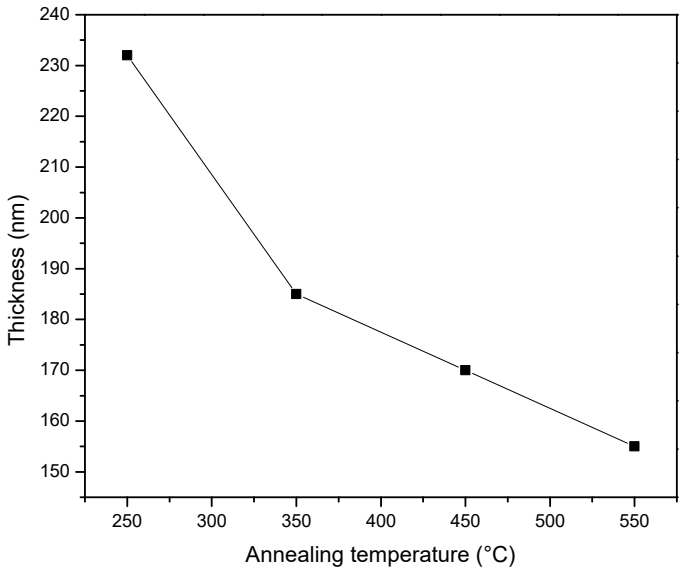

Figure IV. 2. Thickness variation of annealed In_2O_3 thin films.

The thickness of the films has been measured by the weight difference method (mentioned in Chapter III section III.2.1). With the increase of annealing temperature, the thickness of the In_2O_3 films obviously decreases as shown in Figure IV.2. As can be seen, the thickness of thin film is reduced from 232 nm at 250 °C to 155 nm at 550 °C. The decrease could be originated by the increment of material density owing to the evaporation of organic residual coming from the precursor solution [167].

IV.2.2. Structural study

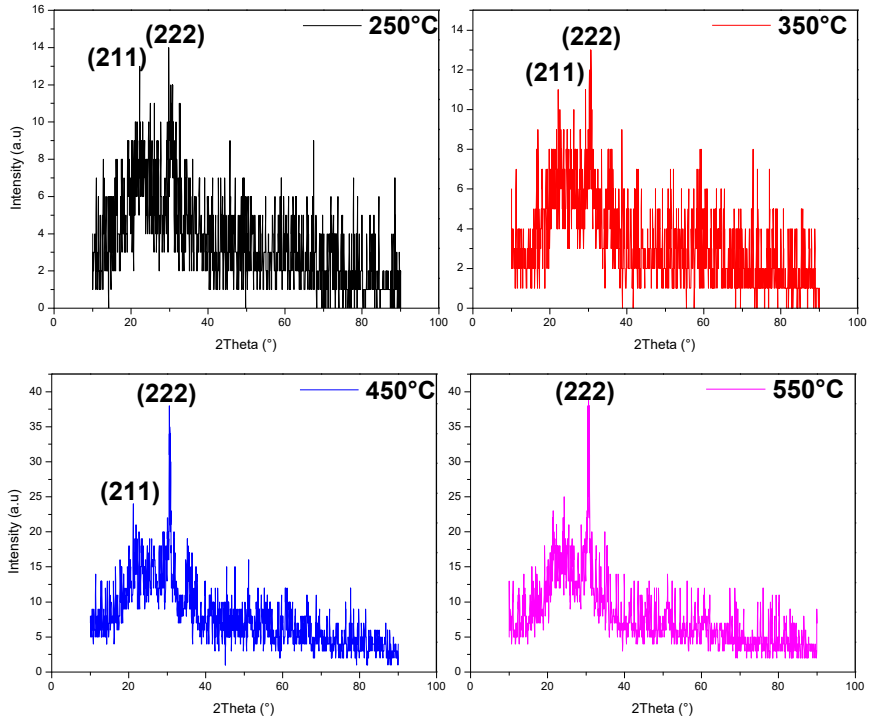

Figure IV. 3. Variation of XRD patterns of In_2O_3 thin films prepared at different annealing temperatures.

Figure IV. 3 shows the X-ray diffraction patterns of deposited In_2O_3 thin films at different annealing temperature in air. Diffraction analysis suggests that all the films are polycrystalline in nature. XRD patterns of the thin films indicated the cubic structure of polycrystalline In_2O_3 with diffraction of two peaks correspond to (211) and (222) planes. This is in good agreement with JCPDS data (JCPDS No. 06-0416). As can be seen from the diffraction patterns, the (222) plane is the predominant orientation. The increment along (222) orientation could be explained as, with the increase of annealing temperature In_2O_3 crystallites gain enough energy and orient themselves along (222) plane as it possesses highest atomic packing density and minimum surface energy. As reported by Sandoval-Paz and Ramirez-Bon [168], the orientation of the

grains in specific crystallographic directions is related with minimization of free surface energy density of the film and the energy density of the interface between the film and substrate. From the high intensity of the (222) peak, it can be seen that <111> is the preferred direction of crystal growth in all these films. Also, the (222) plane is a close packed plane in In_2O_3 cubic bixbyite structure with lowest surface energy [169]. Furthermore, the intensity of the (222) diffraction peak is clearly increased with increasing the annealing temperature, implying the improvement of crystalline structure. Wang et al. [170] reported that, as increasing annealing temperature, the defects in the films decrease and the crystal quality of the films is enhanced.

Table IV. 1. Micro-structural parameters of In_2O_3 thin films formed at different annealing temperatures.

Annealing temperature	**Bragg's angle**	**Lattice constant**	**Crystallite size**	**Dislocation density**	**Strain**
(°C)	2Theta (°)	*a* (Å)	D (nm)	δ (10^{15} line/m^2)	ε (10^{-3})
250	30.56	10.132	12	6.94	2.66
350	30.50	10.150	12	6.94	2.66
450	30.72	10.080	23	1.89	1.33
550	30.64	10.105	23	1.89	1.33

From the diffraction (222) peak positions, various structural parameters like lattice constant (*a*), dislocation density (δ) and strain of In_2O_3 thin films at different annealing temperature were presented in Table IV. 1. The lattice constant is 10.118 Å for the bulk In_2O_3 crystal that has a cubic structure [171]. The values of lattice constant for the films annealed at 250°C and 350°C are larger than the lattice constant of bulk crystal. This referred that the unit cell is elongated, and tensile force exists in the crystal lattice of the film. However, after annealing at higher temperatures, the lattice constant decreases and is almost close to the bulk one for the film annealed at 550 °C, which indicates that the tensile strain in the In_2O_3 films is gradually relaxed as the annealing temperature increases and it is almost fully relaxed for the sample annealed at 550 °C.

As estimated from the (222) peak (Table IV.1), the crystallite size of the films increases from 12 to 23 nm with the increase of annealing temperatures from 250°C to 550 °C, due to the improvement in the crystallinity of the films [172]. Caglar et al. [173] explained that by considering the thermal annealing induced coalescence of small grains by grain boundary diffusion which caused major grain growth. Moreover, Sengupta et al. [174] reported that at high temperatures, atoms had enough diffusion activation energy to occupy the energetically

favorable site in the crystal lattice and eventually grains with the lower surface energy became larger. Furthermore, it is observed from Table IV.1 that the strain and dislocation density of the prepared In_2O_3 films decrease with the increase of annealing temperature. This may be due to the increase in crystallite size and improvement in the stoichiometry of the film grown at higher annealing temperature [175]. Rao et al. [176] suggested that the decrease in strain is basically due to the fact that the atoms get higher energy to adjust their position in the lattice during annealing. In the latter, we conclude that crystal defects plays important role in the value of crystallite size.

IV.2.3. Optical study

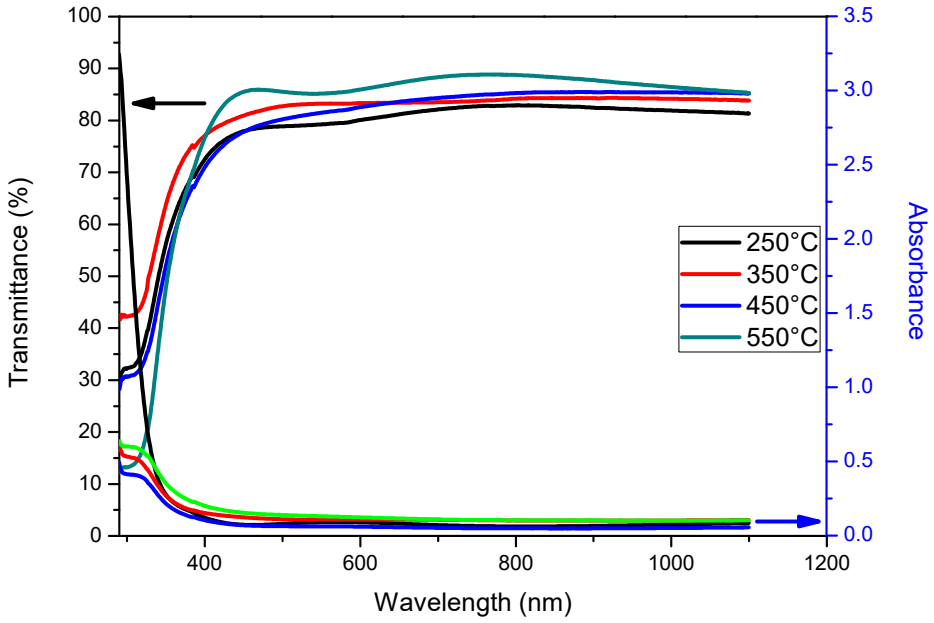

Figure IV. 4. The transmission and absorbance spectra of In_2O_3 thin film annealed at different temperatures.

The knowledge of optical properties of materials has a great significance in the designing and analysis of optoelectronic devices. Moreover, optical measurements are extensively used for characterization of the quality of the materials [177]. The optical transmittance and absorbance spectra with wavelengths from 290 to 1100 nm of In_2O_3 films annealed at different temperatures are shown in Figure IV. 4. This figure shows that all samples have good absorbance in the ultraviolet regions and low absorbance in visible and near-infrared regions. The average transmittance value within the visible region was found in the vicinity of 80% for the film deposited at 250°C and for the films prepared at 350°C, 450°C and 550°C reaches to 82%, 83% and 86%, respectively. So, the transmittance of the films has been found to increase with

annealing temperature in the visible region. Many authors report that the increase in transmittance of the films obtained by annealing is related to an increase in crystallinity of the films and the improvement of crystallinity leads to decrease in optical scattering and defects [178,179]. In [180], it was shown that the increase in transmittance of films with annealing temperature may be attributed to the improvement in the crystallinity and surface homogeneity of the films. In addition, the figure showed that the transmittance is high above 400 nm and it rises slowly with wavelength in the higher wavelength region (above 400 nm) and falls sharply in the shorter wavelength region (below 400 nm). As mentioned earlier, this sharp fall in transmittance in the shorter wavelength region is indicative of direct optical absorption in the films.

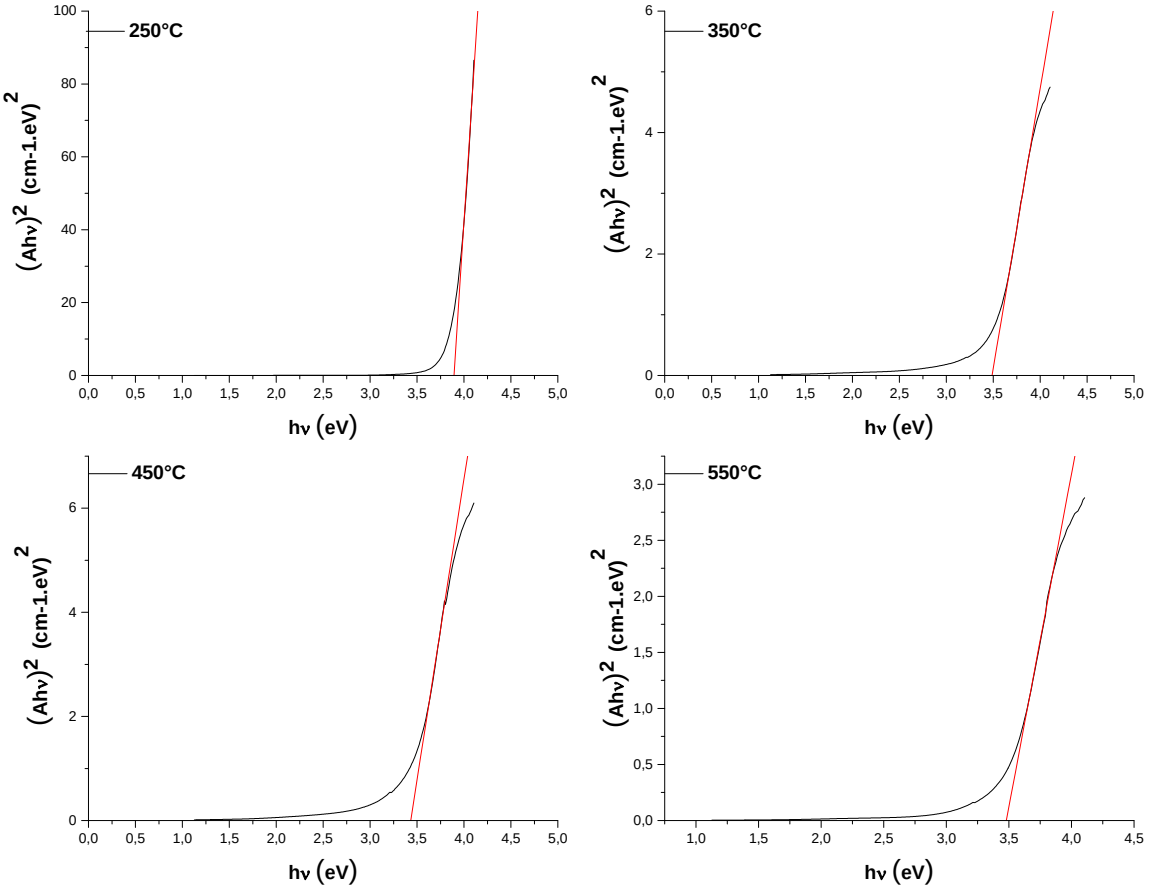

Figure IV. 5. The plots of $(Ahv)^2$ versus photon energy (hν) for the prepared In_2O_3 thin films at various temperatures.

The energy gap (E_g) values depend, in general, on the film crystal structure, the arrangement and distribution of atoms in crystal lattice. The band gap of In_2O_3 films was calculated from the

$(Ahν)^2$ versus photon energy (hν) by extrapolation of the straight line of the plot of $(Ahν)^2$ versus photon energy (hν) for the different annealing temperatures, as shown in Figure IV.5.

The variation of energy band gap for In_2O_3 thin films as function of annealing temperature is presented in Figure IV. 6. It is observed that the values of band gap decrease with the increase of annealing temperature. With the increase of annealing temperature upto 450°C, the band gap value decreases to 3.41 eV. Furthermore, the band gap value increases with the increase of annealing temperature at 550°C. Many author reports that annealing process improves the crystallinity and increases crystallite size of the films that results in decreasing defects concentration as well as reduce the strain in the films; therefore, the optical band gap energy decreases [178,181]. However, the band gap slightly increased for annealed film at 550°C. This tendency may occur due to the high transmittance (see Figure IV. 4) into the film at this elevated temperature, as reported by Sanjeev et al. and Arif et al. [182,183].

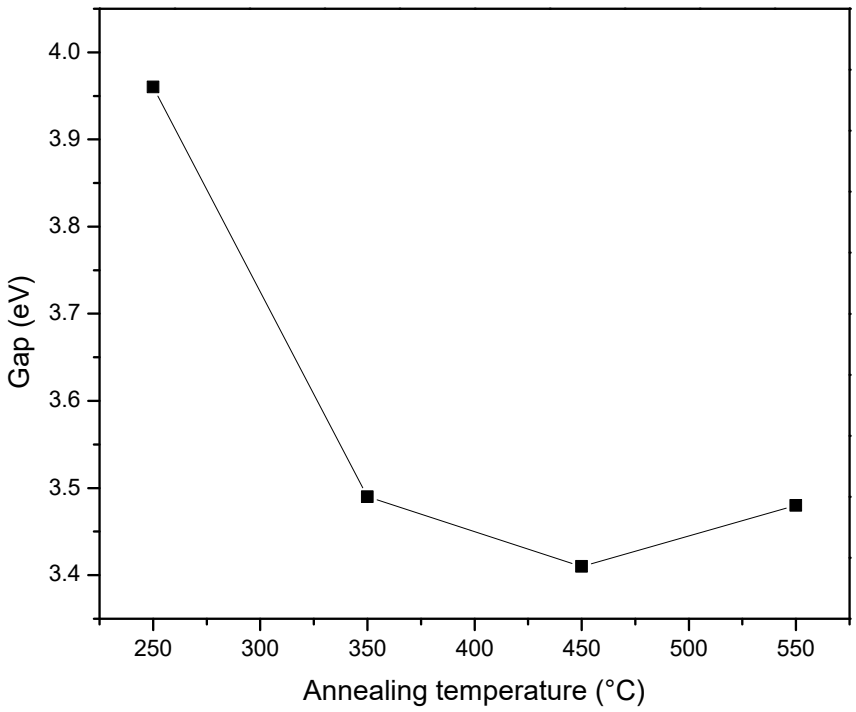

Figure IV. 6. The energy band gap of In_2O_3 thin film at different annealing temperatures.

The Urbach tail is an essential parameter used to estimate the level of crystallinity and structural defect or degree of disorder present in the film materials. Generally, the optical transmittance and optical band gap structure affected by the width of localized states available in the films which are known as Urbach tail. This exponential tail appears in the low crystalline, poor crystalline, the disordered and amorphous materials because these materials have localized

states which extended in the band gap [184].

Figure IV.7 shows the Ln(A) versus (hυ) curve of annealed In_2O_3 films at different temperature. The Urbach energy (E_u) was estimated by taking the reciprocal slope of the straight line of plotting Ln(A) against the incident photon energy (hν).

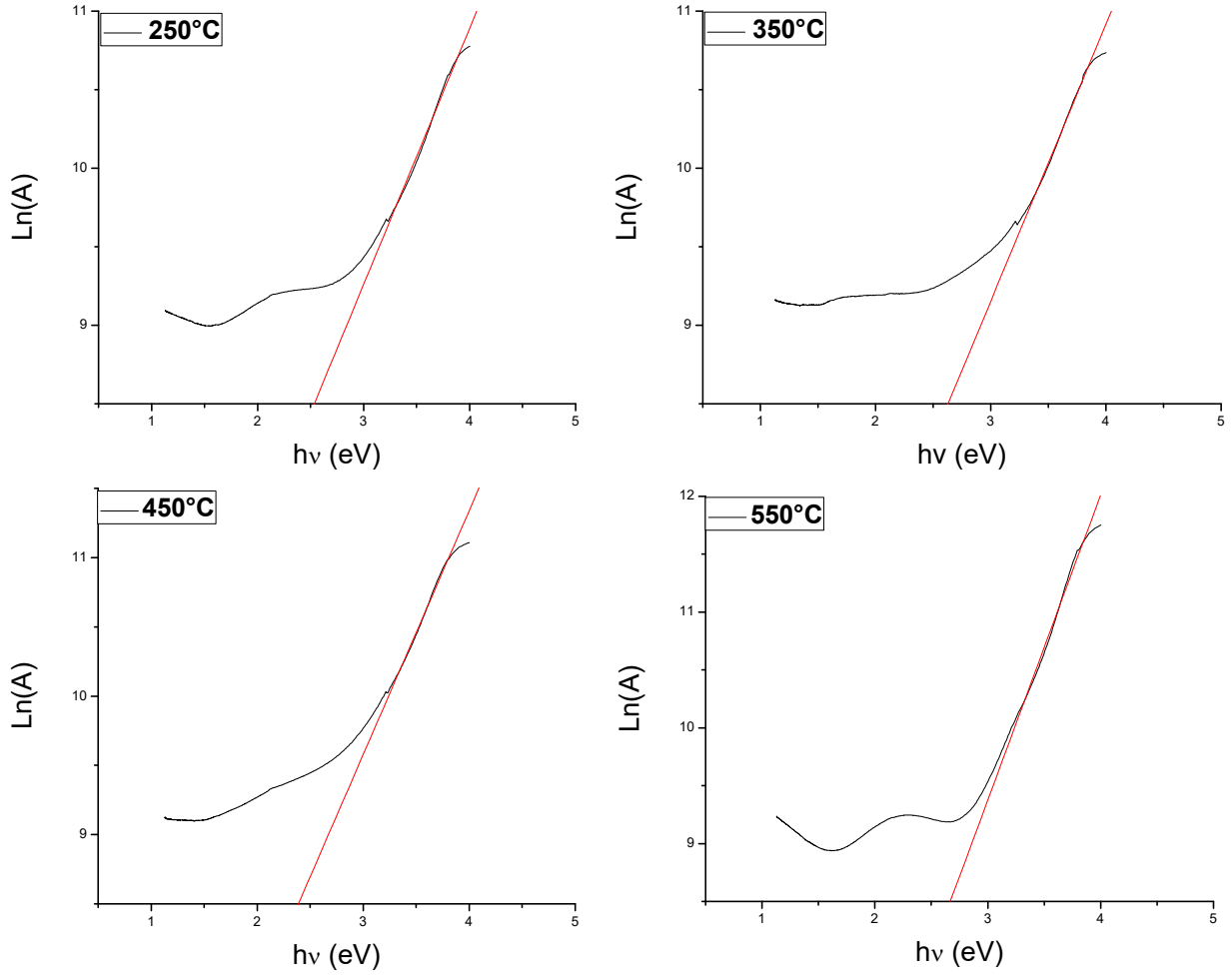

Figure IV. 7. Ln(A) vs hν of annealed In_2O_3 films at different temperature.

As shown in Figure IV.8, the Urbach energy or the width of the band tail decreases with the increases of annealing temperature. This behavior proves that the degree of structural disorder decreases with the increase of annealing temperature. It is obvious that the film exhibit minimum structural disorder when the films are annealed at 550°C. This may due to the improvement of crystallinity and minimization of strain and dislocation density; therefore, the defects in annealed In_2O_3 thin films reduced. The results obtained by Rahman et al. [185] suggest that the reduction in E_u values are, generally, governed by the diminution of the localized density of states around the tails of the absorption edges, increase in crystallinity, decrease in the degree of disorderliness and a relaxation of the distorted bonds. The reduction in Urbach energy also indicates the improvements of the films crystal quality.

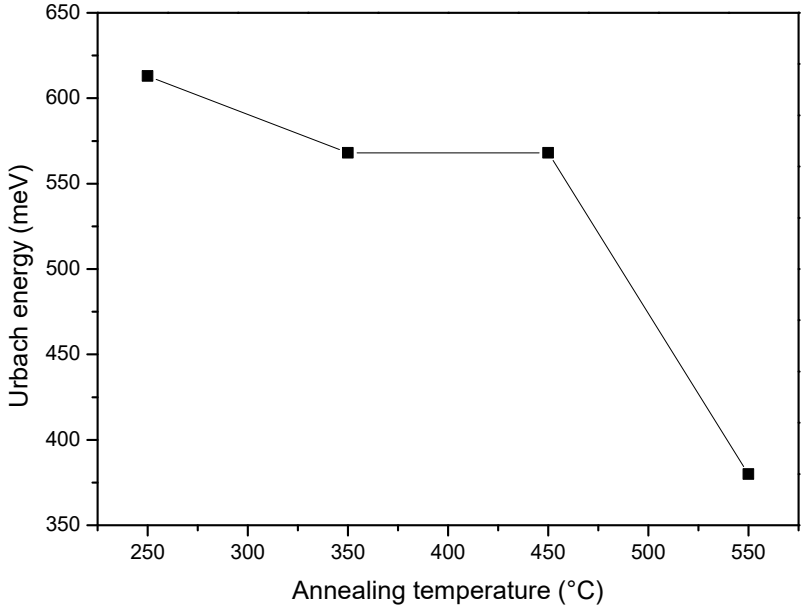

Figure IV. 8. Urbach energy of annealed In_2O_3 thin films.

IV.2.4. Electrical study

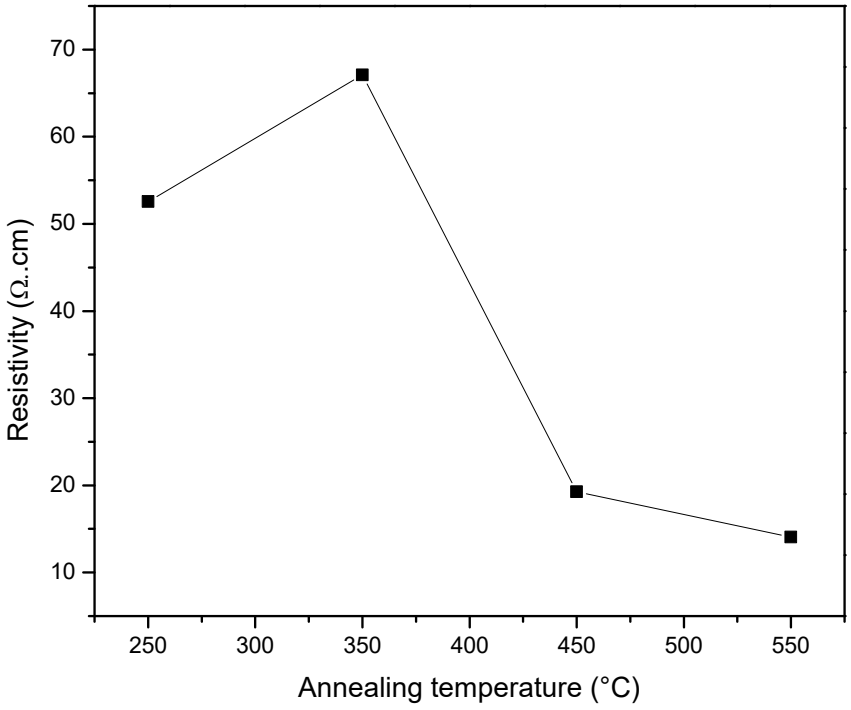

Figure IV. 9. Resistivity of In_2O_3 thin films with different annealing temperatures.

The variation of In_2O_3 films resistivity as a function of annealing temperature is shown in Figure IV. 9. We can see from this figure, as the annealing temperature increases to 350 °C, the resistivity gradually increases to the maximum value of 67.07 Ω.cm. However, further increase in annealing temperature, the resistivity of the films decrease gradually to the value of 14.05 Ω.cm and this may be due to the increase in the mobility of the charge carriers and the increase in the carrier concentration [186]. Generally, the decrease of the resistivity means that the conductivity increase. The increase in conductivity of the films with annealing temperature is due to the growth of crystallite size and improvement of crystallinity [187]. This inference on the improvement of crystallinity of the films with increasing annealing temperature is consistent with the present XRD results. In addition, Wang et al. [188] indicated that the possible reason for the increase in conductivity is that the annealing process has the effect of increasing crystallite size and crystallinity of the film, as mentioned before, which therefore results in less grain boundary scattering. Lastly, the minimum value of the resistivity for annealed In_2O_3 film at 550°C temperature makes the film find wide applications in the field of optoelectronics.

IV.3. Conclusion

In summary, In_2O_3 thin films have been successfully deposited by sol gel spin coating method on microscopic glass substrates. The films have been annealed in a furnace at different temperatures (250, 350, 450 and 550 °C). The film thickness measured by weight difference method decreases with annealing process. The XRD results reveal that the deposited thin films have a polycrystalline nature with cubic structure. As the annealing temperature increase, the crystallinity and crystallite size increase. The film transmission in visible region is about 86% at 550°C sample. Also, the optical band gap narrowed with annealing temperature from 3.98 to 3.47 eV. Moreover, from electrical studies, the electrical resistivity decreases with increase in annealing temperature and a minimum electrical resistivity of 14.05 Ω.cm was obtained for the film coated at 550 °C. Therefore, it is very clear from the present work that the annealing temperature plays an important role in varying the physical properties of the prepared thin films. Finally, we can say that we have prepared In_2O_3 thin films with good optical and electrical properties which can be used in many optoelectronic and photovoltaic applications.

Chapter V: Impact of titanium doping on indium oxide thin films properties

It is well known that the properties of the thin films are affected by deposition parameters such as precursor concentration, post-annealing temperatures, film thickness and dopant concentration, etc. This chapter presents a detailed explanation of the preparation and characterization of Ti-doped In_2O_3 thin films deposited using sol-gel spin coating method. The influence of Ti concentration on the properties of In_2O_3 thin films is also discussed in detail. Doping with Ti is primarily done to achieve high transparency, stability and high conductivity of the In_2O_3 thin films to use them in the low-cost optoelectronic device applications.

V.1. Experimental details

V.1.1. Preparation of In_2O_3 films

Titanium doped indium oxide (InTiO) thin films with different concentrations (0, 5, 10, 15 mol.%) were prepared on glass substrates by sol gel spin coating method. Indium (III) nitrate hydrate [$In(NO_3)_3.xH_2O$], absolute ethanol (C_2H_5OH), acetylacetone ($C_5H_8O_2$) and titanium (IV) isopropoxide [$Ti(OCH(CH_3)_2)_4$] were used as the starting precursors, solvent, stabilizer and titanium (Ti) doping source, respectively. The concentration of the indium (III) nitrate hydrate was 0.15 M and the volume ratio of actylacetone to ethanol was maintained at 1:10. The prepared solutions were stirred at 50 °C for two hours to yield clear and homogenous solutions. After aging for 48 h at room temperature, the resultant solutions were dropped onto glass substrates, which were rotated at 4000 rpm for 30 s. After each coating step, the films dried at 250 °C for 10 min to evaporate the solvent and remove organic residuals. The spin coating process was repeated six times to achieve the desired film thickness. Finally, all the samples were annealed in furnace at 500 °C for 2 h to obtain good crystalline films.

V.1.2. Films characterization

The structural characterization of InTiO thin films were performed by X-ray diffraction (X'PERT PRO), the optical characterization was investigated by UV-Visible spectrophotometer (Perkin Elmer LAMBDA 25) in the range of 250-1100 nm. The room temperature photoluminescence (PL) spectra were measured by a spectrophotometer (Perkin Elmer LS50B) with an excitation wavelength of 325 nm and fourier transform infrared (FTIR) was carried by BRUKER VERTEX-80V spectrometer. Electrical conductivity was achieved using four probe method.

V.2. Results and discussion

V.2.1. Structural study

The X-ray diffraction spectra for undoped and Ti doped indium oxide (InTiO) thin films

deposited on glass substrates using sol gel process are shown in Figure V. 1. The spectra indicate that all the films are polycrystalline in nature and crystallize in a cubic structure according to JCPDS card (06-0416) with preferential crystallographic (222) plane. The growth along the predominant (222) plane may be attributed to minimization of the crystal surface free energy [189]. We observe other weak peaks in the XRD patterns correspond to (211), (400), (431), (440) and (622) planes, which revealed that InTiO films were crystallized very well. Doping by Ti led to an obvious reduction or even disappearance in intensities of XRD peaks corresponding to lattice planes such as (431) and (211). The disappearance and reduction in intensities of XRD peaks of some lattice planes imply the presence of a large number of vacant lattice sites, destroyed periodicities in some crystal planes and local lattice disorders [190]. Ohyama et al. [191] studied the effect of aluminum content on the structure of ZnO:Al films, and thought the decrease of predominant peak could be due to the segregation of dopant components at the grain boundary, though no impurity phases were found from the XRD patterns. The possible reason for no diffraction peaks observed in XRD patterns for TiO_2 phase is due the complete miscibility of Ti components in the proposed composition [192].

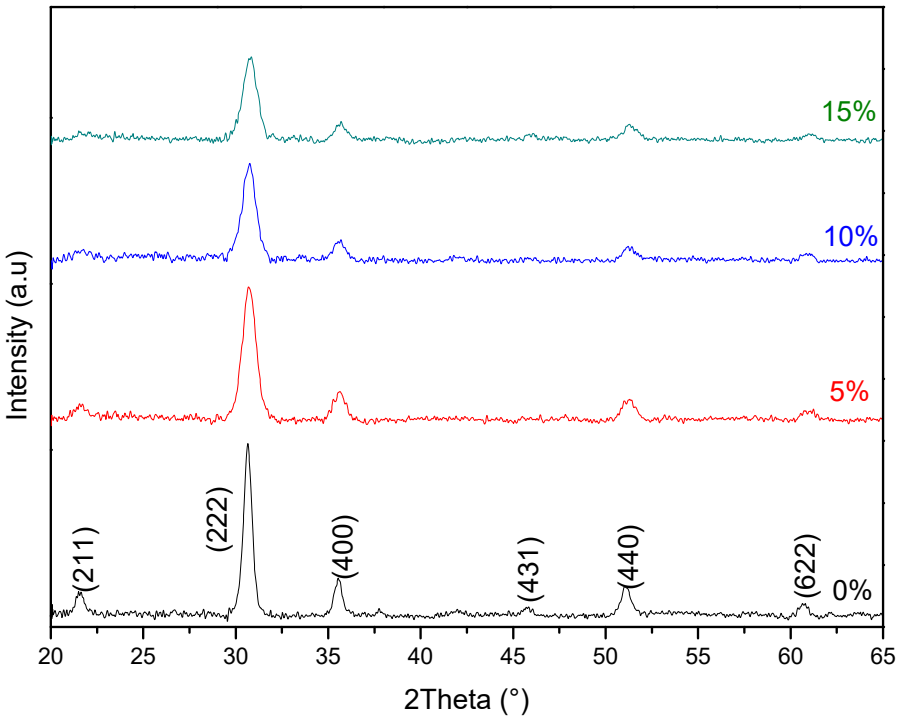

Figure V. 1. X-ray diffraction spectra of In_2O_3 films with different Ti concentrations.

As shown in Figure V. 2, a slight shift in the position of (222) peak to higher angle was observed, indicating a reduction in the lattice constant (see Figure V.3 (b)), which might be due to the increased oxygen vacancies in the film surface [193]. As reported by Chun et al. [194], the

higher angle shift of the XRD peaks suggests the decrease of the lattice constant. The decrease of the lattice constant of In_2O_3 crystals can be estimated to be Δa = 0.041 Å, corresponding to a 0.41% decrease. Since the ionic radius of Ti^{4+} (0.61 Å) is smaller than that of In^{3+} (0.80 Å), the substitution of Ti on In sites in the In_2O_3 lattice can reduce the lattice constant. The XRD peak shift of the In_2O_3 lattice to the higher angle was also observed from the Ga_2O_3–In_2O_3 films [195] and Zr doped In_2O_3 [130]. In addition, Zhang et al. [196] reported that the shift of strong (222) peak position to higher angle region is due to the residual stress developed in the films because of difference in the ionic radius between In^{3+} and Ti^{4+}. The shift of (222) peak indicates successful doping of Ti in the indium oxide films. As the ionic radius of the doping element is small, so there is a limit doping level that must not be exceeded in order to not destroy the unit cell.

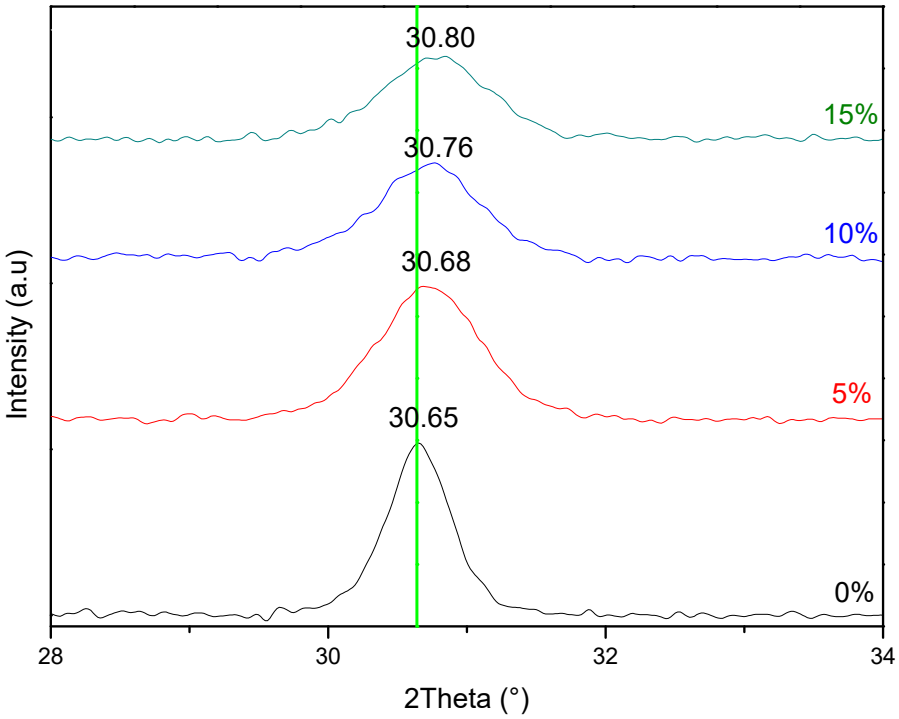

Figure V. 2. Main (222) peak shifting of InTiO thin films.

Figure V. 3 presents the variation of grain size, strain, lattice constant and dislocation density with Ti concentration. It can be seen that the grain size reduces from 13.29 nm for pure In_2O_3 to 6.98 nm for 15 mol.% Ti-doped In_2O_3 thin film (Figure V.3 (a)). It shows that the In_2O_3 grain size tend to decrease with the Ti-doping concentration increasing. It is probably because of the large strain in the films which affects the normal growth of In_2O_3 grains [197]. The decrease in grain size suggests reduced crystallinity with increased grain boundary. Also, the possible reason could be the disturbance of grain growth by stress due to the difference in ion radius between

titanium and indium. Ajili et al. [198] indicated that the decrease of grain size may be attributed to the increasing number of centers during incorporation of the doping into the host material. On the other hand, the strain and dislocation density increase with Ti concentration (Figure V.3 (a) and (b)). The different size between Ti^{4+} (0.61 Å) and In^{3+} (0.80 Å) radius cause the strain field that disturb grain growth process.

Since the dislocation density and the strain are the manifestation of dislocation network in the films, the increase in the strain and the dislocation density indicates the formation of lower quality films with Ti doping concentration [199]. From the above results, it is concluded that Ti doping plays an important role in the crystal orientations of In_2O_3 films and effectively modifies the microstructure of the In_2O_3 films.

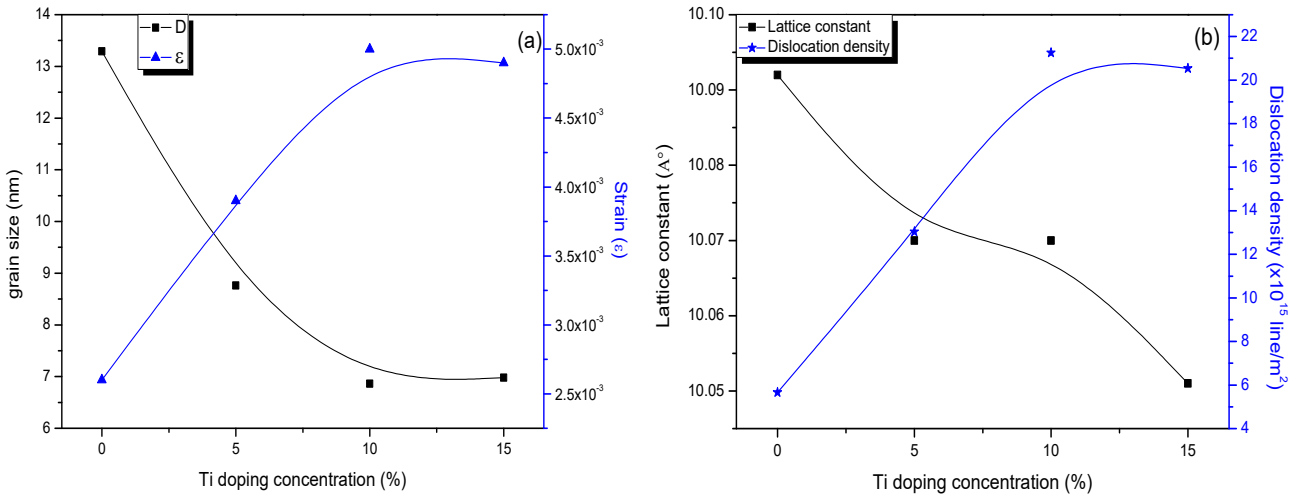

Figure V. 3. Variation of (a) grain size and strain (b) lattice constant and dislocation density with Ti doping concentration.

V.2.2. Optical study

The optical transmission spectra of prepared InTiO thin films at different doping concentrations measured in the wavelength region from 250 to 1100 nm are shown in Figure V. 4. It is found that the undoped and Ti doped indium oxide films exhibit a high transmittance in the range of 87–93% in the visible region with a sharp fundamental absorption edge. This sharp fall in transmission near the fundamental absorption edge is an identification of the good crystallinity of the films [200]. The high optical transmission with Ti doping concentration may be related to low scattering of light. Moreover, In_2O_3 films doped with 10 and 15 mol.% Ti exhibits a high optical transmittance reach to 93% in the visible region. Alqahtani et al. [201] said that high transmission may be ascribed to the improvement of stoichiometry. Also, The

films show the presence of some interference fringes, which might be due to the characteristic of interference between light and nano-structured materials [131]. Li et al. [149] suggest that the interference fringes in transmittance spectra could be attributed to homogenous and smooth of films surface. Linearity is observed in the first case as shown in Figure V. 4 (inset); we can conclude that the direct transitions dominate in undoped and Ti doped indium oxide films.

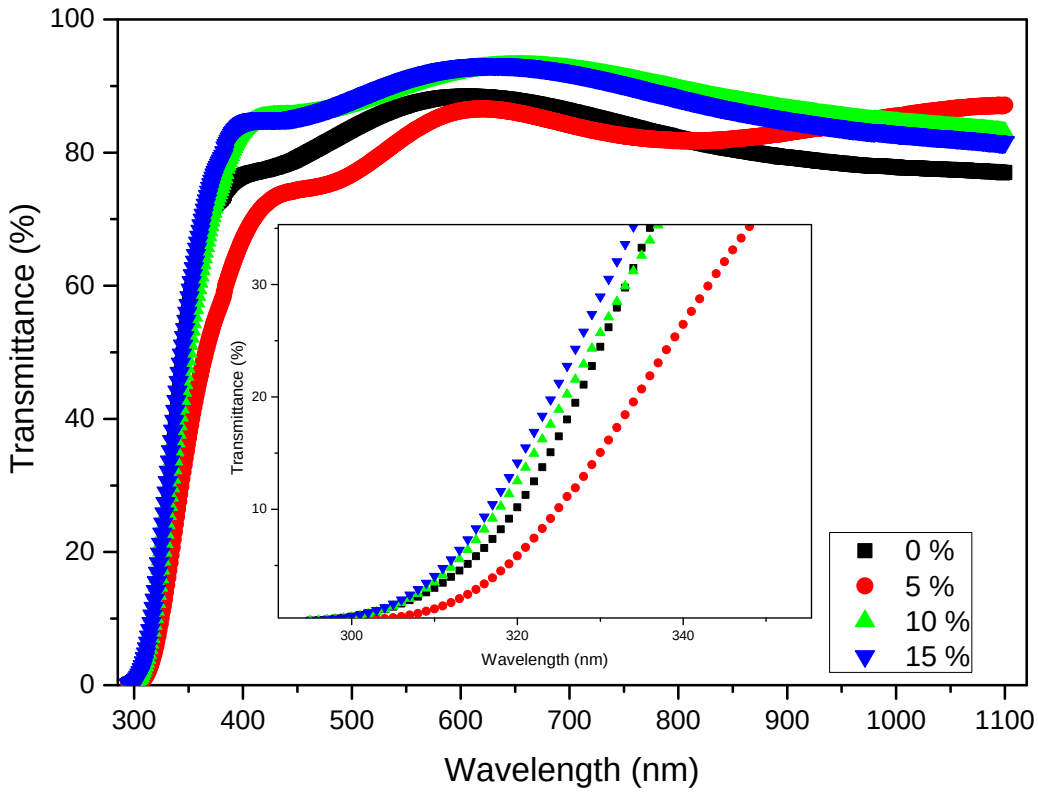

Figure V. 4. Optical transmittance spectra of Ti doped In_2O_3 thin films.

Figure V.5 (a) shows the plots of $(\alpha h\nu)^2$ against $(h\nu)$ in order to estimate the band gap values of the deposited films. The curve of $(\alpha h\nu)^2$ vs $(h\nu)$ has straight line portion and the band gap has been estimated by extrapolating the straight line to intersect the photon energy axis. The intersection point is the band gap value in eV.

The Urbach energy is estimated by plotting $Ln(\alpha)$ vs. $(h\nu)$ and fitting the linear portion of the curve with a straight line. The reciprocal of the slope of this linear region yields the value of E_u, as shown in Figure V. 5 (b).

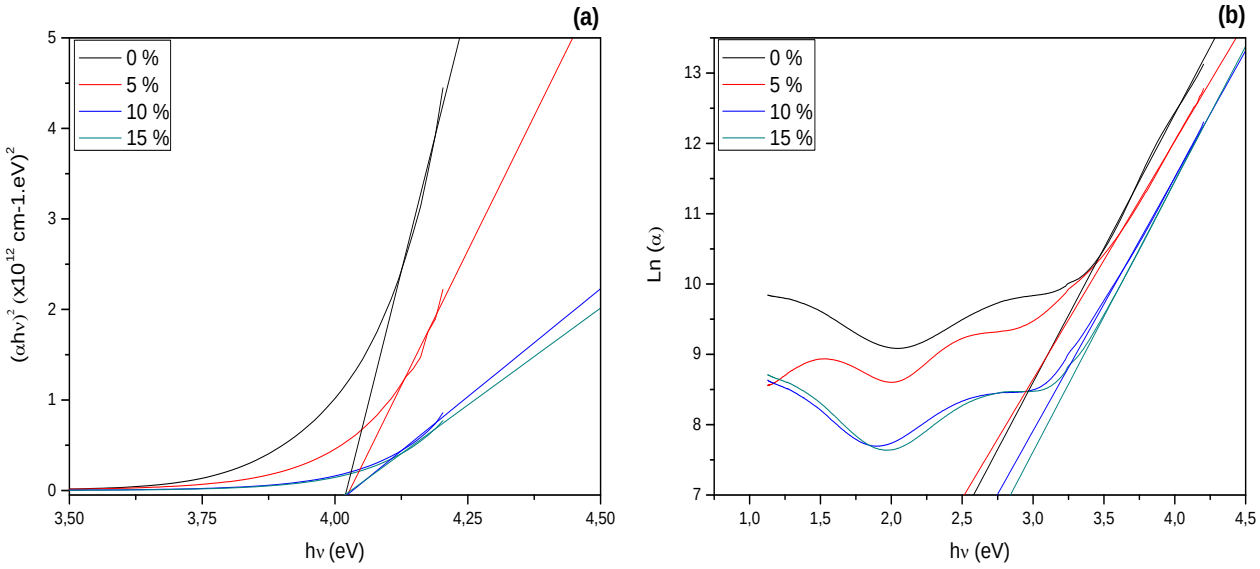

Figure V. 5. Plots of: (a) $(\alpha h\nu)^2$ vs (hν); (b) Ln(α) versus (hν).

The optical band gap (E_g) and Urbach energy (E_u) of Ti doped indium oxide thin films are given in Table V. 1. As can be seen, the band gap is almost constant for pure and Ti doped In_2O_3 thin films at 4 eV value. While, The Urbach energy value of 262 meV of the undoped film increases to the value of 295 meV for 5 mol.% Ti sample and then it starts to decrease to the values of 278 and 260 meV for 10 mol.% Ti and 15 mol.% Ti samples, respectively. As estimated, increasing Ti content did not affect the band gap. The constant band gap with Ti doping could be attributed to the low concentration of dopants which make no shift in the band gap value [202]. In the work of Shanmugapriya et al. [203] the band gap was found to decrease from 3.40 to 3.30 eV with increasing Ti doping. This decrease in the band gap has been attributed to shrinkage effect, which is frequently observed in n-type semiconductors. While doping, the shrinkage of the band gap energy was due to the induced shifting of the conduction band minimum and valence band maximum. However, in [204] it was shown that the E_g is found to increase with increase Ti doping level, which is ranging between 3.4 and 3.8 eV. The increase in E_g explained by the basis of the Burstein–Moss (BM) effect, an energy band widening effect resulting from the increase in the Fermi level in the conduction band of degenerated semiconductors.

Table V. 1. Band gap and Urbach energy of InTiO thin films.

Doping concentration (mol.%)	Optical band gap (eV)	Urbach energy (meV)
0	4.02	262
5	4.02	295
10	4.00	278
15	4.02	260

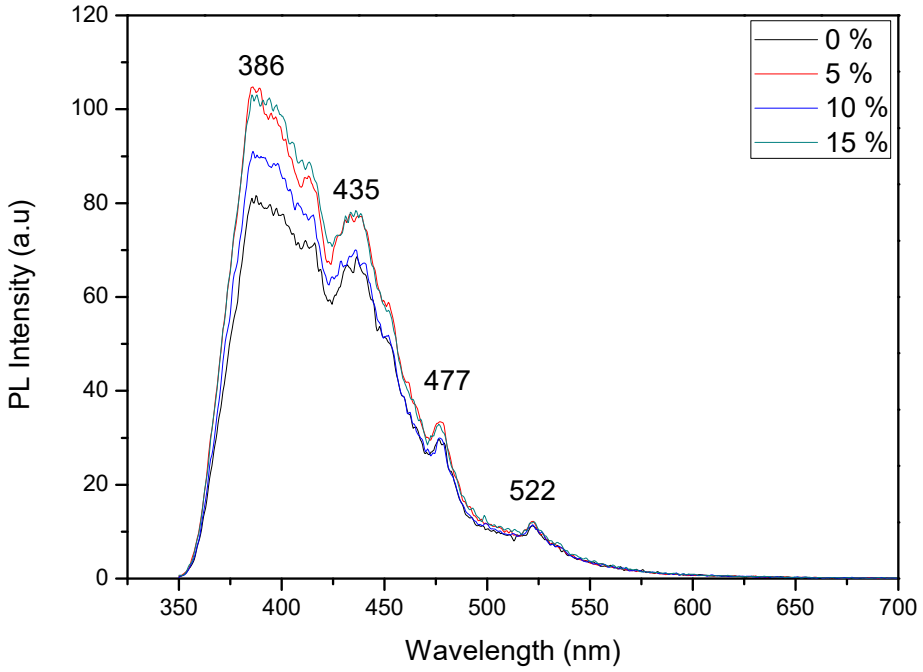

Figure V. 6. Photoluminescence (PL) spectra of InTiO films.

Basically, the luminescence property of the films has a close relation with the film crystallinity because the density of defects in film decreases with the improvement of the crystallinity [205]. The room temperature photoluminescence (PL) spectra of prepared Ti doped In_2O_3 thin films are shown in Figure V. 6. The figure reveals four peaks centered at 386, 435, 477 and 522 nm associated with ultraviolet (UV), violet, blue and green emissions, respectively. The strong UV emission peak is related to near band edge (NBE) emission, and it originates due to the recombination of the free excitons through an exciton–exciton collision process [206]. Whereas, The other emission peaks are due to the presence of structural defects such as oxygen vacancies within In_2O_3 crystal lattice [207]. The violet-blue emission peaks at 435 and 477 nm indicated that a new defect levels are introduced into the band gap by the Ti doping [208].

Moreover, this violet-blue emission could be attributed to the O, In and/or In/O vacancies centers, which is also in agreement with the reported values [209,210]. The origin of green emission band at 522 nm is generally ascribed to deep level (DL) defects such as surface defects and singly ionized oxygen vacancies [163]. Indeed, there is an increase in PL intensity in the presence of Ti^{4+} compared to undoped film, this confirm that the substitution of Ti^{4+} ions caused an increase in defects. Generally, the cubic In_2O_3 is a typical n-type semiconductor, has an oxygen-deficient structure and the oxygen vacancies can induce the formation of new energy levels in the band gap [87].

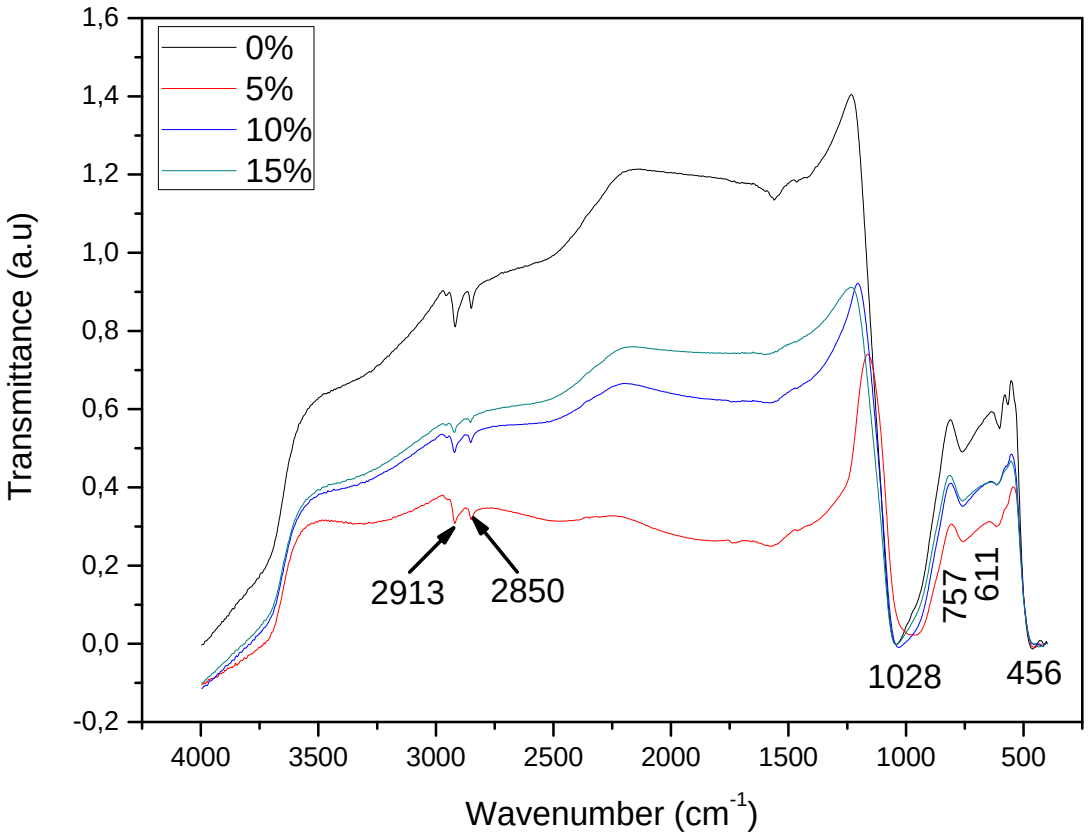

Figure V. 7. FTIR spectra of Ti doped In_2O_3 thin films.

FTIR spectroscopy is very useful tool for investigating vibrational properties and chemical composition of synthesized materials. The FTIR spectral analysis of un-doped and Ti-doped In_2O_3 thin films are shown in Figure V. 7. As can be seen, six main bands were observed at 456, 611, 757, 1028, 2850 and 2913 cm^{-1}. Jothibas et al. [164] said that the In–O stretching vibrations are usually found in the region 800-300 cm^{-1}. So depending on that, the weak bands at 456, 611 and 757 cm^{-1} are attributed to In–O stretching bond. Panneerdoss et al. [157] suggest that the

presence of the entire vibrational patterns of In–O bond in the low frequency region is due to the stability and heavy mass of In_2O_3. The strong broad band at 1028 cm^{-1} is assigned to C–C–H bending, mixed with stretching C–C vibrations of AcAc [211]. The absorption bands at 2850 and 2913 cm^{-1} are due to the C-H stretching bonds of the organic compounds [160]. Furthermore, Renard et al. [213] have demonstrated that the two bands detected at 2850 and 2913 cm^{-1} could be assigned to the symmetric and asymmetric CH_2 stretching vibration modes.

V.2.3. Electrical study

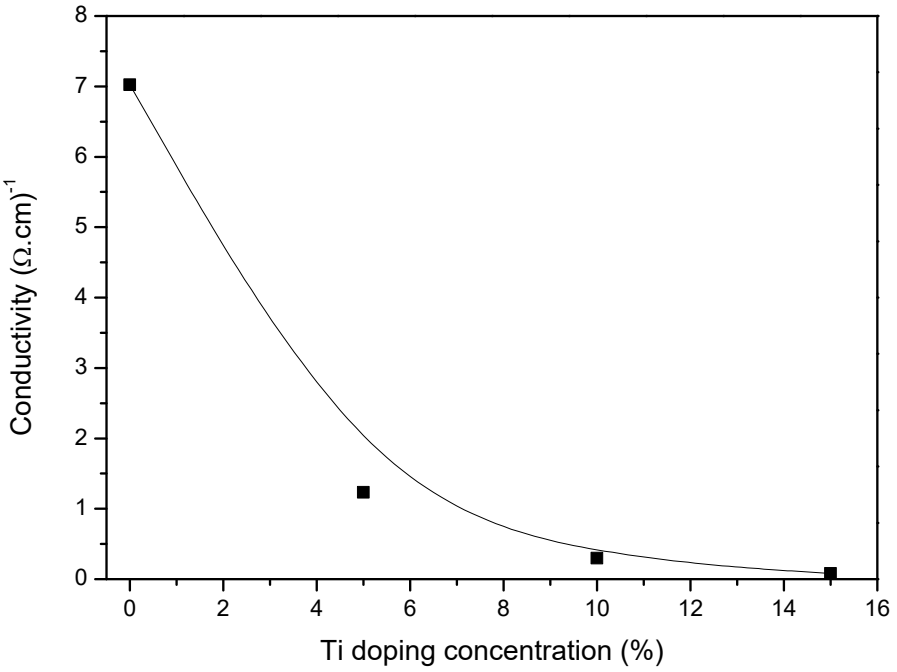

Figure V. 8. Conductivity of prepared InTiO thin films.

The measured electrical conductivity of undoped and Ti doped indium oxide thin films is given in Figure V. 8. It can be seen that the conductivity is decreased from 7.02 to 7×10^{-2} $(\Omega.cm)^{-1}$ as increasing Ti concentration. We obtained a maximum electrical conductivity value at 7.02 $(\Omega.cm)^{-1}$ for pure In_2O_3 thin film. The reason for the decrease in conductivity is that some Ti atoms may occupy interstitial positions and may also form defects in the structural lattice, which acts as a carrier traps rather than electron donors [214]. Manjula et al. [215] suggest that the decrease of grain size means deterioration of crystalline quality of In_2O_3 films with Ti doping and an increase of total grain boundary fraction in the films, which can enhance grain boundary scattering, thus, result in a decrease of electrical conductivity. This result confirmed by XRD and grain size variations. From this we conclude that the electronic transport property for the In_2O_3 thin films is entirely related to the microstructure of the films and doping concentration.

V.3. Conclusion

Transparent conducting indium oxide thin films with different compositions (0, 5, 10, 15 mol.% Ti) were successfully prepared by sol gel spin coating technique. The influence of titanium (Ti) doping concentration on structural, optical and electrical properties of In_2O_3 films was investigated. The following conclusions are derived after these investigations:

- The X-ray diffraction patterns revealed that prepared InTiO films are polycrystalline with preferential (222) plane of cubic structure. The change observed in the peak position of (222) plane confirms the substitutions of Ti atoms in In–O lattice. The grain size was found to decrease from 13.29 to 6.98 with Ti doping.
- The optical measurements show that the transmittance of the films has improved to 93 % for 10 and 15 mol.% Ti and the optical band gap was almost constant (~ 4 eV).
- The room temperature photoluminescence spectra of Ti doped In_2O_3 films exhibit four emission peaks: UV emission peak (at 386 nm), violet emission peak (at 435 nm), blue emission peaks (at 477 nm) and green emission peak (at 522 nm).
- FTIR spectra confirmed the presence of In–O, C–C–H, C–H and CH_2 stretching vibration bonds.
- Four probe measurements show that titanium doping in indium oxide thin films effectively reduces its conductivity from 7.02 to 7×10^{-2} $(\Omega.cm)^{-1}$.

According to these results, we conclude that titanium doped indium oxide thin films are suitable for optoelectronic applications and the sol gel spin coating technique is appropriate for producing In_2O_3 films with good quality.

Chapter VI: Structural, optical and electrical properties of Cu-doped In_2O_3 thin films

Indium oxide doped with metals has been widely used for numerous applications in magnetic semiconductors (Mn doped In_2O_3 nanoparticle) [216], solar cells (Ti doped In_2O_3 thin films) [217], optoelectronic devices (Sn doped In_2O_3), gas sensors and photocatalytic degradation (Zn doped In_2O_3) [218]. In wide band gap semiconductors, doping with impurities often induce dramatic changes in structural, optical, electrical and magnetic properties. Cu-doped In_2O_3 films, together with Sb-doped SnO_2 films, can be used as the ohmic contact for GaN based high performance light emitting diodes. The optical and magnetic properties of Cu-doped In_2O_3 powders have been studied [219]. However, the possible influence of Cu doping on the structural, optical and electrical properties of In_2O_3 films deposited by sol gel spin coating has not yet been investigated. In this chapter, the sol-gel method, which offers the greatest possibility for preparing a film with large area at low cost for technological applications, has been chosen to prepare the undoped and Cu-doped In_2O_3 films. Structural, optical and electrical modifications were discussed in details.

VI.1. Experimental details

VI.1.1. Preparation of In_2O_3 films

Undoped and Cu-doped In_2O_3 films were prepared on glass substrates by the sol-gel method. The precursor solutions were prepared as follows: Indium (III) nitrate hydrated [$In(NO_3)_3.xH_2O$], and copper (II) acetate hydrate [$Cu(CO_2CH_3)_2.H_2O$] were used as starting materials, absolute ethanol (C_2H_6O) as solvent, and acetylacetone ($CH_3COCH_2COCH_3$) as a stabilizer. All solutions were stirred for 2 h at 50°C. Cu doping was achieved by the introduction of appropriate amount of cupric acetate. In the process of doping, Cu content was varied from 0 to 4 mol.%. Undoped and Cu-doped In_2O_3 films were deposited on glass substrates by spin coating at room temperature, with a spinning rate of 4000 rpm for 30 s. After that the films were heated in air at 250°C for 10 min to dry and remove organic materials in the films. This procedure was repeated 6 times to achieve desired film thickness. Finally, the undoped and Cu-doped In_2O_3 were annealed in air at 500°C for 2 h.

VI.1.2. Films characterization

The phase and crystal structure were investigated using a Rigako miniflex (XRD) (2Theta from 20 to 65°). The surface morphology and chemical composition were studied using a scanning electron microscope (SEM) and energy dispersive X-ray (EDX), respectively. The optical properties of the films were characterized using a Perkin Elmer (Lamda25) UV–Vis spectrophotometer. The electrical resistivity measurement was done using four probe method.

VI.2. Results and discussion

VI.2.1. Structural study

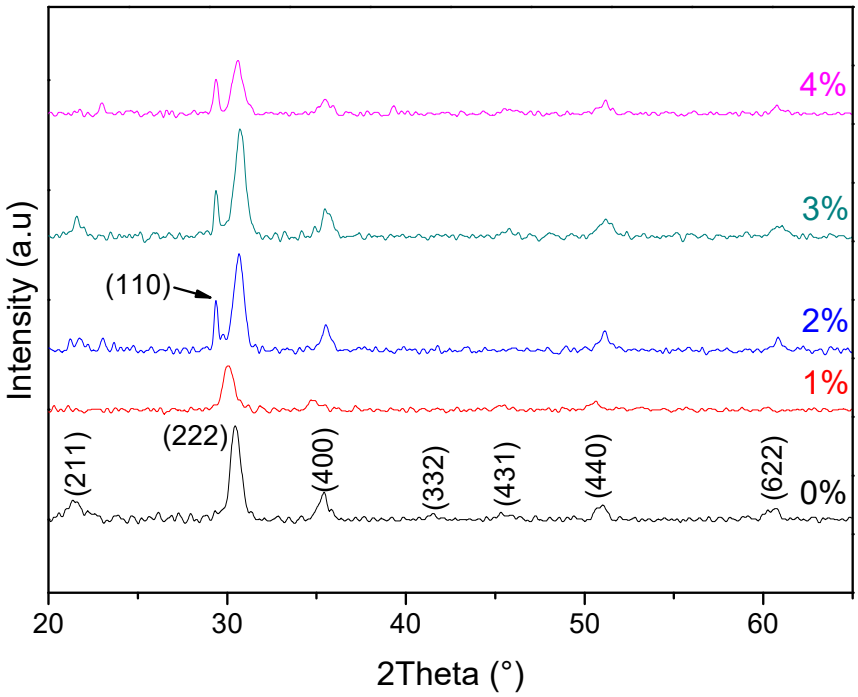

Figure VI. 1. X-ray diffraction patterns of In_2O_3 films with (Cu = 0 – 4 mol.%).

Figure VI. 1 shows the X-ray diffraction patterns of undoped and Cu doped indium oxide thin films. The undoped In_2O_3 exhibits well defined diffraction reflections at 2Theta = 21.45, 30.36, 35.49, 41.55, 46.48, 51.27 and 60.86° corresponding to (211), (222), (400), (332), (431), (440) and (622) planes, respectively. These peaks belong to bixibyte cubic structure with a space group of Ia-3 (206). Presence of various peaks suggest the polycrystalline nature of the films [161]. However, there is a peak appeared at 2Theta = 29.36° corresponding to (110) plane for 2, 3 and 4 mol.% of Cu samples corresponding to the cubic structure of Cu_2O phase. This suggested that the doping of In_2O_3 films by a high percentages of Cu affect on the crystalline structure of the films. At 1 mol.% Cu doping, The intensity of all peaks decreases suggesting deterioration of the crystallinity of indium oxide films due to the incorporation of defects in the lattice sites [220]. At 2 mol.% and 3 mol.% doping, the diffraction intensity of peaks increase sharply, indicating that the added amount of Cu ions enhances the crystallinity of In_2O_3 films. Therefore, we speculate that Cu ions play a crystal seed role during the formation of In_2O_3 particles. The increasing peaks after Cu doping may result due to the fact that Cu ions start to substitute In ions in the cubic lattice, determining better crystallinity and (222) growth orientation of In_2O_3 films. The same trend was observed in previously reported Cu-doped ZnO films [221], and also Ti-doped ZnO

films [222]. Moreover, Salaken et al. [223] suggest that the improvement of the crystalline quality of 2 mol.% and 3 mol.% Cu doped thin films compared to 1 mol.% Cu is attributed to the creation of new nucleation centers from the dopant atoms for the growth of In_2O_3 crystals. However, the crystalline quality is degraded again when Cu-doping concentration is 4 mol.%. This is probably connected with the following two factors: (1) the newer nucleation centers reach saturation [224]; (2) due to the difference of ionic radius between Cu^{2+} (0.73 Å) and In^{3+} (0.80 Å), when a large number of Cu^{2+} replace In^{3+} in lattice sites substitutionally, lattice distortion is intensified, resulting in larger strain in the films and consequently affecting the normal growth of In_2O_3 crystals.

The lattice constants for undoped and 1 mol.% Cu doped In_2O_3 films are 10.198 and 10.347 Å, which are larger than the value of standard bulk In_2O_3 (10.118 Å). Unlike, the lattice constants of 2, 3 and 4 mol.% Cu which are less than the standard value. The lattice parameters of all samples are summarized in Table VI. 1. The effect of Cu concentration on the unit cell of indium oxide can be divided to two effects:

(i) The expansion of the lattice constant for undoped and 1 mol.% Cu doped In_2O_3 films is an indication of interstitial doping (Cu^{2+} ions occupy interstitial sites).

(ii) Contraction of the lattice parameter *a* at 2, 3 and 4 mol.% Cu doping is happened when the dopant (Cu^{2+}) substituted the host cation (In^{3+}) and when the ionic radius of the dopant are lower than the host. This phenomena is possible because the ionic radius of Cu^{2+} ion (R_{Cu} = 0.73 Å) is smaller than the ionic radius of In^{3+} (R_{In} = 0.80 Å).

Furthermore, at higher doping levels (Cu>1 mol.%), the lattice parameter *a* was slightly increased by increasing Cu concentration. This confirmed that In ions substituted by Cu ions in cubic lattice which in turn hence promotes the crystallinity. As reported by Rubel et al. [225], when the ionic radius of dopant is smaller than that of the host, suggesting that when Cu^{2+} replaces In^{3+} in the lattice substitutionally, it results in a smaller lattice constant (*a*) than that of undoped film.

Table VI. 1. 2Theta, lattice constant *a*, crystallite size and strain.

Cu concentrations (mol.%)	2Theta (°)	Lattice constant (Å)	Crystallite size (nm)	Strain ($\times 10^{-3}$)
0	30.47	10.198	12.15	2.8
1	30.08	10.347	11.37	3.0
2	30.65	10.108	12.12	2.9
3	30.72	10.112	11.88	2.9
4	30.59	10.115	11.27	3.0

The calculated crystallite size and strain values for undoped and Cu doped samples at different concentrations are tabulated in Table VI. 1. As can be seen, the crystallite size is decreased from 12.15 nm (Cu = 0 mol.%) to 11.37 nm for the In_2O_3 thin film doped at 1 mol.%. However, opposite tendency is observed for 2 mol.% Cu doping level; that is, the crystallite size is found to increase to reach value 12.12 nm, almost similar to undoped one. After that, the crystallite size decreased again to a minimum value of 11.27 nm for the 4 mol.% Cu doped thin film. This behavior of the crystallite size may be explained by the improvement and deterioration of the crystalline state of the films. In general, the increase of X-ray peak intensity leads to decrease in full width at half maximum (FWHM) indicating enhancement of crystallinity and increase in crystallite size. This result can be confirmed by XRD patterns (see Figure VI.1). In addition, the obtained values of strain were varied from 2.8×10^{-3} to 3.0×10^{-3} for undoped and Cu doped thin films. The minimum value of strain (2.8×10^{-3}) has been recorded for the undoped films, while, the maximum value of strain (3.0×10^{-3}) has been recorded for the films doped at 1 mol.% and 4 mol.%. Moreover, the minimum value of strain (2.9×10^{-3}) obtained for Cu doped films shows that this film is less strained which might be due to the successful replacement of In^{3+} ions with Cu^{2+} ions in the host lattice [226].

VI.2.2. Surface and morphological study

Figure VI. 2 shows the SEM images of undoped and Cu-doped In_2O_3 thin films fabricated by the sol gel spin coating technique with different copper mol.% concentrations. Surface morphology analysis shows that 1, 3 and 4 mol.% Cu doped In_2O_3 thin films exhibit uniform, dense grains and smooth surface, which indicates the good crystal quality of the films. However, at 0 and 2 mol.% Cu doping concentrations, the formation of non-uniform and non-compact agglomerates with few defects such as voids and pores is observed, promoting a rougher and less smooth surface. Furthermore, the undoped, 1 mol.%, 3 mol.% and 4 mol.% Cu-doped In_2O_3 nanostructured films had nearly the same surface morphology.

The elemental analysis of undoped and Cu-doped In_2O_3 thin films was made by energy dispersive X-ray spectroscopy. The EDX spectra of In_2O_3:Cu films (Figure VI. 3) confirm the presence of Cu in the films. The presence of Si element in undoped and Cu-doped In_2O_3 films might be probably from the glass substrate. The weight and atomic percentage compositions of In, Cu and O in the thin films are presented in Table VI.2. It is clearly seen from the table that the amount of In element decreases with increasing Cu content, which very well supports the successful substitution of dopants in the In sites.

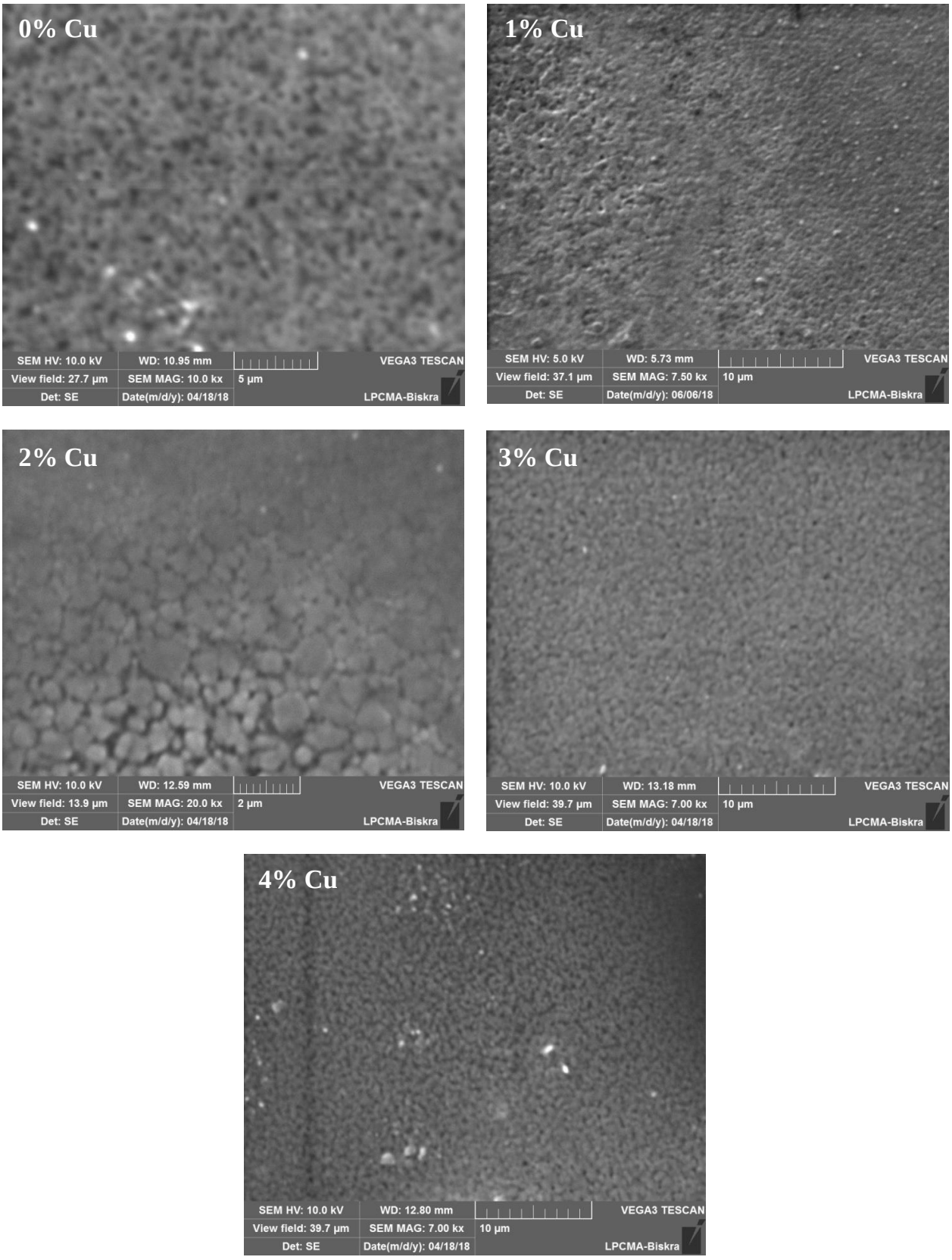

Figure VI. 2. SEM images of pure and Cu doped indium oxide thin films.

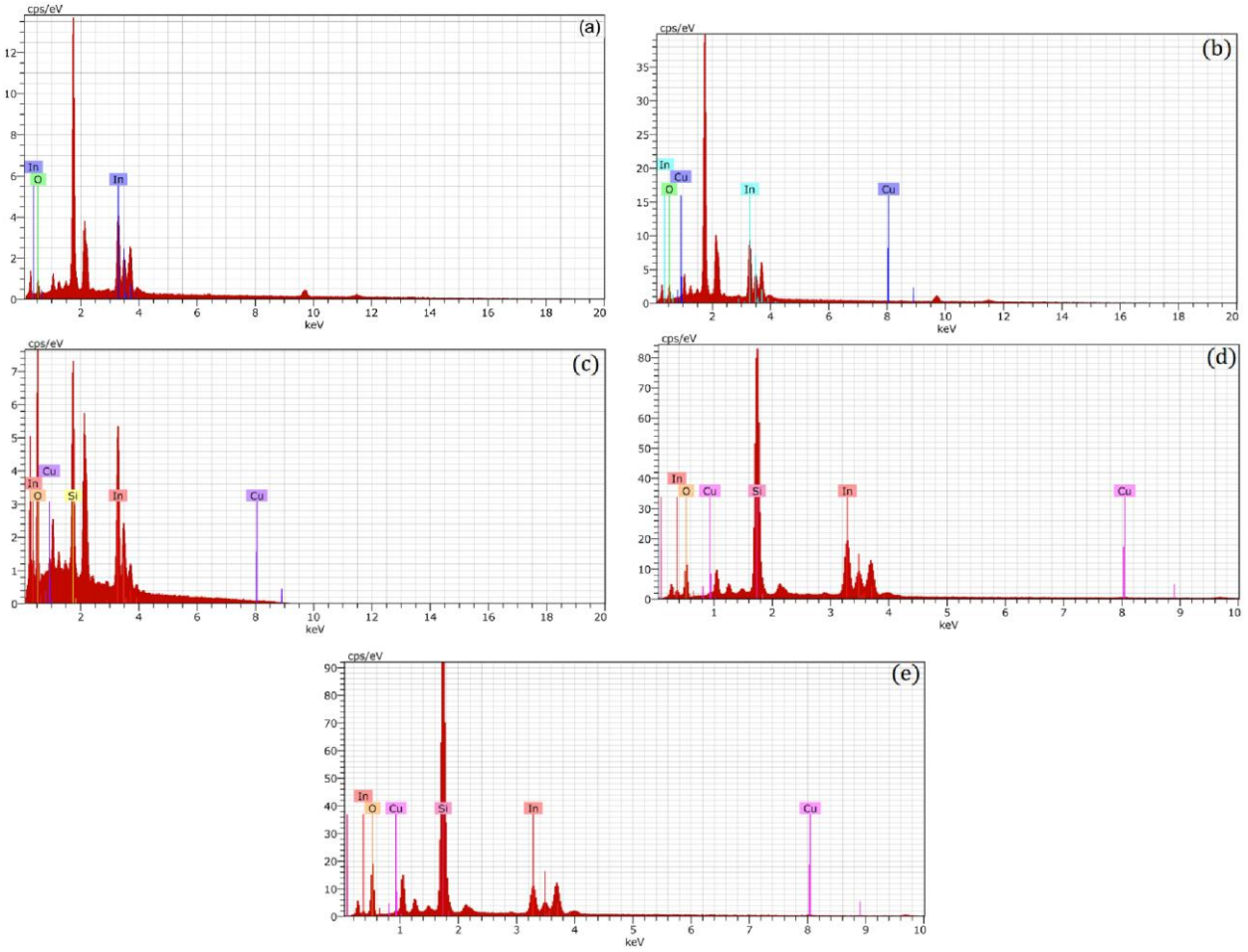

Figure VI. 3. EDX spectra of undoped and Cu-doped In_2O_3 films: (a) undoped, (b) 1 mol.% Cu, (c) 2 mol.% Cu, (d) 3 mol.% Cu, (e) 4 mol.% Cu.

Table VI. 2. Results of quantitative elemental analysis of Cu-doped In_2O_3 thin films.

Material	**Elements**					
	wt.%			at.%		
	In	Cu	O	In	Cu	O
Undoped In_2O_3	66.81	0	17.74	25.63	0	74.07
In_2O_3: 1 mol.%	66.97	0.20	32.83	22.11	0.12	77.78
In_2O_3: 2 mol.%	56.27	2.80	26.37	18.14	1.63	61.03
In_2O_3: 3 mol.%	37.79	1.16	25.91	10.23	0.57	50.32
In_2O_3: 4 mol.%	23.70	0.78	35.65	5.34	0.32	57.63

VI.2.3. Optical study

Figure VI. 4 displays the optical transmittance of prepared thin film samples with various Cu doping concentrations using UV–Vis spectrophotometer at wavelength range 200–1100 nm. The

figure shows that the average transmittance of the films in the visible light range (i.e., 400–800 nm) decreased from 91% to 83% as the doping concentration was increased from 0 to 4 mol.%. The high transmittance value for undoped and Cu doped In_2O_3 thin films may be attributed to its highly crystalline nature [227]. In addition, the high transmission (≥ 80%) is understood because In_2O_3 is a semiconductor with wide direct band gap (>3.5 eV). The high transmittance values of undoped and Cu doped In_2O_3 thin films indicated that the films could be used as a window layer in solar cells. The slight decrease in transmittance at higher doping levels (at 3% and 4%) is credited to an increase in photon scattering due to crystal defects caused by doping or an increase in the metal-to-oxygen ratio in the film [228]. Indeed, the metal-to-oxygen ratio may affect the transmission if the sample is metal-rich; it can result in low transmission [229]. Mugwanga et al. [230] studied Al doped ZnO thin films and showed that the decrease in transmission over the visible range as the concentration of aluminum increases is due to free carriers coupling to the electric field hence increasing the reflection. Furthermore, the optical absorption at the absorption edge corresponds to the transmission from the valence to the conduction band, while the absorption in the visible region corresponds to some localized energy states in the band gap [231].

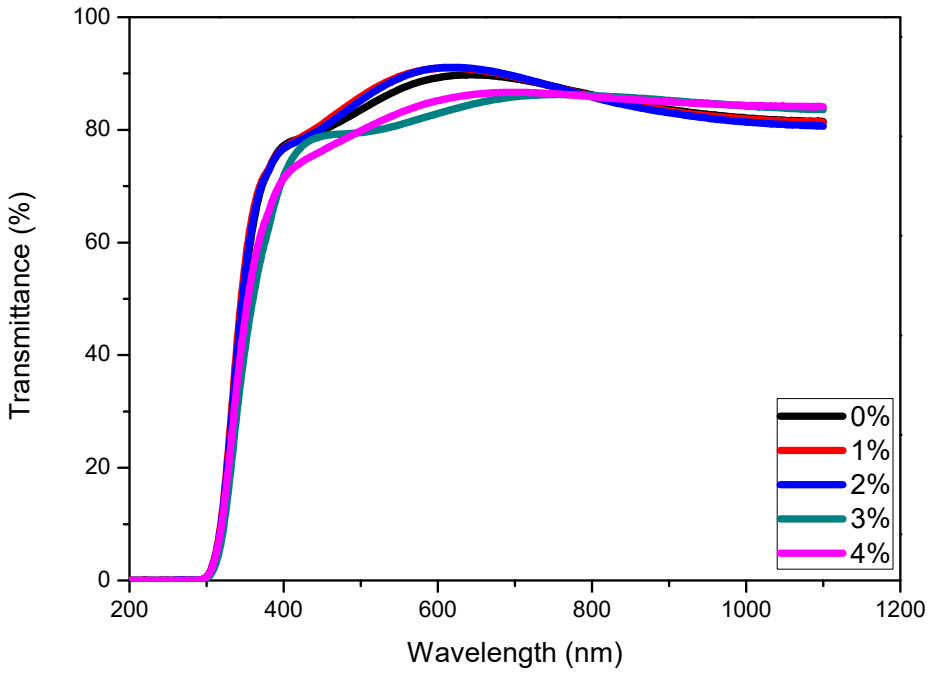

Figure VI. 4. Transmittance of undoped and Cu doped In_2O_3 thin films.

The optical band gap (E_g) and Urbach energy (E_u) of Cu doped indium oxide thin films are shown in Figure VI. 5. The E_g values are 3.98, 4.05, 4.07, 4.01 and 3.99 eV for the undoped and 1 mol.%, 2 mol.%, 3 mol.% and 4 mol.% of Cu-doped In_2O_3 thin films, respectively. Whereas,

the E_u values were found to vary from 246 to 304 meV with increasing Cu doping concentration. From energy gap values we infer two points. One is from the undoped to 2 mol.% Cu doped thin film, we observe that E_g value increases. The second is with the increase in the doping concentration from 2 mol.% to 4 mol.%, we observe that the E_g value decreases. The first one can be explained as follows. It is known that the blue shift of optical band gap can be attributed to the increase of Cu concentration, which creates free carriers in the host In_2O_3. The excess electrons occupy the lowest states in the conduction band and enhance the effective band gap. This behavior is called Burstein-Moss (BM) effect [232–234]. Increase of Fermi level in conduction band due to BM effect is responsible for the increase of energy band gap. According to BM effect, band gap should increases with increase of Cu content. After certain limit of Cu concentration, band gap of sample starts to reduce. Berggren and Sernelius [235] suggest that the exchange and Coulomb interactions among the free carriers in the conduction band and carrier-impurity scattering leads to a downward shift of conduction band and upward shift of valence band. So a renormalization of band gap occurs due to many body effects, such as electron-electron, electron-ion, hole-ion, hole-hole which causes narrowing in the optical band gap of samples [236].

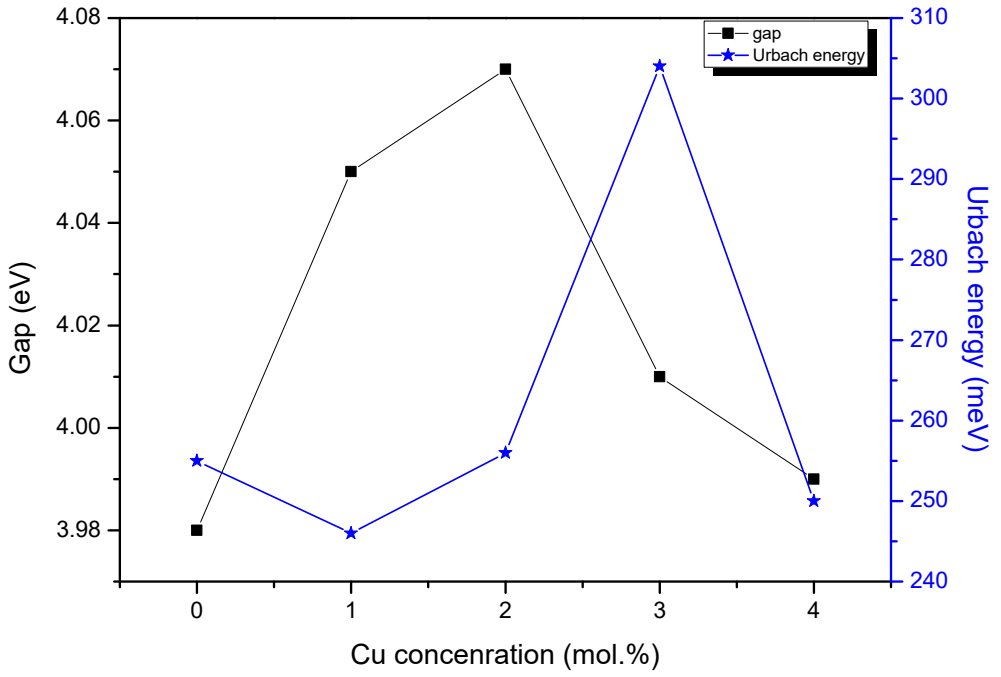

Figure VI. 5. The variation of band gap and Urbach energy.

VI.2.4. Electrical study

The electrical measurements were carried out using a four point probe setup. The variation of

electrical resistivity of In_2O_3 films as a function of Cu-doping concentration is shown in Figure VI. 6. As can be seen, all films exhibit a low resistivity about 1.77×10^{-3} – 6.34×10^{-3} (Ω.cm). Typically, non-stoichiometric undoped In_2O_3 thin films exhibit low resistivity due to the native defects of oxygen vacancies and indium interstitials [237]. We found that the resistivity increase from 1.77×10^{-3} at 0 mol.% Cu to 6.34×10^{-3} (Ω.cm) at 3 mol.% Cu concentration. It is known that Cu atoms are expected to be acceptors when substituting In atoms in In_2O_3. Oxygen vacancies (V_O) and interstitial indium (In_i) are donors in In_2O_3 while interstitial oxygen (O_i) and indium vacancies (V_{In}) are acceptors in In_2O_3 [238,239]. The electron density is compensated by holes generated by acceptors, especially substitutional Cu atoms, and hence the resistivity is increased. Increasing Cu content will result in stronger compensation and hence larger resistivity. As reported by Islam et al. [214], the reason for the increase in resistivity is that some Cu atoms may form defects such as CuO and/or Cu_2O, which acts as a carrier traps rather than electron donors. However, at 4 mol.% Cu doped film, the electrical resistivity decreased to reach value 1.79×10^{-3} (Ω.cm) close to the resistivity value of undoped In_2O_3 film. This could be related to the deterioration of crystallinity, thereby enhancement in lattice distortion. This result can be confirmed by XRD data.

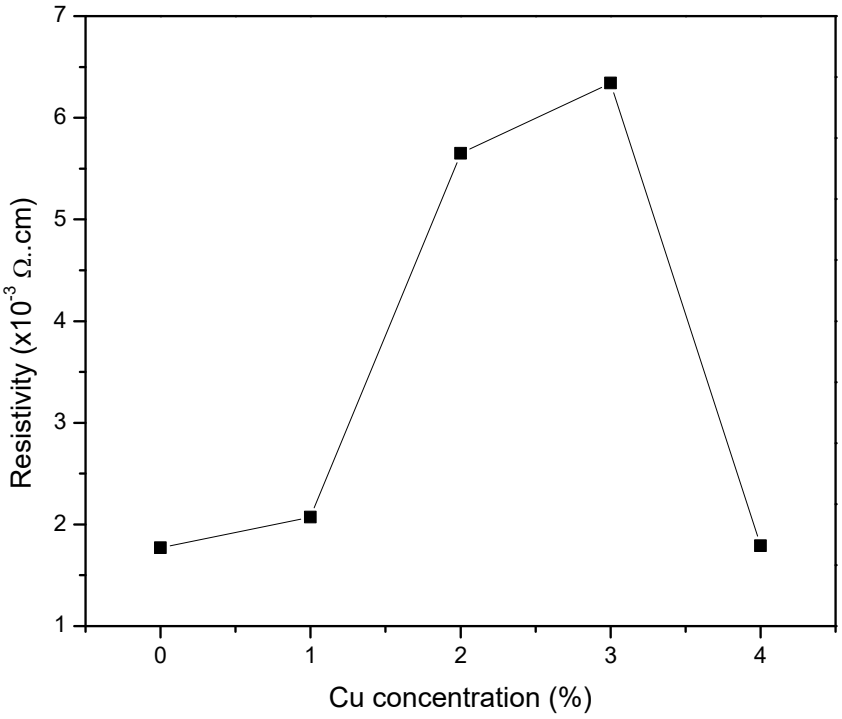

Figure VI. 6. Resistivity of prepared Cu doped In_2O_3 thin films.

VI.3. Conclusion

High quality In_2O_3 and Cu-doped In_2O_3 nanocrystals thin films have been prepared by a simple sol–gel method followed spin coating technique. All films have polycrystalline phase of In_2O_3 cubic structure. However, the trace of secondary phase related to Cu compound has been detected for 2, 3 and 4 mol.% of Cu samples corresponding to the cubic structure of Cu_2O phase. This means that Cu dopant is strongly affects the microstructure of In_2O_3 system. The lattice constant for undoped and Cu doped In_2O_3 films is found to be vary in the range of 10.108-10.347 Å. While, the values of crystallite size and strain were found to be about 11.27–12.15 nm and 2.8×10^{-3}–3.0×10^{-3}, respectively. The optical transmittance decreased with the increment of Cu doping concentration from 91% to 83% in the visible region. The band gap values of the pure and Cu-doped In_2O_3 films have been found to increase from 3.98 to 4.07 eV when Cu ≤ 2 mol.% and decrease to 3.99 eV when Cu > 2 mol.%. All films exhibit a low resistivity in the range of 1.77×10^{-3} – 6.34×10^{-3} (Ω.cm) made them susceptible for application in photovoltaic field.

CONCLUSION AND FUTURE OUTLOOK

Undoped and doped In_2O_3 thin films have been successfully prepared by sol gel via spin coating technique for optoelectronic and photovoltaic applications. The films have been deposited on glass substrates. The structural and optical properties of the deposited films have been analyzed using X-ray diffraction (XRD), UV-VIS spectroscopy, photoluminescence spectroscopy (PL) and Fourier transform infrared spectroscopy (FTIR). The chemical state of elements in the deposited films has been analyzed using energy dispersive X-ray spectroscopy (EDX). The electrical properties of the deposited films have been obtained by four probes method.

Based on the results obtained from four parts of the present work, the following conclusions are made:

Effect of molar concentration on structural, morphological, optical and electrical properties of In_2O_3 thin films has been investigated. XRD analysis confirms the cubic structure of the deposited films with a preferential (222) orientation. SEM images showed the homogenous and uniform distribution of In_2O_3 films without any voids or cracks. EDX spectra revealed the presence of In and O elements in the prepared films. Films exhibited a high optical transparency that reaches up to 90% in the visible range. In addition, the optical band gap energy (E_g) decreases from 4.04 to 3.88 eV. The room temperature PL measurements revealed three peaks corresponding to the NBE (peak at 390 nm) and DL emissions (peaks at 485 and 532 nm). The presence of In–O and In–O–H absorption bands has been confirmed by FTIR. The electrical conductivity increases from 0.58 to 25 $(\Omega.cm)^{-1}$.

The annealing temperature impact on the structural and optical properties of In_2O_3 thin films deposited on glass substrates has been discussed. All the films exhibited a preferred (222) orientation due to minimization free surface energy. As the annealing temperature increases, the intensity of the (222) peak increases indicating that the crystalline quality of the deposited films improves upon annealing. Analysis of UV-VIS spectra revealed that the transmittance of the films increased from 80% to 86% in the visible region with increasing annealing temperature. Also, optical band gap decreases from 3.98 to 3.47 eV and electrical resistivity of the films decreases from 67.07 to 14.05 Ω.cm as annealing temperature increase.

Titanium doped In_2O_3 thin films have been deposited on microscopic glass substrates. XRD patterns revealed that Ti doped In_2O_3 films are polycrystalline with a preferential (222) plane of

cubic structure irrespective of the Ti doping level. The observed change in main (222) peak position confirms the substitutions of Ti atoms in In_2O_3 lattice. The grain size was found to decrease from 13.29 to 6.98 with Ti doping enhanced. The films exhibit high transmittance up to 93% at 10 and 15 mol.% of Ti concentrations with no big change in optical band gap (4 – 4.02 eV). The room temperature photoluminescence spectra of Ti doped In_2O_3 films show four emission peaks: UV emission peak (at 386 nm), violet emission peak (at 435 nm), blue emission peaks (at 477 nm) and green emission peak (at 522 nm). FTIR spectra confirmed the presence of In–O, C–C–H, C–H and CH_2 stretching vibration bonds. The conductivity of thin films effectively reduces from 7.02 to 7×10^{-2} $(\Omega.cm)^{-1}$ with increase Ti doping concentration.

Undoped and Cu doped In_2O_3 thin films have been deposited on glass substrates. All films have polycrystalline nature of In_2O_3 cubic structure with detecting the presence of secondary phase (110) plane related to Cu compound corresponding to the cubic structure of Cu_2O phase. The peak intensity of the (222) plane is stronger in both undoped and Cu doped films. The lattice constant for undoped and Cu doped In_2O_3 films is found to be vary in the range of 10.108-10.347 nm. UV-Visible analyses revealed a decrease of films transmission from 91% to 83% in the visible region with increasing Cu concentration. The band gap values of the pure and Cu-doped In_2O_3 films were in the range 3.98 – 4.07 eV. All films revealed a low resistivity in the range of 1.77×10^{-3} – 6.34×10^{-3} (Ω.cm) make these films suitable for optoelectronic applications.

In the present work, an attempt is made to optimize transparent conducting properties of In_2O_3 films using sol gel spin coating technique which make them a suitable for optoelectronic applications. To achieve this goal, several process parameters like molar concentration, annealing temperature, Ti and Cu doping level are investigated. Among these parameters, doping the In_2O_3 films by Cu is the most successful and efficient for the better electrical conductivity and optical transmittance of the films, which make these films suitable for optoelectronic applications such as solar cells and gas sensors.

Transparent conducting films deposited on rigid glass substrates have been extensively studied in recent years, because they combine the attractive features of highly visible transparency and electrical conductivity. However, as well known, glass is too heavy and brittle and may be easily deformed, especially in certain applications, such as smart card, electronic mapping and flat panel displays where flexibility and lightweight are needed. Therefore transparent conducting films deposited on flexible substrates such as polyimide and polyethylene terephthalate (PET) could overcome these problems and it is necessary to investigate the characteristics of the oxide thin films deposited on flexible substrates. Furthermore, finding a way to improve the electrical properties of the In_2O_3 thin films prepared by sol gel spin coating

process is needed. So varying other parameters could be necessary such as rotation speed of the substrate, pre-heating temperature, substrates type (like silicon, ITO…etc), precursors type and co-doping...etc.

REFERENCES

[1] M. Qin, J. Ma, W. Ke, P. Qin, H. Lei, H. Tao, X. Zheng, L. Xiong, Q. Liu, Z. Chen, Perovskite solar cells based on low-temperature processed indium oxide electron selective layers, ACS Appl. Mater. Interfaces. 8 (2016) 8460–8466.

[2] J. Kennedy, P.P. Murmu, J. Leveneur, V.M. Williams, R.L. Moody, T. Maity, S.V. Chong, Enhanced power factor and increased conductivity of aluminum doped zinc oxide thin films for thermoelectric applications, J. Nanosci. Nanotechnol. 18 (2018) 1384–1387.

[3] Z. Chen, W. Li, R. Li, Y. Zhang, G. Xu, H. Cheng, Fabrication of highly transparent and conductive indium–tin oxide thin films with a high figure of merit via solution processing, Langmuir. 29 (2013) 13836–13842.

[4] P. Chen, X. Yin, M. Que, X. Liu, W. Que, Low temperature solution processed indium oxide thin films with reliable photoelectrochemical stability for efficient and stable planar perovskite solar cells, J. Mater. Chem. A. 5 (2017) 9641–9648.

[5] T.A. Kuku, Heat mirror characteristics of photolytically produced indium tin oxide thin films, Sol. Wind Technol. 3 (1986) 53–58.

[6] E.J. Bjornard, W.A. Meredith Jr, Antireflection coating for a temperature sensitive substrate, 1996.

[7] W.-Y. Chung, G. Sakai, K. Shimanoe, N. Miura, D.-D. Lee, N. Yamazoe, Preparation of indium oxide thin film by spin-coating method and its gas-sensing properties, Sens. Actuators B Chem. 46 (1998) 139–145.

[8] S.K. Park, J.I. Han, W.K. Kim, M.G. Kwak, Deposition of indium–tin-oxide films on polymer substrates for application in plastic-based flat panel displays, Thin Solid Films. 397 (2001) 49–55.

[9] N. Tripathi, S. Rath, V. Ganesan, R.J. Choudhary, Growth dynamics of pulsed laser deposited indium oxide thin films: a substrate dependent study, Appl. Surf. Sci. 256 (2010) 7091–7095.

[10] X. Li, W. Miao, Q. Zhang, L. Huang, Z. Zhang, Z. Hua, Preparation of molybdenum-doped indium oxide thin films using reactive direct-current magnetron sputtering, J. Mater. Res. 20 (2005) 1404–1408.

[11] S.M. Rozati, T. Ganj, Transparent conductive Sn-doped indium oxide thin films deposited by spray pyrolysis technique, Renew. Energy. 29 (2004) 1671–1676.

[12] A. Attaf, A. Bouhdjer, H. Saidi, M.S. Aida, N. Attaf, H. Ezzaouia, On tuning the preferential crystalline orientation of spray pyrolysis deposited indium oxide thin films, Thin Solid Films. 625 (2017) 177–179.

[13] L. Dong, G.S. Zhu, H.R. Xu, X.P. Jiang, X.Y. Zhang, Y.Y. Zhao, D.L. Yan, L. Yuan, A.B. Yu, Preparation of indium tin oxide (ITO) thin film with (400) preferred orientation by sol–gel spin coating method, J. Mater. Sci. Mater. Electron. 30 (2019) 8047–8054.

[14] F. Shan, S.W. Chang, J.-H. Koh, S.-J. Kim, Effect of Spin Coating Speed on the Electrical Performances of Solution-Processed Indium Zinc Oxide Thin-Film Transistors, J. Nanosci. Nanotechnol. 16 (2016) 12871–12874.

[15] S. Ullah, R. Branquinho, A. Santa, F. De Matteis, R. Martins, I. Davoli, G. Gonçalves, E. Fortunato, Boosting highly transparent and conducting indium zinc oxide thin films through solution combustion synthesis: influence of rapid thermal annealing, Semicond. Sci. Technol. 33 (2018) 105004.

[16] M. Misra, D.-K. Hwang, Y.C. Kim, J.-M. Myoung, T.I. Lee, Eco-friendly method of fabricating indium-tin-oxide thin films using pure aqueous sol-gel, Ceram. Int. 44 (2018) 2927–2933.

[17] T.J. Coutts, T.O. Mason, J.D. Perkins, D.S. Ginley, Transparent conducting oxides: status and opportunities in basic research, Proc Electrochem Soc. 99 (1999) 274–288.

[18] S.A. Knickerbocker, A.K. Kulkarni, Calculation of the figure of merit for indium tin oxide films based on basic theory, J. Vac. Sci. Technol. Vac. Surf. Films. 13 (1995) 1048–1052.

[19] K. Badeker, Electrical conductivity and thermo-electromotive force of some metallic compounds, Ann Phys. 22 (1907) 749.

[20] A.J. Freeman, K.R. Poeppelmeier, T.O. Mason, R.P.H. Chang, T.J. Marks, Chemical and Thin-Film Strategies for New Transparent Conducting Oxides, MRS Bull. 25 (2000) 45–51.

[21] M.M. Bagheri-Mohagheghi, M. Shokooh-Saremi, The influence of Al doping on the electrical, optical and structural properties of SnO_2 transparent conducting films deposited by the spray pyrolysis technique, J. Phys. Appl. Phys. 37 (2004) 1248.

[22] Y. Shigesato, N. Shin, M. Kamei, P.K. Song, I. Yasui, Study on fluorine-doped indium oxide films deposited by RF magnetron sputtering, Jpn. J. Appl. Phys. 39 (2000) 6422.

[23] K.L. Chopra, S. Major, D.K. Pandya, Transparent conductors—a status review, Thin Solid Films. 102 (1983) 1–46.

[24] A.L. Dawar, J.C. Joshi, Semiconducting transparent thin films: their properties and applications, J. Mater. Sci. 19 (1984) 1–23.

[25] T.J. Coutts, X. Wu, W.P. Mulligan, J.M. Webb, High-performance, transparent conducting oxides based on cadmium stannate, J. Electron. Mater. 25 (1996) 935–943.

[26] T. Minami, New n-type transparent conducting oxides, MRS Bull. 25 (2000) 38–44.

[27] H. Enoki, T. Nakayama, J. Echigoya, The Electrical and Optical Properties of the ZnO-

SnO_2 Thin Films Prepared by RF Magnetron Sputtering, Phys. Status Solidi A. 129 (1992) 181–191.

[28] H. Un'no, N. Hikuma, T. Omata, N. Ueda, T. Hashimoto, H. Kawazoe, Preparation of $MgIn_2O_{4-X}$ Thin Films on Glass Substrate by RF Sputtering, Jpn. J. Appl. Phys. 32 (1993) L1260.

[29] T. Minami, H. Sonohara, S. Takata, H. Sato, Highly Transparent and Conductive Zinc-Stannate Thin Films Prepared by RF Magnetron Sputtering, Jpn. J. Appl. Phys. 33 (1994) L1693.

[30] R.J. Cava, J.M. Phillips, J. Kwo, G.A. Thomas, R.B. Van Dover, S.A. Carter, J.J. Krajewski, W.F. Peck Jr, J.H. Marshall, D.H. Rapkine, $GaInO_3$: A new transparent conducting oxide, Appl. Phys. Lett. 64 (1994) 2071–2072.

[31] S.C. Dixon, D.O. Scanlon, C.J. Carmalt, I.P. Parkin, n-Type doped transparent conducting binary oxides: an overview, J. Mater. Chem. C. 4 (2016) 6946–6961.

[32] Y. Liu, Y. Li, H. Zeng, ZnO-Based Transparent Conductive Thin Films: Doping, Performance, and Processing, J. Nanomater. 2013 (2013) e196521.

[33] D.O. Scanlon, G.W. Watson, On the possibility of p-type SnO_2, J. Mater. Chem. 22 (2012) 25236–25245.

[34] A. Walsh, J. Buckeridge, C.R.A. Catlow, A.J. Jackson, T.W. Keal, M. Miskufova, P. Sherwood, S.A. Shevlin, M.B. Watkins, S.M. Woodley, A.A. Sokol, Limits to Doping of Wide Band Gap Semiconductors, Chem. Mater. 25 (2013) 2924–2926.

[35] D.J. Griffiths, Introduction to Electrodynamics, 3rd edition, Prentice Hall, Upper Saddle River, N.J, 1999.

[36] E.C. Jordan, K.G. Balmain, Electromagnetic waves and radiating systems, (1968).

[37] M.V.G. Menon, K. Ravindran, R.R. Nayar, P.K. Nair, K.P. Rao, N.A. Menon, Properties of elemental materials, TATA McGraw-Hill Publishing Co. Ltd., Bombay-New Delhi, 1972.

[38] E.A. Forsh, A.M. Abakumov, V.B. Zaytsev, E.A. Konstantinova, P.A. Forsh, M.N. Rumyantseva, A.M. Gaskov, P.K. Kashkarov, Optical and photoelectrical properties of nanocrystalline indium oxide with small grains, Thin Solid Films. 595 (2015) 25–31.

[39] S.A. Palomares-Sanchez, B.E. Watts, D. Klimm, A. Baraldi, A. Parisini, S. Vantaggio, R. Fornari, Sol-gel growth and characterization of In_2O_3 thin films, Thin Solid Films. 645 (2018) 383–390.

[40] M. Girtan, G. Folcher, Structural and optical properties of indium oxide thin films prepared by an ultrasonic spray CVD process, Surf. Coat. Technol. 172 (2003) 242–250.

[41] R.L. Weiher, R.P. Ley, Optical properties of indium oxide, J. Appl. Phys. 37 (1966) 299–

302.

[42] P. Erhart, A. Klein, R.G. Egdell, K. Albe, Band structure of indium oxide: Indirect versus direct band gap, Phys. Rev. B. 75 (2007) 153205.

[43] E. Fortunato, D. Ginley, H. Hosono, D.C. Paine, Transparent conducting oxides for photovoltaics, MRS Bull. 32 (2007) 242–247.

[44] C. Wang, V. Cimalla, G. Cherkashinin, H. Romanus, M. Ali, O. Ambacher, Transparent conducting indium oxide thin films grown by low-temperature metal organic chemical vapor deposition, Thin Solid Films. 515 (2007) 2921–2925.

[45] C.G. Granqvist, Transparent conductive electrodes for electrochromic devices: a review, Appl. Phys. A. 57 (1993) 19–24.

[46] D. Zhang, C. Li, S. Han, X. Liu, T. Tang, W. Jin, C. Zhou, Ultraviolet photodetection properties of indium oxide nanowires, Appl. Phys. A. 77 (2003) 163–166.

[47] S.-Z. Huang, L.I.N. Wei, W.-Z. Chen, Gas sensitivity of indium oxide, Trans. Nonferrous Met. Soc. China. 19 (2009) s80–s82.

[48] O. Bierwagen, Indium oxide—a transparent, wide-band gap semiconductor for (opto) electronic applications, Semicond. Sci. Technol. 30 (2015) 024001.

[49] J.R. Bellingham, W.A. Phillips, C.J. Adkins, Electrical and optical properties of amorphous indium oxide, J. Phys. Condens. Matter. 2 (1990) 6207.

[50] Y.-H. Tak, K.-B. Kim, H.-G. Park, K.-H. Lee, J.-R. Lee, Criteria for ITO (indium–tin-oxide) thin film as the bottom electrode of an organic light emitting diode, Thin Solid Films. 411 (2002) 12–16.

[51] D.S. Bhachu, D.O. Scanlon, G. Sankar, T.D. Veal, R.G. Egdell, G. Cibin, A.J. Dent, C.E. Knapp, C.J. Carmalt, I.P. Parkin, Origin of high mobility in molybdenum-doped indium oxide, Chem. Mater. 27 (2015) 2788–2796.

[52] Y. Abe, N. Ishiyama, Titanium-doped indium oxide films prepared by dc magnetron sputtering using ceramic target, J. Mater. Sci. 41 (2006) 7580–7584.

[53] S.K. Vishwanath, T. An, W.-Y. Jin, J.-W. Kang, J. Kim, The optoelectronic properties of tungsten-doped indium oxide thin films prepared by polymer-assisted solution processing for use in organic solar cells, J. Mater. Chem. C. 5 (2017) 10295–10301.

[54] S. Cho, Structural, optical, and electrical properties of RF-sputtered indium oxide thin films, J. Korean Phys. Soc. 60 (2012) 2058–2062.

[55] R.W.G. Wyckoff, Crystal structures, John Wiley & Sons, 1964.

[56] D.E. Proffit, D.B. Buchholz, R.P. Chang, M.J. Bedzyk, T.O. Mason, Q. Ma, X-ray absorption spectroscopy study of the local structures of crystalline Zn–In–Sn oxide thin films, J. Appl. Phys. 106 (2009) 113524.

[57] C.R. Stanek, K.J. McClellan, B.P. Uberuaga, K.E. Sickafus, M.R. Levy, R.W. Grimes, Determining the site preference of trivalent dopants in bixbyite sesquioxides by atomic-scale simulations, Phys. Rev. B. 75 (2007) 134101.

[58] Y. Liu, W. Xu, D.-B. Liu, M. Yu, Y.-H. Lin, C.-W. Nan, Enhanced thermoelectric properties of Ga-doped In_2O_3 ceramics via synergistic band gap engineering and phonon suppression, Phys. Chem. Chem. Phys. 17 (2015) 11229–11233.

[59] D.B. Buchholz, Q. Ma, D. Alducin, A. Ponce, M. Jose-Yacaman, R. Khanal, J.E. Medvedeva, R.P. Chang, The structure and properties of amorphous indium oxide, Chem. Mater. 26 (2014) 5401–5411.

[60] R.D. Shannon, New high pressure phases having the corundum structure, Solid State Commun. 4 (1966) 629–630.

[61] M. Epifani, P. Siciliano, A. Gurlo, N. Barsan, U. Weimar, Ambient pressure synthesis of corundum-type In_2O_3, J. Am. Chem. Soc. 126 (2004) 4078–4079.

[62] R. Bel Hadj Tahar, T. Ban, Y. Ohya, Y. Takahashi, Tin doped indium oxide thin films: Electrical properties, J. Appl. Phys. 83 (1998) 2631–2645.

[63] J.C. Fan, J.B. Goodenough, X-ray photoemission spectroscopy studies of Sn-doped indium-oxide films, J. Appl. Phys. 48 (1977) 3524–3531.

[64] N. Balasubramanian, A. Subrahmanyam, Electrical and optical properties of reactively evaporated indium tin oxide (ITO) films-dependence on substrate temperature and tin concentration, J. Phys. Appl. Phys. 22 (1989) 206.

[65] L. Gupta, A. Mansingh, P.K. Srivastava, Band gap narrowing and the band structure of tin-doped indium oxide films, Thin Solid Films. 176 (1989) 33–44.

[66] J. Szczyrbowski, A. Dietrich, H. Hoffmann, Optical and electrical properties of RF-sputtered indium–tin oxide films, Phys. Status Solidi A. 78 (1983) 243–252.

[67] K. Sreenivas, T. Sudersena Rao, A. Mansingh, S. Chandra, Preparation and characterization of rf sputtered indium tin oxide films, J. Appl. Phys. 57 (1985) 384–392.

[68] N.V. Joshi, Photoconductivity: Art: Science & Technology, Routledge, 2017.

[69] P. Dulal, Optoelectronic Characteristics of Indium Oxide Thin Films, PhD Thesis, Bowling Green State University, 2019.

[70] S. Chaudhuri, A.K. Pal, Development of InP-based solar cells with indium tin oxide films prepared by reactive dc sputtering, Thin Solid Films. 119 (1984) 1–4.

[71] Y. Shigesato, S. Takaki, T. Haranoh, Electrical and structural properties of low resistivity tin-doped indium oxide films, J. Appl. Phys. 71 (1992) 3356–3364.

[72] D. Beena, K.J. Lethy, R. Vinodkumar, V.P. MahadevanPillai, Influence of substrate temperature on the properties of laser ablated indium tin oxide films, Sol. Energy Mater.

Sol. Cells. 91 (2007) 1438–1443.

[73] A. Salehi, The effects of deposition rate and substrate temperature of ITO thin films on electrical and optical properties, Thin Solid Films. 324 (1998) 214–218.

[74] C.G. Granqvist, Radiative heating and cooling with spectrally selective surfaces, Appl. Opt. 20 (1981) 2606–2615.

[75] S.T. Shishiyanu, T.S. Shishiyanu, O.I. Lupan, Sensing characteristics of tin-doped ZnO thin films as NO_2 gas sensor, Sens. Actuators B Chem. 107 (2005) 379–386.

[76] C. Li, D. Zhang, S. Han, X. Liu, T. Tang, C. Zhou, Diameter-controlled growth of single-crystalline In_2O_3 nanowires and their electronic properties, Adv. Mater. 15 (2003) 143–146.

[77] D. Liu, W.W. Lei, B. Zou, S.D. Yu, J. Hao, K. Wang, B.B. Liu, Q.L. Cui, G.T. Zou, High-pressure x-ray diffraction and Raman spectra study of indium oxide, J. Appl. Phys. 104 (2008) 083506.

[78] Z.L. Wang, J. Song, Piezoelectric nanogenerators based on zinc oxide nanowire arrays, Science. 312 (2006) 242–246.

[79] Z.W. Pan, Z.R. Dai, Z.L. Wang, Nanobelts of semiconducting oxides, Science. 291 (2001) 1947–1949.

[80] W.S. Seo, H.H. Jo, K. Lee, J.T. Park, Preparation and Optical Properties of Highly Crystalline, Colloidal, and Size-Controlled Indium Oxide Nanoparticles, Adv. Mater. 15 (2003) 795–797.

[81] C. Li, D. Zhang, X. Liu, S. Han, T. Tang, J. Han, C. Zhou, In_2O_3 nanowires as chemical sensors, Appl. Phys. Lett. 82 (2003) 1613–1615.

[82] K. Soulantica, L. Erades, M. Sauvan, F. Senocq, A. Maisonnat, B. Chaudret, Synthesis of indium and indium oxide nanoparticles from indium cyclopentadienyl precursor and their application for gas sensing, Adv. Funct. Mater. 13 (2003) 553–557.

[83] C. Li, B. Lei, D. Zhang, X. Liu, S. Han, T. Tang, M. Rouhanizadeh, T. Hsiai, C. Zhou, Chemical gating of In_2O_3 nanowires by organic and biomolecules, Appl. Phys. Lett. 83 (2003) 4014–4016.

[84] X. Li, M.W. Wanlass, T.A. Gessert, K.A. Emery, T.J. Coutts, High-efficiency indium tin oxide/indium phosphide solar cells, Appl. Phys. Lett. 54 (1989) 2674–2676.

[85] H. Zhou, W. Cai, L. Zhang, Photoluminescence of indium–oxide nanoparticles dispersed within pores of mesoporous silica, Appl. Phys. Lett. 75 (1999) 495–497.

[86] M.J. Zheng, L.-D. Zhang, G.-H. Li, X.Y. Zhang, X.F. Wang, Ordered indium-oxide nanowire arrays and their photoluminescence properties, Appl. Phys. Lett. 79 (2001) 839–841.

[87] H. Cao, X. Qiu, Y. Liang, Q. Zhu, M. Zhao, Room-temperature ultraviolet-emitting In_2O_3 nanowires, Appl. Phys. Lett. 83 (2003) 761–763.

[88] Q. Ma, H.-M. Zheng, Y. Shao, B. Zhu, W.-J. Liu, S.-J. Ding, D.W. Zhang, Atomic-layer-deposition of indium oxide nano-films for thin-film transistors, Nanoscale Res. Lett. 13 (2018) 4.

[89] M. Sawada, M. Higuchi, S. Kondo, H. Saka, Characteristics of indium-tin-oxide/silver/indium-tin-oxide sandwich films and their application to simple-matrix liquid-crystal displays, Jpn. J. Appl. Phys. 40 (2001) 3332.

[90] H. Kim, J.S. Horwitz, G.P. Kushto, S.B. Qadri, Z.H. Kafafi, D.B. Chrisey, Transparent conducting Zr-doped In_2O_3 thin films for organic light-emitting diodes, Appl. Phys. Lett. 78 (2001) 1050–1052.

[91] G. Korotcenkov, V. Brinzari, A. Cerneavschi, M. Ivanov, V. Golovanov, A. Cornet, J. Morante, A. Cabot, J. Arbiol, The influence of film structure on In_2O_3 gas response, Thin Solid Films. 460 (2004) 315–323.

[92] J.E. Mahan, Physical vapor deposition of thin films, Wiley-Interscience, 2000.

[93] D.M. Mattox, Handbook of Physical Vapor Deposition, William Andrew, 1998.

[94] D.M. Mattox, V.H. Mattox, 50 years of vacuum coating technology and the growth of the Society of Vacuum Coaters, Society of Vacuum Coaters, (2007).

[95] D.M. Mattox, The Foundations of Vacuum Coating Technology, Springer-Verlag, 2003.

[96] L. Eckertová, Physics of Thin Films, Springer Science & Business Media, 2012.

[97] R. Behrisch, Sputtering by Particle Bombardment I: Physical Sputtering of Single-Element Solids, Springer-Verlag, 1981.

[98] W. Westwood, Sputter deposition, AVS Education Committee, 2003.

[99] A.Y. Cho, Growth of III–V semiconductors by molecular beam epitaxy and their properties, Thin Solid Films. 100 (1983) 291–317.

[100] J.E. Reynolds, XXV.—On the synthesis of galena by means of thiocarbamide, and the deposition of lead sulphide as a specular film, J. Chem. Soc. 45 (1884) 162.

[101] K. Chattopadhyay, A. Banerjee, Introduction to Nanoscience and Nanotechnology, Prentice Hall of India, 2009.

[102] D. Dobkin, M.K. Zuraw, Principles of chemical vapor deposition, Springer Science & Business Media, 2003.

[103] Y. Yun, Recent Advances in Carbon Capture and Storage, InTechOpen, 2017.

[104] C.J. Brinker, G.W. Scherer, Sol-gel sciences, Academic Press, 1990.

[105] L.E. Scriven, C.J. Brinker, D.E. Clark, D.R. Ulrich, Better ceramics through chemistry III, Mat Res Soc, 1988.

[106] C.J. Brinker, A.J. Hurd, G.C. Frye, P.R. Schunk, C.S. Ashley, Sol-gel thin film formation, J. Ceram. Soc. Jpn. 99 (1991) 862–877.

[107] D.E. Bornside, C.W. Macosko, L.E. Scriven, Modeling of Spin Coating, J. Imaging Technol. 13 (1987) 122–130.

[108] K.H. Stern, Metallurgical and Ceramic Protective Coatings, Springer Science & Business Media, 2012.

[109] M. Lottiaux, C. Boulesteix, G. Nihoul, F. Varnier, F. Flory, R. Galindo, E. Pelletier, Morphology and structure of TiO_2 thin layers vs. thickness and substrate temperature, Thin Solid Films. 170 (1989) 107–126.

[110] L.L. Hench, D.R. Ulrich, Ultrastructure Processing of Ceramics, Glasses, and Composites, Wiley-Interscience, 1984.

[111] S.J. Kang, Y.H. Joung, H.H. Shin, Y.S. Yoon, Effect of substrate temperature on structural, optical and electrical properties of ZnO thin films deposited by pulsed laser deposition, J. Mater. Sci. Mater. Electron. 19 (2008) 1073–1078.

[112] Y. Raviprakash, K.V. Bangera, G.K. Shivakumar, Preparation and characterization of $Cd_xZn_{1-x}S$ thin films by spray pyrolysis technique for photovoltaic applications, Sol. Energy. 83 (2009) 1645–1651.

[113] B.K. Gupta, O.P. Agnihotri, Structural investigations of spray-deposited CdS films doped with Cu, In and Ga, Philos. Mag. B. 37 (1978) 631–633.

[114] B.E. Warren, X-ray Diffraction, Addison-Wesley, 1969.

[115] Y. Zhao, J. Zhang, Microstrain and grain-size analysis from diffraction peak width and graphical derivation of high-pressure thermomechanics, J. Appl. Crystallogr. 41 (2008) 1095–1108.

[116] F. Szekely, I. Groma, J. Lendvai, Characterization of self-similar dislocation structures by X-ray diffraction, Mater. Sci. Eng. A. 324 (2002) 179–182.

[117] S.T. Thornton, A. Rex, Modern physics for scientists and engineers, Cengage Learning, 2012.

[118] S. Yilmaz, H.B. Ozmen, High performance concrete technology and applications, IntechOpen, 2016.

[119] B.D. Cullity, Elements of x-ray diffraction, Addison-Wesley Publishing Company, 1978.

[120] H.S. Kim, C.S. Kim, S.G. Kim, Preparation of nickel oxide–and nickel–silica nanocomposites by spray pyrolysis, J. Non-Cryst. Solids. 352 (2006) 2204–2212.

[121] M. Walock, Nanocomposite coatings based on quaternary metalnitrogen, PhD Thesis, University of Alabama, 2012.

[122] P.Z. Zambare, Synthesis and characterization of trivalent (Er^{3+}, Tb^{3+}) doped with Sr_2CeO_4

phosphor, Ashok Yakkaldevi, 2017.

[123] J. Solé, L. Bausa, D. Jaque, An introduction to the optical spectroscopy of inorganic solids, John Wiley & Sons, 2005.

[124] R.M. Mohite, Studies of doped and undoped nanostructured zinc oxide thin films for solar cell application, PhD Thesis, Solapur University, 2015.

[125] S. Sheth, Synthesis and Characterization of Catalysts for Photo-oxidation of Water, PhD Thesis, University of Paris-Sud, 2013.

[126] D. Bao, X. Wu, L. Zhang, X. Yao, Preparation, electrical and optical properties of (Pb, Ca) TiO_3 thin films using a modified sol-gel technique, Thin Solid Films. 350 (1999) 30–37.

[127] J.I. Pankove, Absorption edge of impure gallium arsenide, Phys. Rev. 140 (1965) A2059.

[128] D. Redfield, Electric fields of defects in solids, Phys. Rev. 130 (1963) 914.

[129] T.P. Rao, M.S. Kumar, Physical properties of Ga-doped ZnO thin films by spray pyrolysis, J. Alloys Compd. 506 (2010) 788–793.

[130] C. Manoharan, M. Jothibas, S.J. Jeyakumar, S. Dhanapandian, Structural, optical and electrical properties of Zr-doped In_2O_3 thin films, Spectrochim. Acta. A. Mol. Biomol. Spectrosc. 145 (2015) 47–53.

[131] N. Fellahi, M. Addou, A. Kachouane, M. El Jouad, Z. Sofiani, Optical properties of undoped and tin-doped nanostructured In_2O_3 thin films deposited by spray pyrolysis, Eur. Phys. J. Appl. Phys. 74 (2016) 24611.

[132] F. Yakuphanoglu, S. Ilican, M. Caglar, Y. Caglar, The determination of the optical band and optical constants of non-crystalline and crystalline ZnO thin films deposited by spray pyrolysis, J. Optoelectron. Adv. Mater. 9 (2007) 2180.

[133] S. Ummartyotin, J. Juntaro, C. Wu, M. Sain, H. Manuspiya, Deposition of PEDOT: PSS nanoparticles as a conductive microlayer anode in OLEDs device by desktop inkjet printer, J. Nanomater. 2011 (2011) 606714.

[134] Y. Singh, Electrical resistivity measurements: a review, Int. J. Mod. Phys. Conf. Ser., World Scientific, 2013: pp. 745–756.

[135] J.G. Webster, The Measurement, Instrumentation and Sensors Handbook, CRC Press. 1998.

[136] B. Yahmadi, N. Kamoun, C. Guasch, R. Bennaceur, Synthesis and characterization of nanocrystallized In_2S_3 thin films via CBD technique, Mater. Chem. Phys. 127 (2011) 239–247.

[137] T.P. Rao, M.C. Santhoshkumar, Effect of thickness on structural, optical and electrical properties of nanostructured ZnO thin films by spray pyrolysis, Appl. Surf. Sci. 255

(2009) 4579–4584.

[138] S. Sakka, Handbook of Sol-Gel Science and Technology: Processing, Characterization and Applications, Springer, 2005.

[139] L.N. Lau, N.B. Ibrahim, H. Baqiah, Influence of precursor concentration on the structural, optical and electrical properties of indium oxide thin film prepared by a sol–gel method, Appl. Surf. Sci. 345 (2015) 355–359.

[140] A. Bouhdjer, A. Attaf, H. Saidi, H. Bendjedidi, Y. Benkhetta, I. Bouhaf, Correlation between the structural, morphological, optical, and electrical properties of In_2O_3 thin films obtained by an ultrasonic spray CVD process, J. Semicond. 36 (2015) 082002.

[141] M.M. Khan, W. Khan, M. Ahamed, M. Alhoshan, Structural and optical properties of In_2O_3 nanostructured thin film, Mater. Lett. 79 (2012) 119–121.

[142] V.A. Logacheva, T.A. Myachina, A.N. Lukin, A.M. Khoviv, Investigation of oxidation process and properties of indium and tin-based thin-film heterostructures, J. Surf. Investig. X-Ray Synchrotron Neutron Tech. 2 (2008) 444–449.

[143] M. Jothibas, C. Manoharan, S. Dhanapandian, S.J. Jeyakumar, Influence of precursor concentration on sprayed In_2O_3 thin films, Asian J. Chem. 25 (2013) S59.

[144] W. Metaferia, P. Dagur, C. Junesand, C. Hu, S. Lourdudoss, Polycrystalline indium phosphide on silicon using a simple chemical route, J. Appl. Phys. 113 (2013) 093504.

[145] A.M.E. Raj, K.C. Lalithambika, V.S. Vidhya, G. Rajagopal, A. Thayumanavan, M. Jayachandran, C. Sanjeeviraja, Growth mechanism and optoelectronic properties of nanocrystalline In_2O_3 films prepared by chemical spray pyrolysis of metal-organic precursor, Phys. B Condens. Matter. 403 (2008) 544–554.

[146] B.G. Jeyaprakash, R.A. Kumar, K. Kesavan, A. Amalarani, Structural and optical characterization of spray deposited SnS thin film, J Am Sci. 6 (2010) 22.

[147] P. Prathap, Y.P.V. Subbaiah, K.R. REDDY, Effect of precursor molarity on physical properties of In_2O_3 films, Optoelectron. Adv. Mater.-RAPID Commun. 1 (2007) 252–260.

[148] N. Khedmi, M.B. Rabeh, M. Kanzari, Structural morphological and optical properties of $SnSb_2S_4$ thin films grown by vacuum evaporation method, J. Mater. Sci. Technol. 30 (2014) 1006–1011.

[149] X.Y. Li, H.J. Li, Z.J. Wang, H. Xia, Z.Y. Xiong, J.X. Wang, B.C. Yang, Effect of substrate temperature on the structural and optical properties of ZnO and Al-doped ZnO thin films prepared by dc magnetron sputtering, Opt. Commun. 282 (2009) 247–252.

[150] S.S. Shinde, P.S. Shinde, R.T. Sapkal, Y.W. Oh, D. Haranath, C.H. Bhosale, K.Y. Rajpure, Photoelectrocatalytic degradation of oxalic acid by spray deposited nanocrystalline zinc oxide thin films, J. Alloys Compd. 538 (2012) 237–243.

[151] C.D. Lokhande, A.U. Ubale, P.S. Patil, Thickness dependent properties of chemically deposited Bi_2S_3 thin films, Thin Solid Films. 302 (1997) 1–4.

[152] R.S. Mane, C.D. Lokhande, Thickness-dependent properties of chemically deposited Sb_2S_3 thin films, Mater. Chem. Phys. 82 (2003) 347–354.

[153] S. Lugo-Loredo, Y. Peña-Méndez, M. Calixto-Rodriguez, S. Messina-Fernández, A. Alvarez-Gallegos, A. Vázquez-Dimas, T. Hernández-García, Indium sulfide thin films as window layer in chemically deposited solar cells, Thin Solid Films. 550 (2014) 110–113.

[154] J.R. Mohamed, L. Amalraj, Effect of precursor concentration on physical properties of nebulized spray deposited In_2S_3 thin films, J. Asian Ceram. Soc. 4 (2016) 357–366.

[155] A.I.A. Ali, Molarities effect on structural and optical properties of ZnO prepared by spray pyrolysis, Int. J. Sci. Eng. Res. 5 (2014) 2250–2255.

[156] M.P. Sarma, G. Wary, Effect of molarity on structural and optical properties of chemically deposited nanocrystalline PbS thin film, Int. Lett. Chem. Phys. Astron. 74 (2017) 22–35.

[157] I.J. Panneerdoss, S.J. Jeyakumar, S. Ramalingam, M. Jothibas, Characterization of prepared In_2O_3 thin films: The FT-IR, FT-Raman, UV–Visible investigation and optical analysis, Spectrochim. Acta. A. Mol. Biomol. Spectrosc. 147 (2015) 1–13.

[158] Q.H. Li, D. Zhu, W. Liu, Y. Liu, X.C. Ma, Optical properties of Al-doped ZnO thin films by ellipsometry, Appl. Surf. Sci. 254 (2008) 2922–2926.

[159] C.V. Weiss, M.W. Cole, S.P. Alpay, Influence of the precursor solution molarity on the dielectric response of chemical solution deposited strontium titanate thin films on Si, Integr. Ferroelectr. 126 (2011) 7–16.

[160] Z. Jiwei, Y. Xi, Z. Liangying, S. Bo, H. Chen, Orientation control and dielectric properties of sol–gel deposited Ba(Ti, Zr)O_3 thin films, J. Cryst. Growth. 262 (2004) 341–347.

[161] T.V. Vimalkumar, N. Poornima, C.S. Kartha, K.P. Vijayakumar, Effect of precursor medium on structural, electrical and optical properties of sprayed polycrystalline ZnO thin films, Mater. Sci. Eng. B. 175 (2010) 29–35.

[162] P. Babu, K.R. Reddy, R.W. Miles, Precursor concentration effect on the properties of $ZnIn_2Se_4$ layers grown by chemical bath deposition, Energy Procedia. 10 (2011) 177–181.

[163] Y. Li, Y. Bando, D. Golberg, Single-crystalline In_2O_3 nanotubes filled with In, Adv. Mater. 15 (2003) 581–585.

[164] M. Jothibas, C. Manoharan, S. Ramalingam, S. Dhanapandian, S. Johnson Jeyakumar, M. Bououdina; Preparation, characterization, spectroscopic (FT-IR, FT-Raman, UV and visible) studies, optical properties and Kubo gap analysis of In_2O_3 thin films, J. Mol. Struct. 1049 (2013) 239–249.

[165] M.I. Ivanovskaya, E.A. Ovodok, D.A. Kotsikau, Sol-gel synthesis and features of the

structure of Au-In_2O_3 nanocomposites, Glass Phys. Chem. 37 (2011) 560–567.

[166] M. Ghougali, O. Belahssen, A. Chala, Structural, optical and electrical properties of NiO nanostructure thin film, J. Nano- Electron. Phys. 8 (2016) 04059-1–04059-4.

[167] G.T. Delgado, C.Z. Romero, S.M. Hernández, R.C. Pérez, O.Z. Angel, Optical and structural properties of the sol–gel-prepared ZnO thin films and their effect on the photocatalytic activity, Sol. Energy Mater. Sol. Cells. 93 (2009) 55–59.

[168] M.G. Sandoval-Paz, R. Ramírez-Bon, Indium tin oxide films deposited on polyethylene naphthalate substrates by radio frequency magnetron sputtering, Thin Solid Films. 517 (2009) 2596–2601.

[169] Y.S. Jung, J.Y. Seo, D.W. Lee, D.Y. Jeon, Influence of DC magnetron sputtering parameters on the properties of amorphous indium zinc oxide thin film, Thin Solid Films. 445 (2003) 63–71.

[170] H.J. Wang, Y.Y. Zhu, Effect of post-annealing on the structure and optical properties of ZnO films deposited on Si substrates, IOP Conf. Ser. Mater. Sci. Eng. 382 (2018) 022054.

[171] C. Xirouchaki, G. Kiriakidis, T.F. Pedersen, H. Fritzsche, Photoreduction and oxidation of as-deposited microcrystalline indium oxide, J. Appl. Phys. 79 (1996) 9349–9352.

[172] Z. Yuan, X. Zhu, X. Wang, X. Cai, B. Zhang, D. Qiu, H. Wu, Annealing effects of In_2O_3 thin films on electrical properties and application in thin film transistors, Thin Solid Films. 519 (2011) 3254–3258.

[173] Y. Caglar, S. Ilican, M. Caglar, F. Yakuphanoglu, J. Wu, K. Gao, P. Lu, D. Xue, Influence of heat treatment on the nanocrystalline structure of ZnO film deposited on p-Si, J. Alloys Compd. 481 (2009) 885–889.

[174] J. Sengupta, R.K. Sahoo, K.K. Bardhan, C.D. Mukherjee, Influence of annealing temperature on the structural, topographical and optical properties of sol–gel derived ZnO thin films, Mater. Lett. 65 (2011) 2572–2574.

[175] V. Rakhesh, V.K. Vaidyan, Effect of substrate temperature and post deposited annealing on the electrical and photoluminescence characteristics of zinc oxide films deposited by spray pyrolysis, J. Optoelectron. Biomed. Mater. 1 (2009) 281–290.

[176] T.P. Rao, M.S. Kumar, V. Ganesan, Effect of annealing on the structural, optical and electrical properties of ZnO thin films by spray pyrolysis, Indian J. Phys. 85 (2011) 1381.

[177] S.Y. Kuo, W.C. Chen, F.I. Lai, C.P. Cheng, H.C. Kuo, S.C. Wang, W.F. Hsieh, Effects of doping concentration and annealing temperature on properties of highly-oriented Al-doped ZnO films, J. Cryst. Growth. 287 (2006) 78–84.

[178] S.H. Sabeeh, R.H. Jassam, The effect of annealing temperature and Al dopant on characterization of ZnO thin films prepared by sol-gel method, Results Phys. 10 (2018)

212–216.

[179] Y. Chen, W. Yu, Y. Liu, Effects of annealing on structural, optical and electrical properties of Al-doped ZnO thin films, Sci. China Ser. G Phys. Mech. Astron. 47 (2004) 588–596.

[180] A. Zaier, A. Meftah, A.Y. Jaber, A.A. Abdelaziz, M.S. Aida, Annealing effects on the structural, electrical and optical properties of ZnO thin films prepared by thermal evaporation technique, J. King Saud Univ.-Sci. 27 (2015) 356–360.

[181] G.J. Fang, D. Li, B.-L. Yao, Influence of post-deposition annealing on the properties of transparent conductive nanocrystalline ZAO thin films prepared by RF magnetron sputtering with highly conductive ceramic target, Thin Solid Films. 418 (2002) 156–162.

[182] S. Sanjeev, D. Kekuda, Effect of annealing temperature on the structural and optical properties of zinc oxide (ZnO) thin films prepared by spin coating process, IOP Conf. Ser. Mater. Sci. Eng. 73 (2015) 012149.

[183] M. Arif, A. Sanger, P.M. Vilarinho, A. Singh, Effect of annealing temperature on structural and optical properties of sol–gel-derived ZnO thin films, J. Electron. Mater. 47 (2018) 3678–3684.

[184] M.R. Alam, M.M. Rahman, A.T. Karim, M.K.R. Khan, Effect of Ag incorporation on structural and opto-electric properties of pyrolized CdO thin films, Int. Nano Lett. 8 (2018) 287–295.

[185] M.M. Rahman, H.A. Miran, Z.T. Jiang, M. Altarawneh, L.S. Chuah, H.L. Lee, A. Amri, N. Mondinos, B.Z. Dlugogorski, Investigation of the post-annealing electromagnetic response of Cu–Co oxide coatings via optical measurement and computational modelling, RSC Adv. 7 (2017) 16826–16835.

[186] A. Kennedy, K. Viswanathan, N. Krishnamoorthy, K. Pradeev Raj, Effect of substrate temperature on structural, morphological, optical and electrical properties of $MnIn_2S_4$ thin films prepared by nebulizer spray pyrolysis technique, Mater. Sci. Semicond. Process. 48 (2016) 39–44.

[187] A. Kennedy, K. Viswanathan, Study of the influence of substrate temperature on structural, optical, and electrical properties of Zn-doped $MnIn_2S_4$ thin films prepared by chemical spray pyrolysis, Phys. Lett. A. 380 (2016) 2842–2848.

[188] F. Wang, M.Z. Wu, Y.Y. Wang, Y.M. Yu, X.M. Wu, L.J. Zhuge, Influence of thickness and annealing temperature on the electrical, optical and structural properties of AZO thin films, Vacuum. 89 (2013) 127–131.

[189] P. Pujar, R.V. Vardhan, D. Gupta, S. Mandal, A balancing between super transparency and conductivity of solution combustion derived titanium doped indium oxide: Effect of

charge carrier density and mobility, Thin Solid Films. 660 (2018) 267–275.

[190] Z.W. Chen, J.K.L. Lai, C.H. Shek, Insights into microstructural evolution from nanocrystalline SnO_2 thin films prepared by pulsed laser deposition, Phys. Rev. B. 70 (2004) 165314.

[191] M. Ohyama, H. Kozuka, T. Yoko, Sol-gel preparation of transparent and conductive aluminum-doped zinc oxide films with highly preferential crystal orientation, J. Am. Ceram. Soc. 81 (1998) 1622–1632.

[192] P.S. Devi, M. Chatterjee, D. Ganguli, Indium tin oxide nano-particles through an emulsion technique, Mater. Lett. 55 (2002) 205–210.

[193] S. Neeleshwar, C.L. Chen, C.B. Tsai, Y.Y. Chen, C.C. Chen, S.G. Shyu, M.S. Seehra, Size-dependent properties of CdSe quantum dots, Phys. Rev. B. 71 (2005) 201307.

[194] H.J. Chun, Y.S. Choi, S.Y. Bae, H.C. Choi, J. Park, Single-crystalline gallium-doped indium oxide nanowires, Appl. Phys. Lett. 85 (2004) 461–463.

[195] T. Minami, Y. Takeda, T. Kakumu, S. Takata, I. Fukuda, Preparation of highly transparent and conducting Ga_2O_3–In_2O_3 films by direct current magnetron sputtering, J. Vac. Sci. Technol. Vac. Surf. Films. 15 (1997) 958–962.

[196] B. Zhang, X. Dong, X. Xu, P. Zhao, J. Wu, Characteristics of zirconium-doped indium tin oxide thin films deposited by magnetron sputtering, Sol. Energy Mater. Sol. Cells. 92 (2008) 1224–1229.

[197] A. Khayatian, V. Asgari, A. Ramazani, S.F. Akhtarianfar, M.A. Kashi, S. Safa, Diameter-controlled synthesis of ZnO nanorods on Fe-doped ZnO seed layer and enhanced photodetection performance, Mater. Res. Bull. 94 (2017) 77–84.

[198] M. Ajili, N. Jebbari, N.K. Turki, M. Castagné, Effect of Al-doped on physical properties of ZnO Thin films grown by spray pyrolysis on SnO_2: F/glass, Eur. Phys. J. Conf. 29 (2012) 00002.

[199] N.J. Begum, K. Ravichandran, Effect of source material on the transparent conducting properties of sprayed ZnO: Al thin films for solar cell applications, J. Phys. Chem. Solids. 74 (2013) 841–848.

[200] V. Senthamilselvi, K. Saravanakumar, N.J. Begum, R. Anandhi, A.T. Ravichandran, B. Sakthivel, K. Ravichandran, Photovoltaic properties of nanocrystalline CdS films deposited by SILAR and CBD techniques—a comparative study, J. Mater. Sci. Mater. Electron. 23 (2012) 302–308.

[201] M.S. Alqahtani, N.M.A. Hadia, S.H. Mohamed, Effects of V doping on magnetic and optical properties of oxygen-deficient In_2O_3 thin films, Optik. 145 (2017) 377–386.

[202] A.A. Aboud, M. Shaban, N. Revaprasadu, Effect of Cu, Ni and Pb doping on the photo-

electrochemical activity of ZnO thin films, RSC Adv. 9 (2019) 7729–7736.

[203] B. Shanmugapriya, M. Shanthi, P. Dhamodharan, K. Rajeshwaran, M. Bououdina, C. Manoharan, Enhancement of photocatalytic degradation of methylene blue dye using Ti^{3+} doped In_2O_3 nanocubes prepared by hydrothermal method, Optik. 202 (2020) 163662.

[204] S. Parthiban, V. Gokulakrishnan, K. Ramamurthi, E. Elangovan, R. Martins, E. Fortunato, R. Ganesan, High near-infrared transparent molybdenum-doped indium oxide thin films for nanocrystalline silicon solar cell applications, Sol. Energy Mater. Sol. Cells. 93 (2009) 92–97.

[205] M. Jothibas, C. Manoharan, S. Ramalingam, S. Dhanapandian, M. Bououdina, Spectroscopic analysis, structural, microstructural, optical and electrical properties of Zn-doped In_2O_3 thin films, Spectrochim. Acta. A. Mol. Biomol. Spectrosc. 122 (2014) 171–178.

[206] A. Umar, B. Karunagaran, E.K. Suh, Y.B. Hahn, Structural and optical properties of single-crystalline ZnO nanorods grown on silicon by thermal evaporation, Nanotechnology. 17 (2006) 4072.

[207] P.B. Nair, V.B. Justinvictor, G.P. Daniel, K. Joy, V. Ramakrishnan, D.D. Kumar, P.V. Thomas, Structural, optical, photoluminescence and photocatalytic investigations on Fe doped TiO_2 thin films, Thin Solid Films. 550 (2014) 121–127.

[208] Y. Cao, W. Yang, W. Zhang, G. Liu, P. Yue, Improved photocatalytic activity of Sn^{4+} doped TiO_2 nanoparticulate films prepared by plasma-enhanced chemical vapor deposition, New J. Chem. 28 (2004) 218–222.

[209] Z. Liang, X. Yu, B. Lei, P. Liu, W. Mai, Novel blue-violet photoluminescence from sputtered ZnO thin films, J. Alloys Compd. 509 (2011) 5437–5440.

[210] S. Kaleemulla, A.S. Reddy, S. Uthanna, P.S. Reddy, Physical properties of pure In_2O_3 thin films, Optoelectron Adv Mater Rapid Commun. 2 (2008) 782–787.

[211] I. Georgieva, N. Danchova, S. Gutzov, N. Trendafilova, DFT modeling, UV-Vis and IR spectroscopic study of acetylacetone-modified zirconia sol-gel materials, J. Mol. Model. 18 (2012) 2409–2422.

[212] Y. Bouachiba, F. Hanini, A. Bouabellou, F. Kermiche, A. Taabouche, M. Bouafia, S. Amara, S. Sahli, K. Boukheddaden, TiO_2 thin films studied by FTIR, AFM and spectroscopic ellipsometry, Int. J. Nanoparticles. 6 (2013) 169–177.

[213] L. Renard, J. Brötz, H. Fuess, A. Gurlo, R. Riedel, T. Toupance, Hybrid organotin and tin oxide-based thin films processed from alkynylorganotins: synthesis, characterization, and gas sensing properties, ACS Appl. Mater. Interfaces. 6 (2014) 17093–17101.

[214] M. Islam, R.C. Roy, J. Hossain, M. Julkarnain, K.A. Khan, Electrical and optical transport

characterizations of electron beam evaporated V doped In_2O_3 thin films, Mater. Res. 20 (2017) 102–108.

[215] N. Manjula, M. Pugalenthi, V.S. Nagarethinam, K. Usharani, A.R. Balu, Effect of doping concentration on the structural, morphological, optical and electrical properties of Mn-doped CdO thin films, Mater. Sci.-Pol. 33 (2015) 774–781.

[216] A.R. Vazquez-Olmos, J.I. Gomez-Peralta, R.Y. Sato-Berru, A.L. Fernandez-Osorio, Diluted magnetic semiconductors based on Mn-doped In_2O_3 nanoparticles, J. Alloys Compd. 615 (2014) S522–S525.

[217] H. Taha, Z.T. Jiang, D.J. Henry, A. Amri, C.Y. Yin, M.M. Rahman, Improving the optoelectronic properties of titanium-doped indium tin oxide thin films, Semicond. Sci. Technol. 32 (2017) 065011.

[218] X. Sun, X. Liu, X. Deng, X. Xu, Synthesis of Zn-doped In_2O_3 nano sphere architectures as a triethylamine gas sensor and photocatalytic properties, RSC Adv. 6 (2016) 89847–89854.

[219] M. Sasaki, K. Yasui, S. Kohiki, H. Deguchi, S. Matsushima, M. Oku, T. Shishido, Cu doping effects on optical and magnetic properties of In_2O_3, J. Alloys Compd. 334 (2002) 205–210.

[220] R. Karmakar, S.K. Neogi, A. Banerjee, S. Bandyopadhyay, Structural; morphological; optical and magnetic properties of Mn doped ferromagnetic ZnO thin film, Appl. Surf. Sci. 263 (2012) 671–677.

[221] Y. Zhang, L. Mi, Z. Zheng, Study on the structure and optical property of $Zn_{1-x}Cu_xO$ sol–gel thin films on quartz substrate, Phys. B Condens. Matter. 407 (2012) 2254–2257.

[222] H. Chen, J. Ding, S. Ma, Violet and blue-green luminescence from Ti-doped ZnO films deposited by RF reactive magnetron sputtering, Superlattices Microstruct. 49 (2011) 176–182.

[223] S.M. Salaken, E. Farzana, J. Podder, Effect of Fe-doping on the structural and optical properties of ZnO thin films prepared by spray pyrolysis, J. Semicond. 34 (2013) 073003.

[224] L. Xu, X. Li, Influence of Fe-doping on the structural and optical properties of ZnO thin films prepared by sol–gel method, J. Cryst. Growth. 312 (2010) 851–855.

[225] A.H. Rubel, J. Podder, Structural and electrical transport properties of CdS and Al-doped CdS thin films deposited by spray pyrolysis, J. Sci. Res. 4 (2012) 11–19.

[226] K. Usharani, A.R. Balu, Structural, optical, and electrical properties of Zn-doped CdO thin films fabricated by a simplified spray pyrolysis technique, Acta Metall. Sin. Engl. Lett. 28 (2015) 64–71.

[227] H. Kim, C. Gilmore, A. Pique, J.S. Horwitz, H. Mattoussi, H. Murata, Z.H. Kafafi, D.B.

Chrisey, Electrical, optical, and structural properties of indium–tin–oxide thin films for organic light-emitting devices, J. Appl. Phys. 86 (1999) 6451–6461.

[228] A. Kathalingam, K. Kesavan, A.U.H.S. Rana, J. Jeon, H.S. Kim, Analysis of Sn concentration effect on morphological, optical, electrical and photonic properties of spray-coated Sn-doped CdO thin films, Coatings. 8 (2018) 167.

[229] F. Yakuphanoglu, Nanocluster n-CdO thin film by sol–gel for solar cell applications, Appl. Surf. Sci. 257 (2010) 1413–1419.

[230] F.K. Mugwanga, P.K. Karimi, W.K. Njoroge, O. Omayio, Characterization of aluminum doped zinc oxide (Azo) thin films prepared by reactive thermal evaporation for solar cell applications, J Fundam Renew. Energy Appl. 5 (2015) 1000170.

[231] R.K. Mishra, P.P. Sahay, Zn-doped and undoped SnO_2 nanoparticles: A comparative structural, optical and LPG sensing properties study, Mater. Res. Bull. 47 (2012) 4112–4118.

[232] A.P. Roth, J.B. Webb, D.F. Williams, Band-gap narrowing in heavily defect-doped ZnO, Phys. Rev. B. 25 (1982) 7836–7839.

[233] P. Banerjee, W.J. Lee, K.R. Bae, S.B. Lee, G.W. Rubloff, Structural, electrical, and optical properties of atomic layer deposition Al-doped ZnO films, J. Appl. Phys. 108 (2010) 043504.

[234] K.J. Kim, Y.R. Park, Large and abrupt optical band gap variation in In-doped ZnO, Appl. Phys. Lett. 78 (2001) 475–477.

[235] K.F. Berggren, B.E. Sernelius, Band-gap narrowing in heavily doped many-valley semiconductors, Phys. Rev. B. 24 (1981) 1971–1986.

[236] M. Saha, S. Ghosh, V.D. Ashok, S.K. De, Carrier concentration dependent optical and electrical properties of Ga doped ZnO hexagonal nanocrystals, Phys. Chem. Chem. Phys. 17 (2015) 16067–16079.

[237] K. Usharani, N. Raja, N. Manjula, V.S. Nagarethinam, A.R. Balu, Characteristic Analysis on the Suitability of CdO Thin Films Towards Optical Device Applications-Substrate Temperature Effect, Int. J. Thin Films Sci. Technol. 4 (2015) 89–96.

[238] P. Reunchan, X. Zhou, S. Limpijumnong, A. Janotti, C.G. Van de Walle, Vacancy defects in indium oxide: An ab-initio study, Curr. Appl. Phys. 11 (2011) S296–S300.

[239] L.M. Huang, C. Arhammar, C.M. Araújo, F. Silvearv, R. Ahuja, Tuning magnetic properties of In_2O_3 by control of intrinsic defects, EPL Europhys. Lett. 89 (2010) 47005.

List of publications and conferences

Publication

A. Yahia, A. Attaf, H. Saidi, M. Dahnoun, C. Khelifi, A. Bouhdjer, A. Saadi, H. Ezzaouia, Structural, optical, morphological and electrical properties of indium oxide thin films prepared by sol gel spin coating process, Surfaces and Interfaces. 14 (2019) 158–165.

Conferences

A. Yahia and A. Attaf, Effect of molar concentration on properties of indium oxide thin films prepared by sol gel spin coating method, University Mohamed Khider of Biskra, (2017).

A. Yahia, A. Attaf, H. Saidi, M. Dahnoun, C. Khelifi, and A. Saadi, Titanium doped indium oxide thin films deposited via sol gel spin coating process, University Mohamed Khider of Biskra, (2018).